UNIVERSIDAD EAFIT

Engineering School

Design Engineering Research Group (GRID)

A comparative study of the hydrodynamic performance of planing boats through experimental and statistical approaches.

Graduation manuscript presented as partial requirement to obtain the

Master of Science in Engieneering

AUTHOR:

Ing. Erick Santiago Giraldo Pérez

ADVISOR:

Gilberto Osorio-Gomez, PhD.

August 2021

Abstract

Hydrodynamic efficiency emerges as a key characteristic for boats to help migrating to more waterborne sustainable transportation means. This hydrodynamic efficiency can be reached in several ways but all have as a common objective the reduction of the hydrodynamic drag, which depends mostly on the area in contact with water of the boat hull, due to this fluid is responsible for at least 80% of the total hydrodynamic drag generation. For reducing the wetted area, several alternatives have been invented. Planing boats and hydrofoil crafts stand as the most studied of all alternatives and both can be combined to create hydrofoil planing boats with monohull or multihull hull shapes. However, it is not convenient to operate monohull planing boats with hydrofoils in low-depth bodies of water without the need of implementing complex mechanisms to avoid increasing excessively the boat draft. Here, hydrofoil supported catamarans (hysucats) emerge as a compromise solution even with the potential of reaching better hydrodynamic performances than monohulls, and according to the literature, both have not been compared against the other. In this exploratory research project, a monohull, a catamaran and a hysucat hull are compared experimentally together with Savitsky model for planing hulls in order to find the geometry with the lowest hydrodynamic drag. These geometries have the same length, width, draft, submerged volume and weight distribution. Also the dynamic positioning of the boats is studied. The hysucat and the catamaran boats present up to 50% higher drag in planing speeds than the monohull, which may be mostly due to they travel almost horizontally at planing speeds, what makes both having a 50% more wetted area in comparison with the monohull. Some alternatives for improving the hydrodynamic efficiency of the catamaran and the hysucat are proposed.

Keywords: planing boats, hydrofoils, hydrodynamic efficiency, sustainable transport.

Resumen

La eficiencia hidrodinámica surge como una característica clave para que las embarcaciones ayuden a migrar hacia medios de transporte acuÃ¡ticos más sostenibles. Esta eficiencia hidrodinámica puede alcanzarse de varias maneras, pero todas tienen como objetivo común la reducción de la resistencia hidrodinámica, que depende sobre todo del área en contacto con el agua del casco de la embarcación, ya que este fluido es responsable de al menos el 80% de la generación total de resistencia hidrodinámica. Para reducir el área mojada, se han inventado varias alternativas. Los botes de planeo y los botes con hidroalas son las alternativas más estudiadas y ambas pueden combinarse para crear botes de planeo con hidroalas con formas tipo monocasco o multicasco. Sin embargo, no es conveniente operar con embarcaciones de planeo monocasco con hidroalas en cuerpos de agua de baja profundidad sin necesidad de implementar complejos mecanismos para evitar el aumento excesivo del calado de la embarcación. En este caso, los catamaranes apoyados en hidroalas (hysucats) surgen como una solución de compromiso, incluso con el potencial de alcanzar mejores prestaciones hidrodinámicas que los monocascos, y según la literatura, ambos no han sido comparados entre sí. En este proyecto de investigación exploratorio, se comparan experimentalmente un monocasco, un catamarán y un casco hysucat, junto con el modelo de Savitsky para cascos de planeo, con el fin de encontrar la geometría con la menor resistencia hidrodinámica. Estas geometrías tienen la misma longitud, anchura, calado, volumen sumergido y distribución de peso. También se estudia el posicionamiento dinámico de los botes. El hysucat y el catamarán presentan hasta un 50% más de resistencia en velocidades de planeo que el monocasco, lo que puede deberse principalmente a que se desplazan casi horizontalmente a velocidades de planeo, lo que hace que ambos tengan un 50% más de superficie mojada en comparación con el monocasco. Se proponen algunas alternativas para mejorar la eficiencia hidrodinámica del catamarán y del hysucat.

Palabras Clave: Botes de planeo, hidroalas, eficiencia hidrodinámica, transporte sostenible

Acknowledgements

This research has been developed in the framework of the “ENERGETICA 2030" Research Program, with code 58667 in the “Scientific Colombia" initiative, funded by The World Bank through the call “778-2017 Scientific Ecosystems", managed by the Colombian Ministry of Science, Technology and Innovation (Minciencias), with contract No. FP44842-210-2018.

Contents

List of Figures

List of Tables

Chapter 1

Introduction

1.1 Background

Watercrafts are probably the most ancient means of transport that humanity has ever used. It is estimated that the first boats were built more than 8.000 years ago. They played an important role in migration, discovery and colonization in the antiquity, middle ages and discovery ages (Jean Vaucher, 2014). At those ages, the nations with the strongest naval fleet had a great advantage over their military and commercial competition. Water transport brought wealth, economic growth and political importance to the nations adopting this means of transport (Stopford, 2008).

Nowadays, water transport is still a very important means of transport for several applications due to it has the largest carrying capacity and is the most suitable for carrying bulky goods and people over long distances at moderate speeds. According to the European Comission (2020), the inland waterway transport offers a greener and more efficient alternative to road and rail transport considering that its energy consumption per km/ton of transported goods is only 17% of that of road transport and 50% of rail transport.

Figure 1.1 shows the evolution of the amount of passengers transported by year in the European Union in which it can be observed that despite there has been some reduction in passengers in the last decade, 415 million of passengers embarked and disembarked in all ports in 2017 which is similar to the European Union population.

Table 1.2 shows the amount of passengers and goods transported by different means in some leading countries in billions of passengers per kilometer (pkm) and billions of tons per kilometer (tkm) respectively. It can be observed that freight transport is carried out in big part through waterways, specially in Europe where combined inland and sea operations becomes the second means of transport with the highest cargo movement after road transport. In the other hand, despite water transport for passengers is the least used transportation mean in these developed regions, it represents an alternative

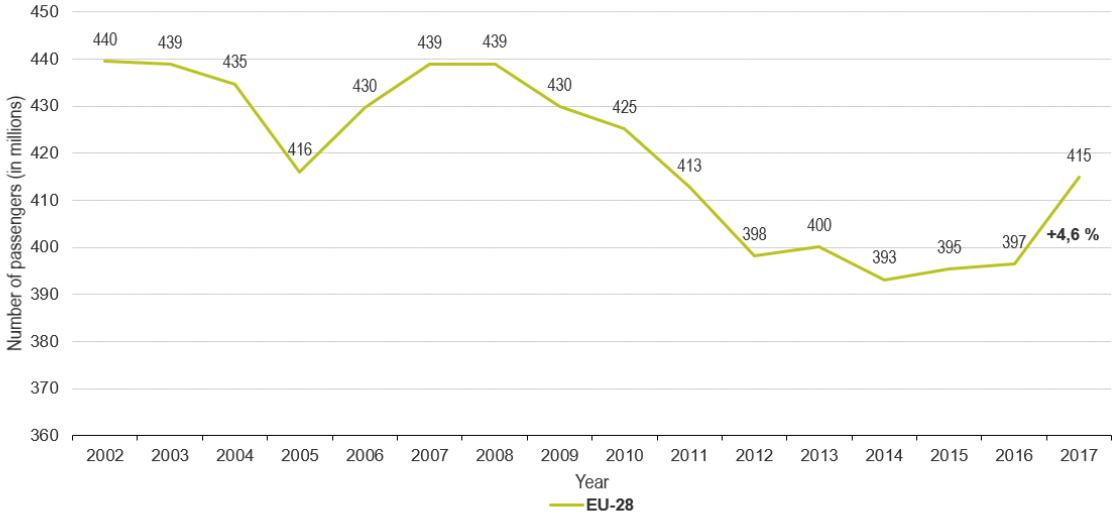

Note: the y-axis is cut.
Source: Eurostat (online data code: mar_mp_aa_cph)

Figure 1.1: Seaborne passengers embarked and disembarked in all ports in EU-28 from 2002 to 2017. Plot retrieved from: `https://ec.europa.eu/eurostat/statistics-explained/index.php?title=Passenger_transport_statistics`

to reduce inland traffic congestion, and even organizations such as the European Comission and the UITP (Union internationale des Transports Publiques) consider it as an opportunity to innovate in a greener mobility (Comission, 2017; Union Internationale des Transports Publics, 2013). Some examples of public fluvial transport systems can be observed in at least 23 cities around the world such as Amsterdam, Copenhagen, Gothenburg, Auckland, Hong Kong, Venice, Istanbul, New York, Sao Paulo and London, to mention a few (Cheemakurthy et al., 2017).

PASSENGER TRANSPORT

billion pkm	EU-28 2016	USA 2016	JAPAN 2015	CHINA 2016	RUSSIA 2016
Passenger car	*4 829.3*	6 315.4 (1)		1 022.9 (2)	
Bus + trolley bus + coach	*552.0*	558.1	71.4		129.8
Railway	450.1	40.2	427.5	1 257.9	124.6
Tram + metro	*105.6*	23.5	(3)		48.7
Waterborne	*25.0*	0.8	*2.9 (4)*	7.2	0.7
Air (domestic/intra-EU-28)	*713.5*	1 079.0	88.2	837.8	215.6

FREIGHT TRANSPORT

billion tkm	EU-28 2016	USA 2015	JAPAN 2015	CHINA 2016	RUSSIA 2016
Road	1 803.5	2 990.2	204.3	6 108.0	234.0
Rail	*411.8*	2 547.3 (5)	21.5	2 375.2	2 344.0
Inland waterways	*147.3*	486.5			67.0
Oil pipeline	*115.1*	1 411.8		419.6 (6)	1 308.0
Sea (domestic/intra-EU-28)	1 180.8	*251.8 (7)*	180.4	9 733.9 (8)	43.0

Notes: (1) USA: including light trucks/vans.
(2) China: including buses and coaches.
(3) Japan: included in railway pkm.
(4) Japan: 2014 value.
(5) USA: Class I rail.
(6) China: oil and gas pipelines.
(7) USA: refers to coastal shipping, 2014 data.
(8) China: both coastwise and inland waterway transport.

Figure 1.2: Passenger and freight transport by different means around the world. Source: (European Comission, 2018)

Nonetheless, currently most of the fuel used to propel these vessels are fossil fuels and the consumption is much higher than in land vehicles. Alternative sources, such as batteries, have a much lower available energy per kilogram and are much more expensive. The higher consumption in watercrafts is mainly because water is 1000 times heavier than air so resistance is much higher. In comparison, a 7.5 meters long classic boat consumes around 15 times more than a family car (Candela speedboat, 2018), and the weight per usable energy of batteries is at least 16 times higher than that of the gasoline (Candela speedboat, 2018). In addition to this, the cost of batteries with respect to the total cost of a car is around 30% (Bullard, 2019). The wide usage of fossil fuels has transformed water transport in a main player of the pollution source in transportation means. According to the European Parliament, only maritime transport was responsible for 4% of the global CO_2 emissions in 2012, and it could grow to 17 % in 2050 if left unregulated (Cames et al., 2015).

This is why most representative maritime organizations around the world such as the International Maritime Organization (IMO) with its MARPOL convention, the European Comission (Comission, 2017), the UITP (Union Internationale des Transports Publics, 2013), among others, are fostering the development of efficient, environmentally friendly and sustainable mobility solutions in order to reduce reliance on fossil fuels and reduce pollutant emissions.

For increasing performance and efficiency of vessels and hence reducing pollutant emissions, aside from implementing alternative energy sources, it is vital to reduce the hydrodynamic resistance without reducing the safety of the vessel. The consumed energy depends on this resistance, of which water causes around a 90% (Faltinsen, 2005). As a rule of thumb, reducing the operational speed, the wetted area, the area formed by the intersection between the vessel and the surface of the water, or the area facing the flow will produce hydrodynamic resistance reduction. However, the first strategy may not be an option for high-speed vessels. The three latter ones can be reduced mainly by minimizing the vehicle weight, creating hydrodynamic lift with hulls with flat bottoms or planing hulls (Savitsky et al., 1964), using hydrofoils (Vellinga, 2009), using hard chines or hull steps in order to cause separation of the flow from the hull (Savitsky and Morabito, 2010), bleeding air to generate air cavities under the hull (Latorre, 1997), among other techniques.

Among these techniques for reducing hydrodynamic resistance, hydrofoils have been one of the most successful for reducing water resistance on vessels and hence increasing performance, which is proved by the amount of vessels that have broken speed records and have achieved high fuel saving since this invention (Vellinga, 2009; Yun and Bliault, 2012). Nowadays, the best high performance boats for competitions use hydrofoils (solar boat race, 2018; Solar Splash, 2012) and electric boats with performances similar to those of combustion engine boats are appearing more constantly around the world regardless of its usage for leisure or for passenger transportation. Boats like Candela (Candela speedboat, 2018) and the Sea Bubbles (Ebbert, 2017) are clear examples.

Hydrofoils are appendages that can be attached to the bottom of almost any type of vessel. They can be attached to monohulls as well as to multihulls. This make them very versatile and a compelling way to increase efficiency of vessels. However, one their biggest limitations is that their proper operation is limited to depth waters in which they can work far away the surface and the bottom, primarily because the foils reduce their performance when close to fluids or elements different than water. Additionally, the foil could collide against a solid element at the bottom of the water body, causing an accident.

Hydrofoils tend to suffer from cavitation in boats working at speeds higher than 25 m/s. Cavitation can be reached at even less speeds if the hydrofoil is not properly designed. Also, they can suffer from ventilation, which occurs when the foil is very close to the water surface. This causes the foil to suck air from the surface, causing the immediate vanishing of the lift (Vellinga, 2009; Faltinsen, 2005).

Another way of reducing hydrodynamic resistance as mentioned before is by replacing traditional curved surfaces at the bottom of the hull by flat surfaces in order to generate a hydrodynamic force pointing upwards or lift. Planing boats take advantage of this principle and the interest on understanding the phenomena is as old as the one with hydrofoils. Planing boats can travel at high speeds without requiring huge amounts of power and energy consumption; and without penalizing stability and manoeuvrability. Planing boats, like hydrofoils, take advantage of hydrodynamic lift in order to reduce the boat sinkage and reduce the wetted area (Savitsky et al., 1964).

Planing boats can be monohulls or multihulls (catamarans). Historically, planing monohulls have been used the most due to their ease of construction and because of the phenomena acting behind scenes for the planing monohull boat is more understood, which allows designers to easily accomplish design objectives. However, planing catamarans have been taking a greater role in high speed vessels for passenger transportation, leisure or competition due to their high efficiency, roll stability at high speeds and smoother rides in rough water conditions (Yun et al., 2018).

As was mentioned before, if a hydrofoil is wanted to be attached in a planing monohull, the designer must make sure the monohull is going to operate in depth waters, so normally monohull hydrofoils operate in channeled rivers, lakes, open seas and bodies of water where a safe depth can be warranted. Hopefully, attaching hydrofoils to planing catamarans may solve these inconvenients due to restrictions. The benefit is twofold: the foils are protected by the demihull keels (at least against the bottom) without increasing the boat draft excessively. These advantages would allow to use hydrofoil catamarans in bodies of water that are more restrictive, such as non-channeled low depth rivers, which are very common in South America and Asia.

This concept of hydrofoil catamarans is relatively new compared to the invention of planing boats and hydrofoils, and the first report of this invention was published by Hoppe (1989). Since then, several successful applications of this concept have been carried out in leisure boats, patrol boats

and ferries with companies like Hysucat, Safehaven Marine, Icarus Marine, among others. Other applications include solar-electric vessel competitions and high speed sailing competitions such as the hydrocontest and the Red Bull Foiling Generation. In this sense, there is an opportunity of replacing classic planing monohulls for hydrofoil supported catamarans, seeking for more efficient designs without incurring in safety penalties.

These efficient designs are nothing but vessels producing a relatively low hydrodynamic resistance, which implies less installed power for traveling at a design speed and hence, less (cheaper) batteries. This resistance can be measured mainly by 3 ways: experimentally, by means of statistical methods, and with numerical methods (CFD).

Experimental methods are the most accepted in the scientific world due to their close representation to reality, but they may be the most expensive and time consuming of all. Statistical methods are the fastest in giving results, but they are the less close to reality due to their simplifications so they are preferably used in early design stages. However, a significant cost reduction can be achieved by testing with scaled models. The family of numerical methods contain several methods, but the most successful of all is computational fluid dynamics (CFD). CFD can be very precise but need validation, is very sensitive to the inputs and can be very computationally expensive and complex. This high cost and complexity can be increased even further if dynamic meshes are used to represent the behavior of planing boats. Furthermore, CFD requires a high skill and expertise that requires a certain amount of time to learn.

In this work, a comparative experimental and statistical study is carried out between a planing monohull, a planing catamaran and a hydrofoil supported catamaran (hysucat) of similar dimensions, weight and weight distribution, in order to determine the geometry with the best hydrodynamic behavior, meaning a low hydrodynamic drag and appropriate dynamic positioning according to the literature. The equation derived by Savitsky et al. (1964) will be used as a tool for a deeper understanding of the planing phenomena and as precursor for designing the experiment. The results derived from this work will help in the evaluations of the implementation of hysucats in water basins where the depth of the water is a restriction.

1.2 Research justification

This thesis is framed in a research project where the objective is to design an electric boat that replaces the current boats operating in Colombian rivers for the public transportation of passengers. Therefore, the designed boat must have similar characteristics to these selected vessels. These vessels are monohull planing boats propelled with fossil fuel engines with an output power of 200 HP that travel at high speeds, concretely at around 55 km/h in average, and are able to convey between 20 and 25 passengers. Figure 1.3 shows an image of the monohull boat.

Figure 1.3: Current monohull boat for the transportation of passengers operating in Colombian rivers

Colombian rivers where these monohull vessels operate have several characteristics that make the operation of boats in general to be more complex, in comparison to the operation in bodies of water in countries or continents such as Europe, which has been a pioneer implementing novel hydrofoil boat designs. These Colombian rivers are low-depth rivers that greatly variate their flow rate along the year due to the seasonal rains and droughts, which makes the depth to also variate (Arcadis Nederland and Jesyca, 2015; Calle, 2016). This high variation in depth, combined with the fact that the bottom of these rivers has very irregular shapes, makes these rivers very dangerous to navigate with motorboats during some seasons in the year. Furthermore, these rivers transport silt in very high concentration rates making unfeasible to install channels as in some European rivers (Restrepo et al., 2018; Higgins et al., 2016; Restrepo et al., 2015).

Implementing an electric boat with similar characteristics would allow to implement a more sustainable mean of transportation with possibly lower transport rates for people in regions where the water transport is representative.

1.3 Research question

How to determine what boat geometry achieves a lower hydrodynamic resistance and an appropriate dynamic positioning at different speeds?

1.4 Objectives

1.4.1 General objective

To compare the hydrodynamic performance of planing boats at several speeds through an experimental and statistical approach, in order to estimate the differences in hydrodynamic resistance and dynamic positioning of a monohull, a catamaran, and a hysucat.

1.4.2 Specific objectives

- To develop a design of experiment with the help of Savitsky method, which allows to determine the difference in hydrodynamic performance between the selected boat geometries.
- To carry out experiments with the selected boat configurations in order to evaluate their hydrodynamic resistance and dynamic positioning at different speeds.
- To analyze the experimental results in order to statistically determine the hull configuration with the lowest hydrodynamic resistance and more appropriate dynamic positioning at different speeds.

1.5 Research Scope

In this work, three boat hulls of different shapes will be evaluated at multiple speeds. These speeds will be in the displacement, preplaning and planing regimes. Here, it will be analyzed total drag and dynamic positional variables such as trim angle, wetted area, sinkage and wetted keel length in a comparative way. This comparative way includes statistical tests such as ANOVA, multiple comparison tests and regression analyses, using statistical methods available in the literature to provide insights for the experimental design. Computational fluid methods are left out of this study.

No ground-truth results are meant to be provided in this study since this requires testing with the full-scale boats or high-cost infrastructure and precise instruments recommended by the International Towing Tank (ITTC) for testing with scaled models.

The amount of useful data collected per run and stabilization of the boat models during a run is subjected to the length of the body of water in which the experiments are carried out. For example, the length of towing tanks certified by the ITTC may have 300 meters in length at least. Despite this,

in this study the experimental tests are carried out in a body of water 100 meters long. This requires a fast stabilization of the boat specially at the highest speeds which may be not achieved sometimes. This lack of stabilization may cause a high dispersion in the data, specially for the data collected with sensors embedded in the boat, which are more sensitive to the boat oscillation during the runs.

1.6 Thesis organization

This chapter starts introducing the importance of the maritime transport around the world and the need of migrating to more sustainable alternatives, especially for planing boats for the transport of passenger or cargo. Some alternatives for reducing the energetic consumption are mentioned and the alternative of a hysucat as a hybrid and compromise solution is raised. According to the mentioned characteristics, this architecture seems to be better suited for the context, which is described in the research justification. This chapter closes with the objective and scope of the project.

Chapter two contains general theory of boat hydrodynamics. A description of the planing phenomena is given and the methods for evaluating important variables of planing boats are mentioned. Following this, The Savitsky equations are described in detail and how they are used to calculate the most important forces according to a typical free body diagram for a planing hull. Also, the modified version of Savitsky equations for catamaran hulls are also explained in detail. Thereafter, some theory about hydrofoils is mentioned, including the available arquitectures, the equations for calculating principal forces, cavitation and ventilation and the influence of shallow operation in the performance of hydrofoils. The chapter closes with a quick revision of non dimensional numbers important in this study and references an ITTC recommended procedure for measuring hydrodynamic resistance in models and scaling up results to real scale.

In chapter three, the methods for measuring the hydrodynamic behavior of planing hulls are discussed in more detail and examples of studies using these methods are given. It is also explained why numerical methods are out of the scope of this work. The chapter closes discussing what studies have compared monohulls, catamarans an hysucats with the previously discussed methods and highlights scenarios not yet evaluated.

Chapter four explains how the statistical chosen method serves for designing the experiment. The rest of the chapter describes in detail the manufactured instruments to carry out the experiments and the experimental setup. Variables included in the analysis are mentioned, as well as the preprocessing of the data collected for this variables in order to carry out the analyses. Also the activities to carry out to fulfill the requirements of a valid fully randomized experiment are touched on. The chapter is wrapped up explaining the statistical tests to carry out the analysis, such as ANOVA and the tests to check compliance of the assumptions, Tukey-HSD test for the multiple comparison test and the regression analysis.

Chapter five presents the description of the hull shapes to be evaluated as well as the hydrofoils that were installed in the catamaran to obtain the hysucat. The inputs to the Savitsky method are shown in detail and the manufacture process of the boat models for the experiments is mentioned. The final part of the chapter is devoted to show and discuss the obtained results according to the previously planned statistical analyses. Results for the ANOVA and their assumptions, for the multiple comparison test and the regression analysis for the drag force, trim angle, wetted area, wetted keel length and sinkage are presented. At the end of this work, the chapter of conclusions draws upon these obtained results.

Chapter 2

Theoretical Framework

2.1 General ship hydrodynamics

In the process of designing a boat, generally the first step in sizing the power required to the boat to reach a required speed is to measure the total drag of the boat. This drag multiplied by the speed is equal to the effective power. Finally, this effective power is multiplied by a series of efficiencies corresponding to the principal components of the propulsion system to obtain the installed power of the engine (Faltinsen, 2005; Molland et al., 2017). Figure 2.1 shows a summary of this design process.

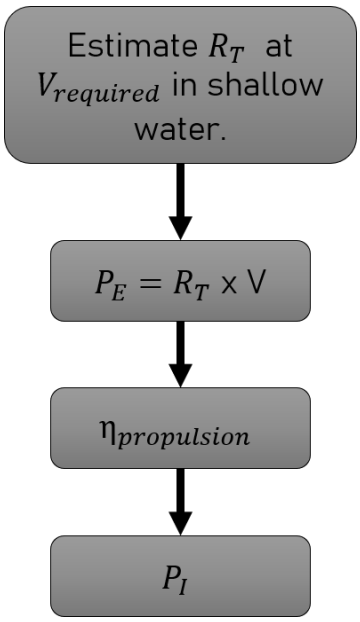

Figure 2.1: Diagram of the process of estimating the installed power of a vessel

Where R_T it the total resistance of the boat, V is the speed of the boat, P_E is the effective power, which is the power after the propeller, $\eta_{propulsion}$ is the global efficiency of the propulsion system and

P_I is the installed power or power generated by the engine. In brief, the installed power is transformed into a force which pushes the boat in a desired direction by means of the transmission and propeller blades. This force always matches resistance at any constant speed. Figure 2.2 shows a free body diagram representing this equilibrium of forces.

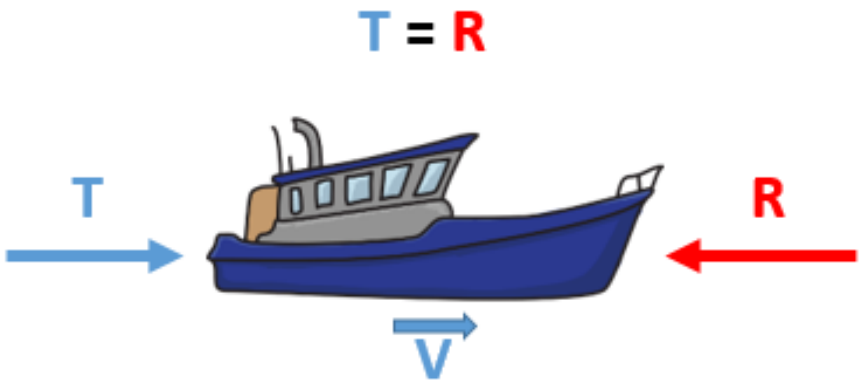

Figure 2.2: Boat propulsion outline

In an electric boat, the installed power must be again multiplied by the efficiency of the electric engine in order to obtain the electric power. Having this electric power, and a distance to travel at a required speed, the amount of energy hence the size and weight of the batteries can be obtained. Equation (2.1) represents the process for transforming the effective power into electric power.

$$P_{EL} = P_E \cdot \frac{1}{\eta_M} \cdot \frac{1}{\eta_T} \cdot \frac{1}{\eta_D} \tag{2.1}$$

In this equation, P_{EL} is the electric power, η_M is the motor efficiency, η_T is the transmission efficiency, and η_D is the propulsive efficiency due to power losses in the propeller. Further efficiency components can be added in more detailed analyses or as long as more propulsive components are added.

2.1.1 Components of total resistance

In the preliminary design of any boat, total resistance is measured in an undisturbed environment, which means that the air and water are completely calm. Under this assumption, the total resistance is divided into four main components Faltinsen (2005); Molland et al. (2017):

- Viscous water resistance, R_v
- Wave-making resistance, or residual resistance, R_w or R_R
- Spray resistance, R_S
- Air resistance, R_{AA}

Therefore, if all the components are added, the total resistance of the boat is obtained with the Equation (2.2).

$$R_T = R_v + R_{AA} + R_S + R_w \tag{2.2}$$

2.1.1.1 Viscous water resistance

It is the main component of resistance which is caused by friction force in the wet area of the hull and is represented by the Equation (2.3):

$$R_v = 0.5 \cdot \rho_W \cdot C_F \cdot S \cdot U^2 \tag{2.3}$$

Where ρ_W is the water density, S is the wet area of the boat, C_F is the friction coefficient and U is the speed of the boat.

2.1.1.2 Wave-making resistance

It is the resistance due to the waves generated by the boat going in a straight line at constant speed in calm water conditions. It is mainly influenced by the ratio between beam and length, displacement, hull shape in the wet zone, Froude number and speed. In shallow water, this component of resistance can be highly influenced by depth.

This component is the largest along with the viscous water resistance and is even larger in high-draft vessels due to it is highly affected by the wetted area S, which in turn is influenced by the submerged volume $\nabla^{1/3}$.

$$R_w = 0.5 \cdot \rho_W \cdot C_w \cdot S \cdot U^2 \tag{2.4}$$

2.1.1.3 Spray resistance

This component depends on the Froude and Reynolds numbers and is very likely to occur at Froude numbers greater than 0.5 when speed is increased. It occurs when there are large stagnant pressures and large pressure gradients at the front of the boat in the free surface area, so the water pierces the free surface and shoots upward in a mixture of air and water. This spray can be reduced by using "spray rails". However, these spray rails cause drag due to other phenomena. Additionally, it is difficult to measure, and can only be reliably determined on full-scale experimental trials.

2.1.1.4 Air resistance

It is the resistance generated by the air flow, without including wind gusts and is represented by the Equation (2.5).

$$R_{AA} = 0.5 \cdot \rho_a \cdot C_D \cdot A \cdot V^2 \tag{2.5}$$

Where ρ_a is the air density, C_D is the Coefficient of resistance of the vessel above the free surface, and A is the cross-sectional area.

Unlike water (where viscous forces dominate), air is dominated by pressure forces, so the cross-sectional area of the vessel above the waterline is taken into account, rather than the wet area.

Because water is 1000 times more dense than air, air makes a low contribution to the total resistance of the vessel. In general, it can contribute 4 to 8 % of the total drag.

Figure 2.3 summarizes the resistance components for total resistance in calm water conditions including some equations and ways to reduce some components like the viscous water resistance and the wave-making resistance. The orange squares represent two types of boats which are the displacement and planing boats. In brief, as the name says, displacement boats goes trough the water displacing the water sideways while planing boats go almost over the water. Planing boats are explained in more detail in section 2.2

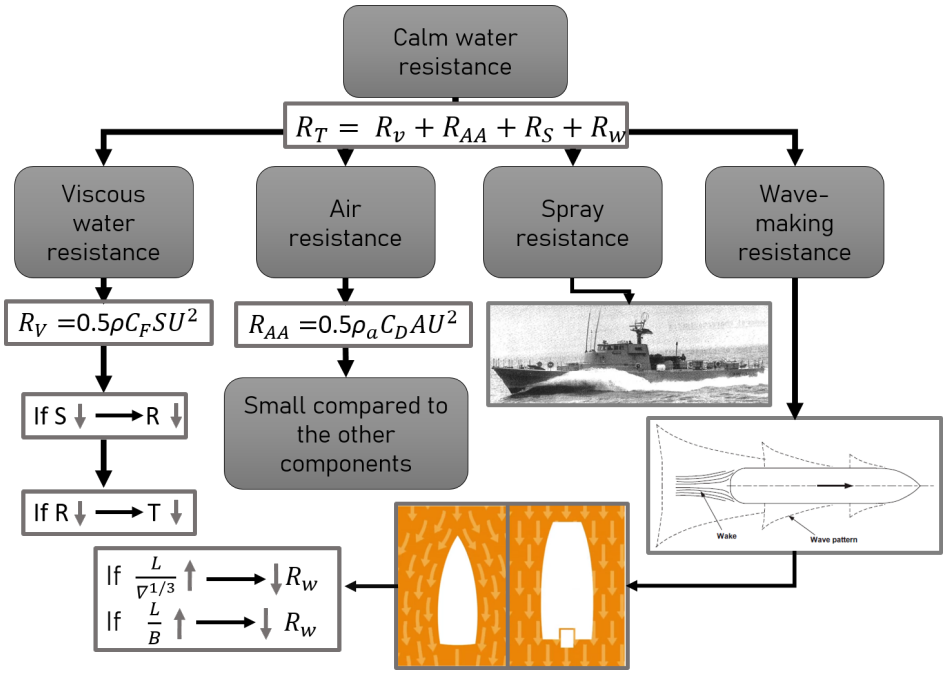

Figure 2.3: Components of total resistance in calm water conditions

In addition to these components in resistance, it is necessary to add that in perturbated conditions waves, wind gusts, maneuvers carried out with the boat, among others, can add up on the total

resistance of the boat and may account up to a 40% more in resistance depending on the operating conditions (Faltinsen, 2005; Molland et al., 2017). It is also worth mentioning that this total resistance in calm water does not account for appendages but for the bare hull only.

According to Figure 2.3, it is possible to reduce the hull resistance by tuning their geometric parameters such as the slenderness ratio ($\frac{L}{\nabla^{1/3}}$) and the length-to-beam ratio ($\frac{L}{B}$). Most authors agree on the fact that slender hulls present lower hydrodynamic resistance. However, as it is described in section 2.2, planing boats need to be wider in order to have enough area for creating the lift that is going to push the hull out of the water surface at Froude numbers over 1-1.2 and make it to enter in the planing regime.

2.2 Planing boats

There are several ways of classifying boats. They can be classified depending on the shape of the hull (rounded bilge, deep-v or flat-bottomed), the amount of hulls (monohull, catamaran, trimaran, etc), the speed regime (slow or high-speed vessels) or by the way the are supported in water (displacement boats, planing boats, hydrofoil boats and air cushion vehicles). Planing boats are high speed vessels with flat bottoms which causes hydrodynamic forces which make the boat come out of the water at a defined speed. These type of boats sometimes combine the flat bottom with v-shaped hulls in order to break the income water, whether it is for breaking a wave or for reaching planing regime easier.

Planing boats go through 3 regimes until reaching planing which are: displacement, pre-planing and planing, so the drag-speed curve differs from that of a displacement boat. Figure 2.4 shows a typical Drag-speed curve for a planing boat. There, it can be observed that there are mainly three regimes: displacement, pre-planing and planing. A planing boat goes through all these regimes as the speed increases.

First, the boat goes trough the displacement regime in which the buoyant force supports almost all the weight of the boat so the boat travels with a sinkage according to the volume it displaces. In this point, a displacement boat would be limited in speed by the front wave formed in front of the bow. Then when increasing the speed, hydrodynamic forces start appearing around the hull up to a point the boat enter a transition to the planing regime. Here, the boat starts 'riding' the wave formed at the bow and reducing its sinkage. Finally at the design speed of the hull, the hydrodynamic forces become much higher than the buoyant forces and the boat finds its trim and sinkage position according to the moments created around the center of gravity of the boat. In this position, the boat has greatly reduced its sinkage, reducing the wetted area, and then the hydrodynamic resistance. This is why in the figure it can be observed that the resistance drops to a small valley after a hump. After this valley, the resistance starts growing again in an exponential fashion.

This planing phenomena is highly time dependent and the hydrodynamic resistance for this type

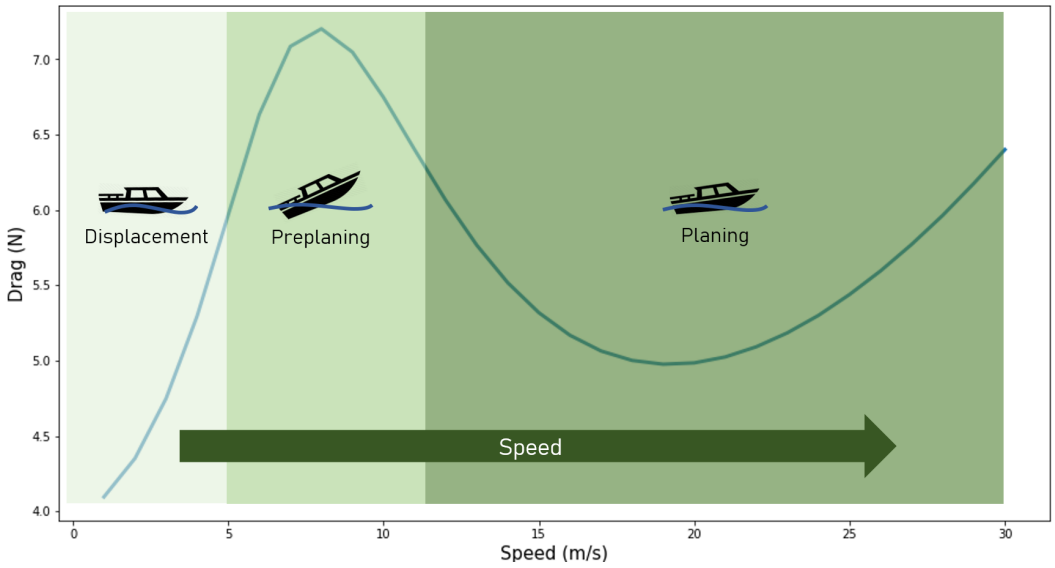

Figure 2.4: Typical planing curve

of vessels can be studied mainly by three methods: Experimental, numerical and statistical. In experimental methods, real-scale or scaled boats are built and tested in water bodies. These water bodies can be towing tanks or lakes to mention a few. Experiments deliver the closest results to reality, but these are generally the most time consuming and expensive of all the methods.

Most relevant numerical methods include Finite Element Method (FEM), Boundary Element Method (BEM) and Finite Volume Method (FVM). FVM constitutes the most computationally expensive method but yields the most precise results of the three. This method consist in solving the Navier-Stokes equations in tiny discrete places surrounding the boat, in order to find the behavior of the fluids around the boat and find the hydrodynamic resistance, among other variables of interest. For a planing boat, whose position depends on the time and the speed, there is a need of using dynamic meshes which can be divided in deformable meshes and overset meshes. Both have been used for simulating planing hulls achieving close results to experiments, but they have in common that are very computationally expensive, the timesteps in the simulation have to be sometimes prohibitevly small and reaching convergence is very difficult, hence the user has to intervene several times in the simulation. Considering this and the available time for the development of the project, this method will not be taken into account in this work.

Statistical methods refer to equations that have been derived from extensive experiments. These are the methods which requires the least amount of time and computational resources in order to obtain information, but they are the least precise due to only the principal geometrical parameters are taken into account and lots of assumptions are made in order to simplify the equations. Some equations like Keith's, Crouch's, Wyman's, Blount & Fox's, and Savitsky's have been used for obtaining the hydrodynamic resistance of planing monohull boats in preliminary design stages, but the most used

is Savitsky's due to its precision, it has a modification for catamarans and also allows to study several variables involved in the planing phenomena. One can see that even though the original paper with the set of equations of Savtisky was published in 1964 (Savitsky et al., 1964), it is still widely used for comparing planing monohulls performance in simulations and experiments. This set of equations have also a modification for planing catamarans with asymmetric demihulls. This set of equations are explained in further detail next.

2.2.1 Savitsky equation for planing hulls

Based in experiments, Savitsky derived a set of empirical equations to describe the lift, drag, wetted area and center of pressure of a planing hull in terms of the speed, trim angle, deadrise angle, principal dimensions and weight of the hull. This set of equations are solved iteratively and some values like the angle of trim of the boat must be assumed.

First, the Equation (2.6) defines the lift coefficient for a flat plate as:

$$C_{L0} = \tau^{1.1} \cdot [0.012 \cdot \lambda^{0.5} + 0.0055 \cdot \frac{\lambda^{2.5}}{{C_v}^2}] \tag{2.6}$$

In which τ is the trim angle of the boat, λ is the mean wetted length-beam ratio (defined by the Equation (2.7)), and, C_v is the speed coefficient (defined by the Equation (2.8)) which is the same than the beam Froude number of the boat.

$$\lambda = \frac{(l_k + l_c) + 2}{b} = \frac{l_m}{b} \tag{2.7}$$

$$C_v = \frac{V}{\sqrt{g \cdot b}} \tag{2.8}$$

Here, l_k is is the wetted keel length, l_c is the wetted chine length, l_m is the mean wetted length, b is the beam of the planing surface, V is the boat speed and g is the gravity.

As planing hulls usually have a deadrise angle β, the Equation (2.6) must be corrected with the Equation (2.9):

$$C_{L\beta} = C_{L0} - 0.0035 \cdot \beta \cdot {C_{L0}}^{0.6} \tag{2.9}$$

Considering that neither C_{L0} nor λ nor $C_{L\beta}$ are given beforehand, $C_{L\beta}$ is calculated through the Equation (2.10):

$$C_{L\beta} = \frac{\Delta}{0.5 \cdot \rho \cdot b^2 \cdot V^2} \tag{2.10}$$

In which Δ is the boat weight.

After finding C_{L0} and λ, the wetted keel length (l_k), the wetted chine length (l_c) and the mean wetted length (l_m) can be obtained. With the Equation (2.11) the distance from transom to point of intersection of hydrodynamic force vector with keel (l_p) can be found (All units in feet and pounds).

$$\frac{l_p}{l_m} = 0.75 - \frac{1}{5.21 \cdot \frac{C_v}{\lambda}^2 + 2.39} \tag{2.11}$$

The correct value for τ is found trough the fulfilling of the equations of equilibrium according to the forces and moments acting on the planing hull. A free-body diagram of these forces and moments is depicted in the Figure 2.5.

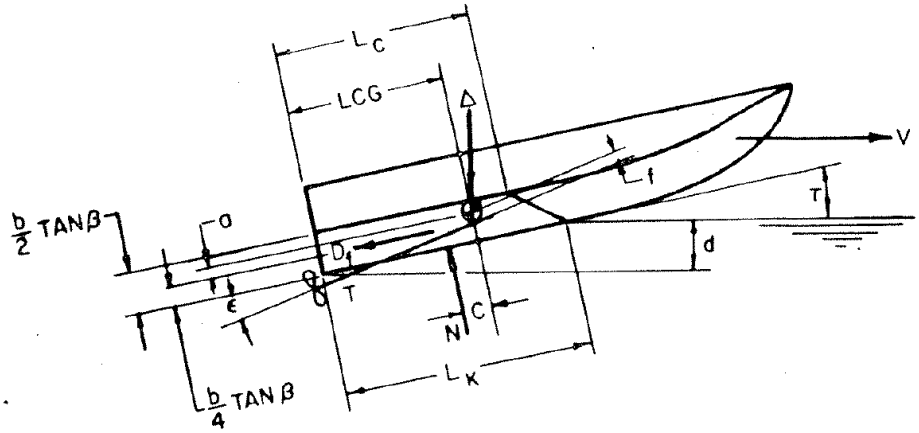

Figure 2.5: Free body diagram of the principal forces in planing regime. Figure taken from the work of Savitsky et al. (1964)

Consequently, the Equations (2.12) to (2.15) are the equation of equilibrium:

$$T \cdot Cos(\epsilon) = \Delta \cdot Sin(\tau) + D_f \tag{2.12}$$

$$R_T = T \cdot Cos(\tau + \epsilon) \tag{2.13}$$

$$\Delta \cdot Cos(\tau) = N + T \cdot Sin(\epsilon) \tag{2.14}$$

$$\Delta \cdot Cos(\tau) \cdot L_{CG} = N \cdot l_p + T \cdot \overline{PT_L} \cdot (Cos(\epsilon) + Sin(\epsilon) \cdot Cos(90° - \epsilon)) \tag{2.15}$$

In which T is the thrust, ϵ is the angle of the thrust, $\Delta \cdot Sin(\tau)$ is the drag due pressure forces, D_f is the drag due to viscous forces, R_T is the total resistance, N is the hydrodynamic lift, L_{CG} is the distance from transom to the longitudinal center of gravity, l_p is the distance from transom to the center of pressure, and $\overline{PT_L} = L_{CG} \cdot Sin(\epsilon) + f$

D_f is defined through the Equation (2.16):

$$D_f = \frac{1}{2} \cdot \rho \cdot S \cdot C_f \cdot v^2 \tag{2.16}$$

In which S is the wetted surface, and, C_f is the coefficient of friction, calculated respectively with the Equations (2.17) and (2.18):

$$S = l_m \cdot b \cdot Sec(\beta) \tag{2.17}$$

and

$$Cf = \frac{0.075}{(log_{10}Re - 2)^2} \tag{2.18}$$

Finally, for obtaining the sinkage of the boat, d, the Equation (2.19) is used:

$$d = L_k \cdot Sin(\tau) \tag{2.19}$$

It is worth mentioning Savitsky obtains the closest results in the planing regime, which is achieved for Froude number values over 1. Another limitation is that it is suited for monohull prismatic vessels with similar geometries to those with which Savitsky obtained the equations. For further details, the reader is invited to go to references (Savitsky et al., 1964) and (Molland et al., 2017).

This model has a modification for asymmetrical catamarans, which was proposed by the studies of Liu and Wang (1979) and Lee (1982). Here, two parameters named the *interference factor*, A, and the *separation ratio*, r, are added to the formulation. For catamarans in which $r < 1$, A can be assumed as $\sqrt{2}$, and, r is expressed through the Equation (2.20):

$$r = \frac{b_1}{b} \tag{2.20}$$

Where b is the width of the hull, and b_1 is the total width of the two demihulls, without including the tunnel width. With this term, Equations (2.6), (2.11), and (2.17) are modified with the Equations (2.21) to (2.23):

$$C_{L0} = \tau^{1.1} \cdot r^{3/2} \cdot [\frac{0.012 \cdot \lambda^{0.5}}{A} + 0.0055 \cdot \frac{\lambda^{2.5} \cdot A}{{C_v}^2 \cdot r}] \tag{2.21}$$

$$\frac{l_p}{l_m} = 0.75 - \frac{1}{5.21 \cdot (\frac{C_v}{\lambda \cdot A})^2 \cdot r + 2.39} \tag{2.22}$$

$$S = b^2 \cdot [r \cdot Sec(\beta) + 2 \cdot \lambda \cdot tan(\tau)] \tag{2.23}$$

2.3 Hydrofoil crafts

A hydrofoil craft is a vessel whose weight is not supported totally over its hull, but over appendages that work as airplane wings. These appendages, called hydrofoils, are related to water as airfoils are to air. As the boat advances through water, a relative speed is created between the hydrofoils and the water. This relative speed causes a resultant force, which can be decomposed in two components. One is an upwards force, or lift force, which pushes the vessel out of the water and the second is a force in the opposite direction of the boat propulsion. The latter is the resistance component. Figure 2.6 illustrates these two force components.

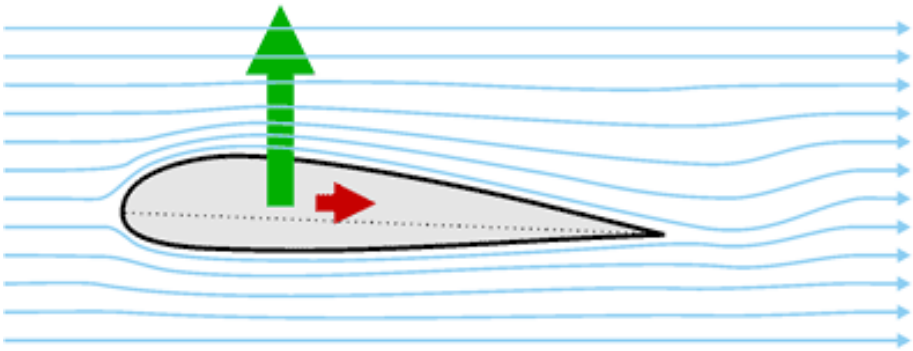

Figure 2.6: Force components in a hydrofoil

After the boat reaches a determined speed, which depends on the specific design of the hydrofoils, the upwards force surpasses the boat weight, the boat comes out of the water and the resistance is drastically reduced. In consequence, hydrofoil crafts generally present a much lower energy consumption than planing monohulls or multihulls since the wet area is greatly reduced (Yun and Bliault (2012)).

The two force components generated by the interaction between the hydrofoil and the flowing water can be calculated with the Equation (2.24) for the Lift, and the Equation (2.25) for the Drag:

$$L = \frac{1}{2} \cdot C_L \cdot \rho_w \cdot S_h \cdot U^2 \tag{2.24}$$

$$D = \frac{1}{2} \cdot C_D \cdot \rho_w \cdot S_h \cdot U^2 \tag{2.25}$$

Where C_L, C_D and S_h are respectively the lift coefficient, the drag coefficient and the hydrofoil area from a plain view. C_L and C_D depend highly on the geometry of the hydrofoil, the angle of attack (α) and the Reynolds number. All these coefficients can be obtained from polar curves in repositories in the web such as airfoil tools or generated from open source softwares such as Xflr-5. The Reynolds number is represented by the Equation (2.26):

$$Re = \frac{\rho_W \cdot U \cdot L}{\mu_W} \tag{2.26}$$

Where L is a characteristic length, which in this case is the hydrofoil chord (c). C_L and C_D increase with α and Re.

Another important coefficient in hydrofoils is the pressure coefficient, C_p, which represents a pressure distribution of the body immersed in a fluid. It can be calculated with the Equation (2.27):

$$C_p = \frac{p - p_\infty}{\frac{1}{2} \cdot \rho_\infty \cdot U^2} \tag{2.27}$$

Where p is the pressure at a determined point and p_∞ is the ambient pressure. This coefficient also depends on the shape of the hydrofoil, the angle of attack and the Reynolds number. This coefficient is smaller in zones around the hydrofoil where the flow speed is higher, which is the suction or upper side of the hydrofoil.

When somewhere around the profile, the local pressure goes under the water vapor pressure, it occurs cavitation. However, this starts being a concern after speeds of 25 m/s (Faltinsen, 2005), which is way beyond the top speeds of the compared boats at real scale and therefore, the study of this phenomenon is out of the scope of this work. Another event that may occur at high speeds is ventilation and occurs when the foil is very close to the water surface and the pressure at the upper part of the profile goes down enough for sucking portions of air. This makes the hydrofoil to instantaneously lose its lift, which may end up in catastrophic consequences. For avoiding this, it is necessary for the hydrofoils to work with the highest depth of submergence possible.

This depth of submergence also plays an important role on the efficiency of the hydrofoils due to the fact that the efficiency is greatly reduced when approaching to the water surface, even at low speeds when cavitation and ventilation are far from occurring. The submergence factor, S, is the percentage of lift that occurs as a function of proximity to the water surface and is given by the Equation (2.28) (Vellinga, 2009), which dictates that profile efficiency begins to be noticeably affected by depths shallower than the profile chord.

$$S = 1 - 0.022 \cdot (\frac{1.5 \cdot C - d}{C})^2 \tag{2.28}$$

Where d is the operating depth of the airfoil with respect to the water surface. The result of this equation is multiplied by the lift of the hydrofoil assuming an infinite operating depth and thus the near-surface lift is obtained.

Finally, other parameters that need to be considered when designing a foil regardless of the fluid are span, aspect ratio, taper ratio, sweep angle, and dihedral angle. All of them depend on the application of the foil and on the context. For example, hydrofoils with high aspect ratio have a higher efficiency but for the case of hysucats, the span is restricted with the width of the tunnel. Authors such as

Vellinga (2009) and Bertin and Smith (1998) give more details about how these geometric parameters affect the performance of the foil and how should they be configured depending on the context.

At the end, the principal design objective is to maximize the hydrofoil lift to drag ratio ($\frac{C_L}{C_D}$) avoiding cavitation and ventilation at maximum, and taking care of the depth of submergence (Faltinsen, 2005; Vellinga, 2009).

2.4 Similarity Principle and dimensional analysis

As mentioned in section 3, experimental tests with scaled models are a reliable and cheaper way of studying the hydrodynamic behavior of planing boats. These tests requires the use of dimensionless Froude and Savitsky numbers.

- **Froude number**

  It is a dimensionless number that allows classifying the flow as supercritical, critical and subcritical and relates the inertial forces to the gravitational forces. It is used very constantly in flow conditions with free surface effects and is given by the Equation (2.29):

$$F_r = \frac{U}{\sqrt{g \cdot L_c}} \tag{2.29}$$

  The Froude number is constantly used as a dimensionless fashion of presenting the speed of a vessel due to it gives a sense of how the speeds regimes for a planing hull are divided independent of its size or weight. Displacement speeds are considered to be at $F_r <= 0.5$, preplaning speeds at $0.5 > F_r <= 1 - 1.2$ and planing speeds at $F_r > 1 - 1.2$.

- **Reynolds number**

  It is a dimensionless number that allows characterizing the flow as laminar, transitional or turbulent. Inertial forces are related to viscous forces. It is defined through the Equation (2.30).

$$R_e = \frac{U \cdot L_c \cdot \rho}{\mu} \tag{2.30}$$

  Where U is the flow velocity, L_c is a characteristic length and, ρ and μ are the density and viscosity of the fluid, respectively.

In order for the data collected from the tests with scaled models to be reliable and similar to the real-scale results of the prototype it is necessary that there is geometric and dynamic similarity between the model and the prototype.

- **Geometric Similarity:** The prototype and the model must have the same geometric proportions and shape, what means the model is a scaled version of the prototype. The scale factor, λ, is usually defined with the relationship between the the lengths of the prototype (L_S) and the model (L_M), such as it is presented in the Equation (2.31):

$$\lambda = \frac{L_S}{L_M} \tag{2.31}$$

- **Dynamic Similarity:** It is achieved when all magnitudes of the flow affecting the model, including velocities, accelerations, forces, pressures, etc, are proportional to those of the prototype, have the same directions and are located at the same locations of the hull in this case. This means non dimensional numbers Froude and Reynolds must be equal for both the prototype and the model. This is impossible due to when scaling down, speeds must be reduced according to Froude and increased according to Reynolds. Furthermore, the gravity force and viscosity effects of water cannot be scaled in a laboratory.

  Fortunately, it is possible to reach partial dynamic similarity thanks to Froude's law of comparison or corresponding speeds, which is reached under the assumption that the Froude numbers of both the model and the prototype are the same (Molland et al., 2017).

The ITTC gives a detailed procedure on how to reach similarity and carry the model-to-ship extrapolation in resistance tests with high speed marine vehicles on his recommended procedure 7.5-02-05-01 (International Towing Tank, 2008). The model-to-ship extrapolation of resistance allows to obtain the components of resistance for the full-scale prototype based on the resistance tests of its scaled model version. In the extrapolation, Equations from (2.2) to (2.5) are used.

Table 2.1 gives the scaling ratio of physical variables according to Froude's law of comparison.

Parameter	**Froude scaling ratio**
Length	λ
Area	λ^2
Volume	λ^3
Velocity	$\lambda^{\frac{1}{2}}$
Time	$\lambda^{\frac{1}{2}}$
Mass	λ^3
Acceleration	1
Force	λ^3
Energy	λ^4
Power	$\lambda^{\frac{7}{8}}$

Table 2.1: Froude scaling ratio for physical variables.

Chapter 3

State of the art

Ever since authors like Clement and Blount (1963), Fridsma (1969), Savitsky et al. (1964) and Hoppe (1989), several studies have been carried out in order to determine the hydrodynamic performance of planing monohulls, multihulls and hydrofoil supported catamarans. These studies have become more important in the last decades due to a demand of a more efficient transport. Three types of approaches to study planing hulls and hydrofoil supported catamarans can be distinguished: Experimental, statistical and numerical. Yousefi et al. (2013) mentioned studies carried out with these techniques in their review article, but more studies have come out since then, so they are reviewed next.

3.1 Experimental

It includes experiments with real scale or reduced scale boats in circulating water channels, towing tanks or with field experiments in different bodies of water. Testing with real scale boats is clearly the most accurate method, but is by far the most expensive and is done mainly for validating a correct design at the final step of the design process. For earlier design stages, tests with scaled models are carried out and the scaling is implemented according to Froude's law of comparison. For scaling up the hydrodynamic performance for the real scale prototype, some corrections are applied according to the ITTC. The ITTC also recommends to use towing tanks (International Towing Tank, 2008), which are water channels in which a trailer or cart is mounted on one or a pair of rails that guide the boat along the water channel. The model for the test is assembled to the cart, which keeps it suspended or completely submerged in the water as needed.

Even though towing tanks exist decades ago, they are still widely used for model testing monohulls, catamarans and hysucats. Some examples are Kim et al. (2013); Sukas et al. (2017); Najafi and Nowruzi (2019) and De Luca and Pensa (2017), who measured experimentally the hydrodynamic performance of different monohulls in calm and rough water, Najafi et al. (2019); Hoppe (1989) who evaluated the resistance reduction in a catamarans with hydrofoils and Broglia et al. (2014); Morabito (2011); Souto-Iglesias et al. (2012); Müller-Graf (1989) and Hu et al. (2020), who tested symmetrical and asymmetrical displacement and planing catamarans with different geometry variations in order to determine interference effects, among several other authors. Despite the advantages of testing in towing tanks, these installations have a high initial investment and are not widely available.

Some alternatives carried out by some authors are to carry out tests towing the models with motor boats (Day et al., 2017; Ozden and Demir, 2009) or with self-propelled tests (Honaryar et al., 2021) in bodies of water, using GPS for measuring the speed, and several types of supports to hold the model boat and measure drag. However, it is hard to control the speed of almost any motorboat and measuring the real speed to which the experiment is executed heavily depends on the precision of the GPS. Furthermore, conditions of calm water and no wind in field experiments are hard to control. For the case of the self-propelled tests no drag is measured, but speed, engine power or propeller revolutions.

3.2 Statistical methods

It groups all the equations derived from experiments, aiming to relate the boat parameters and their operation variables with their hydrodynamic performance. Statistical approaches, like Savitsky et al. (1964), Wyman (1998), Crouch (Skene, 1973), Keith (Sponberg, 2011), and L. Blount and L. Fox (1976), have been extensively implemented in the preliminary study of the hydrodynamic performance

of planing vessels. Out of this methods, Savitsky method is, despite being a little more than 50 years old, the one that best represents the planing phenomenon for single-hull vessels compared to the other methods. This is demonstrated by the large amount of studies which have used it as a benchmark for comparing experimental and numerical studies such as those of Khazaee et al. (2019); Sukas et al. (2017); Ekman et al. (2016) and Yousefi et al. (2014), to mention a few.

This Savitsky method also has a modification for catamarans in which the modification of the lift coefficient of the boat in planing due to an interference factor between the hulls is taken into account (Liu and Wang, 1979; Lee, 1982). These coefficients are used according to the experiments carried out by the authors with catamarans with different hull spacings at different speeds. This is one more advantage for Savitsky's method in comparison with the other methods considered, since none of them allows its application for planing catamarans. Unfortunately, it does not allow applications for hydrofoil supported catamarans.

The Savitsky model is fed with the speed range and some parameters of the boat such as weight, location of the center of gravity, among others, and outputs up to 10 variables, being the hydrodynamic drag, sinkage and the trim angle the most important for this study.

Some numerical studies, which do not have experimental results beforehand, validate with Savitsky model at the expense of only similar geometries considered for developing the Savitsky model can be validated. For instance, Giraldo-Pérez et al. (2020) compared their numerical results with Savitsky and other statistical methods such as Blount & Fox, Crouch and Keith, Yengejeh et al. (2016) in monohulls and assymetrical planing catamarans with Savitsky and (Khazaee et al., 2019), who carried out so with Savitsky for planing monohulls.

3.3 Numerical methods

It is subdivided into Boundary Element Methods (BEM) and Finite Volume Methods (FVM), being the second the most successful and precise but more computationally expensive. BEM methods ignore the viscous properties of water which narrows their applicability mostly for high speed vessels. In FVM methods, it is sought to approximately solve the Navier-Stokes equations, which describe the behavior of water and air moving around the boat (Yousefi et al., 2013). FVM methods are implemented trough Computational Fluid Dynamics (CFD) simulations.

CFD simulations of planing hulls are complicated due their inherent tendency to change their position according to the speed, which makes it necessary for the mesh to adapt to these movements. This makes these simulations very unstable mostly due to pressure over the hull can easily shoot up, which implies the timesteps must be greatly reduced to avoid this unstabilities (down to 1e-4 seconds). Due to this, researchers not having the available computational resources, end up scaling down the boats for the simulations and using high processing computers with dozens of processors (Kandasamy

et al., 2011; Fu et al., 2014; Yousefi et al., 2014; Frisk and Tegehall, 2015; Sukas et al., 2017). Scaling down the models for the simulations may end up in adding more errors because of unrealistic physics modelling.

These simulations share the same idea of towing tanks, but they are virtual laboratories in which all the external variables are controlled. Here, correct predictions of hydrodynamic performance heavily depends on the correct setup of the simulation and that is why it is always recommended to have experimental results to validate the simulation results. Most authors carrying CFD simulations on watercrafts for measuring the hydrodynamic performance, compare with previously executed experiments or with experiments available in the literature (Honaryar et al., 2021; Najafi and Nowruzi, 2019; Sukas et al., 2017; Yousefi et al., 2014; Fu et al., 2014; Hu et al., 2020; Kim et al., 2018).

Another fact that makes numerical simulation hard to execute, is that simulating a vessel with appendages that are small compared to the size of the hull and that influence the position of the hull depending on the speed, such as hydrofoils, increases the level of complexity and computational cost of the simulation. This is due to much higher levels of mesh resolution are required around these appendages in order to pressures over them to be correctly developed (Kandasamy et al., 2011; Faison, 2014).

In consequence, even though CFD methods are in constant development, modelling and simulating of planing hulls and hydrofoil phenomenon require a high level of expertise and requires a very high computational power to reach stability and results close to reality, so, they are out of the scope of this study.

3.4 Comparative studies between monohulls, catamarans and hydrofoil supported catamarans

The methods mentioned before give different levels of precision compared to the real scale results and give different levels of insights. Their application depends on the level of expertise and the computational, monetary and time resources avaliable. However, when evaluating monohull or multihulls vessels with or without appendages, these methods are normally combined to complement each other. They have as main objective, to estimate the drag generated at a determined speed for the hull, in addition to other variables such as angle of trim, sinkage and wetted area.

On this basis, most authors agree on the fact that monohulls are more efficient at speeds beyond the preplaning regime compared to catamarans of similar principal dimensions and displacement, mainly due to catamarans have an extra resistance component, which is the interference resistance due to the interaction of both demihulls (Molland et al., 2017; Yun et al., 2018; Faltinsen, 2005). This interference resistance depends on the speed range and the demihull separation and is the lowest

for asymmetric catamarans travelling at speeds beyond the preplaning regime, due to lower waves are generated because of the flat internal faces and the low entrance angle in the internal side of the demihulls (Tuck and Lazauskas, 1998). This geometry is usually used for planing catamarans which required to go at high speeds (Yun et al., 2018). These possible variations of the shape of a catamaran makes it somewhat difficult to determine which between a monohull and a catamaran of similar principal dimensions, displacement and weight distribution is more efficient at different speeds and authors usually differ.

Some authors have compared catamarans with monohulls at different speeds. For example, Müller-Graf (1989) and Sherman and Fisher (1975) carried out several experimental resistance tests for catamarans and monohulls with hard chines at preplaning and planing speeds. The considered catamarans were symmetric, semi-symmetric and asymmetric with different demihull spacings. For the study of Müller-Graf (1989), the monohull presented the highest total resistance in the preplaning regime, followed by the catamarans with resistance a 20-25% lower. In the planing regime, the behavior was inverted and the monohull presented the lowest total resistance, 16% lower than the the symmetric and asymmetric catamarans. In contrast, Sherman and Fisher (1975) reported the monohull as having the less resistance at preplaning and planing speeds, with differences up to 11%.

Thomas et al. (2007) and Seif and Amini (2004), compared the hydrodynamic performance of monohulls and catamarans with statistical methods. Thomas et al. (2007) developed a decision-making tool for choosing between a catamaran and a monohull for a ferry covering a route in Australia. After taking into account economical and technical feasibilities, the catamaran was selected. Here, the resistance of both types of hull was calculated with Holtrop and Mennen (1982) for displacement monohulls and Müller-Graf (1989) for the catamarans. Seif and Amini (2004), compared a planing monohull and a planing catamaran of equal displacement at different speeds using Savitsky for monohulls and its modification for catamarans. The Monohull performed around 30% better at planing speeds (Froude numbers from 2.5 to 5) until both resistance curves converged at a Froude number of 6. Davidson et al. (2011) carried out a qualitative comparison between displacement monohulls and catamarans for cargo duties. Here, hydrodynamic and structural costs were considered, concluding that catamarans may have lower capital and operating costs. Even though in these studies the hydrodynamic performance played an important role for making decisions, these results were not validated against experimental or, at least, numerical methods.

Souto-Iglesias et al. (2012); Zaghi et al. (2011); Srinakaew (2017) and Broglia et al. (2014) compared, experimentally and numerically, symmetrical catamarans with different demihull spaces with a monohull in displacement regime (0.1<=Fr<=0.7). Both studies found the monohull had around 20% less resistance and less sinkage and trim angle at Fr<=0.5. Beyond this Froude number, the hydrodynamic performance of the monohull started to be similar to that of the catamarans with the

highest spaces between the demihulls.

Yun et al. (2018), in his very complete review of high speed catamarans, argue that asymmetric planing catamarans present higher resistance than monohulls at Froude numbers starting at 2, with catamarans having around 35% more resistance than monohulls. In contrast, trim angle is slightly higher for the monohull between Froude numbers of 2 and 3 with 4-5°, while for the catamarans is around 3-4.5°.

Some authors, have carried out experimental comparisons between catamarans and hysucats. The first author was Hoppe (1989), who investigated the hydrodynamic drag performance, showing a reduction of 41% for the hysucat at Froude numbers higher than 2, and up to 4.5. He published the patent of the hysucat in 1986 (Hoppe, 1986). Around one year after, Gerdsen and Jabbusch (1987) published a similar design.

In the next decade, several hysucat concepts were developed (Hoppe, 2001). The author reported that a reduction in resistance of up to 40% was reached when installing the foils in previously designed and operated catamarans.

Kandasamy et al. (2011) carried out the only study with CFD in hysucats that was possible to find in the literature, which was based in previous experimental results. However, this study did not compare the hydrodynamic performance against catamarans.

Lately, Najafi et al. (2019) carried out an experimental comparison between an asymmetric catamaran and a hysucat at different speeds, installing foils with three different profiles. They reported that the only regime where there was a significant reduction in hydrodynamic drag was at low and medium planing speeds, with a reduction in drag for the hysucat of 9 to 20% depending on the used hydrofoil profile. For displacement, preplaning and high planing speeds, there was not a significant reduction in drag. The hysucat travels at trim angles 2-3° lower than the catamaran during all the evaluated speeds.

In summary, at displacement speeds, the hydrodynamic behavior of monohulls and catamarans is very similar. At preplaning regime, authors differ on what geometry between a catamaran and a monohull present a better hydrodynamic performance. At this speed regime, foils start working so a reduction in the hydrodynamic drag is expected in hysucats in comparison to catamarans. Finally, at planing speeds regimes authors agree on the fact that monohulls have a lower drag than catamarans with differences ranging from 11% up to 35%. Reductions in drag for hysucats in comparison to catamarans are between 9 and 41%. This hydrodynamic drag depend on the dynamic positioning of the boat at the different speeds, which is described by variables as trim angle, sinkage and wetted area. As explained in chapter 2, the lower the sinkage and the wetted area, the lower the drag. With respect to the trim angle, ideally the hull should be supported mostly on the stern (rear) at the bottom, with the bow (forward) out of the water. Savitsky et al. (1964) found that the optimum trim

angle for planing speeds for prismatic monohulls is between 4 and 5°, and something similar should be for catamarans and hysucats.

Despite the amount of research that has been carried out in planing boats according to the literature review, it was not possible to find a study comparing the hydrodynamic performance of a monohull, a catamaran and a hysucat with experimental and statistical methods. According to this, it is reasonable to explore the possibility of a hysucat to perform hydrodynamically better than a monohull due to the percentages of reduction in drag reported above.

Chapter 4

Research proposal

In this chapter, the methodology proposed to answer the hypothesis (see subsection 4.2) is explained. This study is an exploratory-type research since even though the variables to measure are known, it is not certain what hull or treatment has a better hydrodynamic behavior. For answering the hypotheses, a classical scientific method is used, in which the data derived from the experiments is constantly checked for rejecting the hypothesis or not. The Figure 4.1 shows the outline of the proposed methodology.

This chapter is divided in sections according to the steps in the methodology. The sections are:

- Inputs of the methodology
- Research hypotheses
- Application of Savitsky method
- Experimental design
- Comparison between hull geometries

4.1 Inputs of the methodology

The methodology works for comparing any hull shape, including monohulls, multihulls and it is not limited to planing hulls, but can also be used for displacement hulls or for hulls with appendages such as hydrofoils. The methodology also can be used for comparing more than two shapes. For comparing the geometries it is necessary for them to fulfill three requirements in order to be comparable:

- They must have similar principal dimensions: Length, beam (width) and height.
- They must have the same total weight or submerged volume.

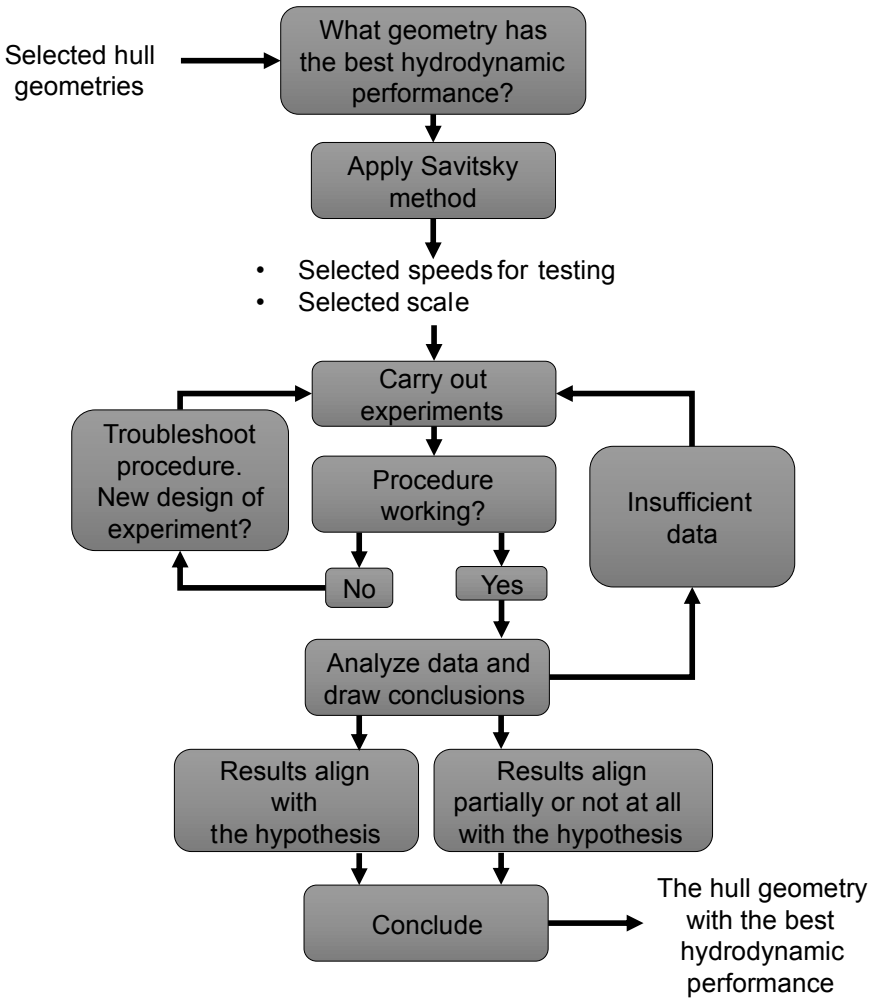

Figure 4.1: Proposed research methodology. Scientific method.

- They must have the center of gravity located at the same point due to it greatly affects the planing behavior.

For this work, three hulls are chosen. A monohull, a catamaran and a catamaran with hydrofoils or hysucat.

4.1.1 Monohull

It is selected due to it is widely used for transporting people or cargo at high speeds and has been the default shape for planing boats during most of 50 years. This high usability is due to its simplicity in construction and operational versatility; and due to the planing phenomena is more understood for this shape. A disadvantage for this shape is that for low-depth bodies of water, hydrofoils cannot be attached to it because the draft of the boat is greatly increased. In addition, it is not convenient for the hull to emerge completely out of the water in some contexts; for example, low-depth not-channelled

rivers, which are very common out of Europe. In this context, the hydrofoil would not be protected in a hypothetical crash against the river bottom.

4.1.2 Catamaran

The catamaran is also selected because of their high efficiency at high speeds if properly designed, higher roll stability and because allows to install a hydrofoil between the demihulls without increasing the hull draft at all. In this location, the hydrofoils are intended to partially push the hull out of the water. Even though this does not provide a drag reduction equal to the case the hull completely emerges out the water surface, it may provide a substantial reduction in drag of up to 41% in catamarans as reported in chapter 3.

4.1.3 Hydrofoils

The objective of the hydrofoils is to reduce the submerged volume of the craft at the design speed and in consequence, reduce the hydrodynamic drag. The idea behind this target is that the tunnel upper part raises out of the water and travels only supported by the hydrofoils and the demihulls.

The demihulls, in addition to supporting the vessel by buoyancy forces and support the boat in planing, provide protection to the hydrofoils from possible collisions with the river bottom and reduce the likelihood of collisions with floating elements in the river. The demihulls help to the hull stability, mainly in pitch and roll at zero speeds and in planing regime. Due to this, it is not necessary to have control surfaces on the hydrofoils or variable angles to keep stable the hull.

The profile for the hydrofoils and their general geometric parameters are selected according to some recommendations found in the literature (Vellinga, 2009; Najafi and Nowruzi, 2019).

4.2 Research Hypotheses

According to the reviewed literature and the advantages the hysucat may bring in comparison, two hypotheses arise, which are intended to be answered with the methodology proposed herein:

- The catamaran presents a higher hydrodynamic drag at planing speeds.
- When installing a hydrofoil in the catamaran, the reduction in the hydrodynamic drag is enough to be less than that of the monohull, at the same nominal planing speed.

4.3 Application of Savitsky method

4.3.1 Selection of the speeds for towing tests

According to the theory behind the Savitsky method described in 2.2.1, several output variables can be obtained at different speeds. As the drag is the most important variable, it is used here to select the speeds at which the models are towed. An important consideration is to select enough speeds in order to achieve a proper resolution of the curve of hydrodynamic drag vs speed, specially at the speeds where inflections occur in the curve.

The input variables for the Savitsky model are given for the real-scale prototype and are the boat weight, the longitudinal center of gravity, some principal geometrical parameters of the hull and the speed.

The most important output variables in order to measure the hydrodynamic performance are drag, trim angle, wetted area, wetted keel length and sinkage, at different speeds. The conventional Savitsky method is used for the monohull and a modified version is used for the catamaran. It was not possible to find a version for hysucats in the literature review. Appendix C contains the code of Savitsky method.

4.3.2 Selection of the scale

Another important input is the scale to which the tests are to be carried out. The decision depends on the maximum speed that is going to be reached with the scaled models and in the available infrastructure, including the length of the body of water in which the models are to be towed.

It is important to mention that according to Froude law of similarity the closer the scale to the real scale, the higher the speeds (closer to the real scale speeds). Therefore, the higher the vibrations and load exerted over the infrastructure with which the model is towed, which implies a higher noise in the collected data. Also, the lower the scale, the higher the errors to be encountered in the results due to some properties of the fluids are not scalable, such as the viscous properties.

4.4 Experimental design

The experiment setup is inspired in the ITTC recommended procedure 7.5-02-05-01 (International Towing Tank, 2008), so the procedure is followed where possible.

4.4.1 Data collection

The main objective of the experiment is to tow the models at different speeds and measure the variables of interest. Figure 4.2 shows the variables of interest. It should be ensured that the experiments are

carried out in similar environmental conditions, and variables of temperature and wind speed are measured to check a constant behavior. Ripples and small waves in the water must be avoided as possible.

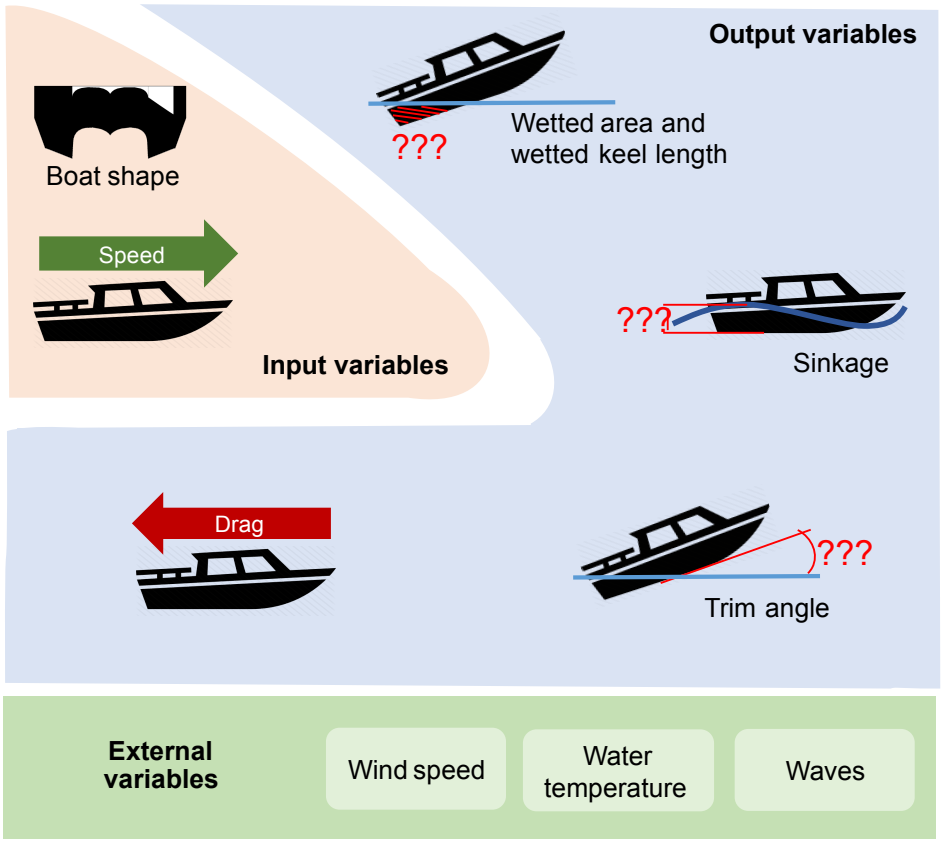

Figure 4.2: Outline of the variables to be collected.

It should also be ensured that the models are at least, two lengths away any wall sideways and at least one length away any wall downwards in order for them to not interfere in the experiments. The models are to be weighted after every 15-20 runs, checking the center of gravity is in the same place.

The experiment is a complete randomized design experiment in order for the external effects to be homogeneous between the evaluated treatments. Here, it is assumed that there are only two sources of variability, the treatments themselves and the variability due to external sources.

The experiment has two input variables, but for convenience, the comparisons for drag and trim are made at the same speed. This transforms the experiment into a single-factor experiment, in which there are three treatments, which are the hull geometries.

The hull models are towed from zero speed to the selected speed for the run, allowing the boat to stabilize and keep the speed the longest according to the longitude of the body of water. This process is to be executed at least 3 times per treatment at every speed in order to have significant statistical data.

Even though the data is taken during all the run, it is necessary to select only the time frame where the speed and drag are stable. A time frame of a run is considered stable if it lasts at least 5 seconds and if it achieves a standard deviation and a mean value that depend on the scale of the models that are to be towed and in the precision of the sensors to measure the speed and drag force. These values are specified in section 5.3.1. The definition of these criteria was inspired by the ITTC recommended procedure 7.5-02-05-01 (International Towing Tank, 2008), whose requirements in terms of instrument precision and low dispersion of the data collected are much higher, but are difficult to reach in the project due to technical and economic limiting factors.

With the application of the criteria, it should be expected a normal distribution for all the variables, which allows to average the results for each run. With averaging results, pseudo-replication is avoided due to the points taken for a single run cannot be considered as different samples because they are dependent of each other.

4.4.2 Comparison between hull geometries

For comparing the treatments, the output variables are assumed to be taken at the intended speeds, which are the speeds selected with the Savitsky method. Here, the collected speeds should have a normal distribution for each run, in which their mean should be very near the intended speed (No more than 0.2 m/s away). With this assumption, it is possible to carry out the ANOVA analysis and multiple comparison tests for each speed between the treatments. For the multiple comparison test, it is selected Tukey-HSD.

The three ANOVA assumptions are checked with both statistics and charts. For the assumption of normal distribution of residuals, Shapiro tests is carried out. Charts of distribution of the residuals and QQ-plots are also used. For asserting the assumption of homogeneity of variances, Barlett and Levene tests are carried out and residuals are plot according the treatment, in order to visualize their range of variation. Lastly, for testing the assumption of independence of errors, Durbin & Watson tests are carried out and residuals are plotted according to the order the runs are taken. These methods for checking ANOVA assumptions are referred and explained in detail by Gutiérrez Pulido and Salazar (2004). The chosen significance level for evaluating all the statistical hypotheses is 5%.

The statistical hypotheses to be tested for each intended speed with the multiple comparison test are, according to section 4.2, the following for the drag:

$$H_0 : \mu_{catamaran} = \mu_{monohull} \tag{4.1}$$

$$H_a : \mu_{catamaran} > \mu_{monohull} \tag{4.2}$$

and

$$H_0 : \mu_{hysucat} = \mu_{monohull} \tag{4.3}$$

$$H_a : \mu_{hysucat} < \mu_{monohull} \tag{4.4}$$

and the following for the dynamic positioning variables (trim angle, wetted area, wetted keel length and sinkage):

$$H_0 : \mu_{catamaran} = \mu_{monohull} \tag{4.5}$$

$$H_a : \mu_{catamaran} \neq \mu_{monohull} \tag{4.6}$$

and

$$H_0 : \mu_{hysucat} = \mu_{monohull} \tag{4.7}$$

$$H_a : \mu_{hysucat} \neq \mu_{monohull} \tag{4.8}$$

Where μ is the mean for each variable. Note that the monohull is always the reference. In the case where there is the need of finding what treatment has a greater or lower output than the other, the Tukey-HSD test p-values does not provide this information by its own. This information can be obtained from the plot of the confidence intervals for the mean for each treatment or 'mean plot'.

Chapter 5

Case study

In this chapter, results of the method proposed in the previous chapter are shown. First, the catamaran geometry and the hydrofoil designs are described. Then the inputs to the Savitsky model according to the geometries are presented. With this information, speeds and scale for the towing tests are selected. After this, the experimental design including the materials and instruments are presented. The chapter closes presenting results of the experimental and statistical methods for evaluating the hydrodynamic performance of the three hull geometries at the intended speeds.

5.1 Description of hull geometries

Figure 5.1 shows the front views of the selected three boats. The particular monohull shape was selected due to it is the most used geometry for transporting passengers at high speeds in the context of interest according to the description given in the research justification in section 1.2.

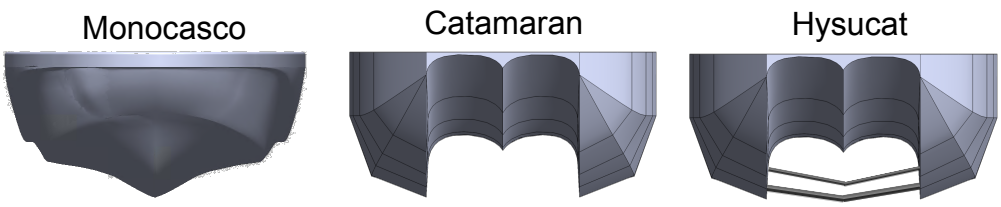

Figure 5.1: Proposed hulls for the experiments.

5.1.1 Description of the catamaran hull

The catamaran hull was designed thinking on the requirements of the zone of interest according to the context described in the research justification. The design was carried out under the project Energética 2030 (Mejia-Gutierrez et al., 2021). The restrictions and requirements were derived from a preliminar study carried in the works of Mira et al. (2020) and Giraldo-Pérez et al. (2020). Some important restrictions and requirements related to the form of the hull were: width, draft, required power at cruise speed, total weight of the boat at maximum load, passenger capacity, available area in deck and available volume for batteries for a fully electric boat.

Between the demihulls, the more turbulent the water the more affected the performance of the hydrofoils will be, so the demihulls have flat inner walls to minimally disturb the flow inside the tunnel. These flat walls also helps reducing the interference resistance of the catamaran (Yun et al., 2018).

The upper part of the tunnel has a V-shaped geometry in order to facilitate the breaking of the water flow facing the vessel and to induce the planing regime more easily. A significant portion of the tunnel remains under the water surface to provide greater buoyancy to the vessel, but at cruising speed it raises above the water surface due to the combined planing effect and to the assistance of the hydrofoils. On the inside, the hull has a deadrise angle of 22° near the bow and ends at 5° towards the stern of the boat. This change of angle allows that when the boat is in a displacement regime, the deadrise angle facing the water is sharper and facilitates the task of cutting through the water waves. Additionally, a lower deadrise angle at the stern of the boat helps to concentrate most of the hull lift at the stern in order to enter in planing regime and keep the front of the boat out of the water, thus reducing the drag.

The geometrical parameters were chosen according to a market study, in which hysucat-type vessels with similar dimensions and capacities in terms of number of passengers and operating speeds were taken into account. Tables 5.1 and 5.2 contain the geometrical parameters of the hull and the dimensionless hull numbers, respectively.

Figures A.1, A.2 and A.3 of the appendix A, show the hull lateral, rear and frontal bodyplans of the catamaran hull, as well as its sketch drawing respectively.

5.1.2 Description of the hydrofoils

Figure 5.2 shows the objective reduction for the catamaran with the hydrofoils for the upper part of the tunnel to completely emerge out of the water as mentioned in subsection 4.1.3. For the crest located at the middle of the upper part of the tunnel not to touch the water surface, it is necessary for the boat to travel as horizontal as possible.

The hydrofoils are arranged in a traditional configuration, similar to that of an airplane. The main foil is located slightly forward of the center of gravity, supporting around 86% of the weight

Total length	7.9 m
Total beam	2.12 m
Wetted length	7.5 m
Distance between demihulls	1 m
Freeboard height (Max. load)	0.4 m
Draft (Max. load)	0.7 m
Total height	1.1 m
Displacement	4.3 m^3

Table 5.1: Principal dimensions of the catamaran hull. These parameters are the same for the monohull, excepting there are not demihulls.

Parameter / Variable	**Formula**	**Value**
Longitudinal Froude number	$F_l = \frac{V}{\sqrt{g \cdot L}}$	1.7
Volumetric Froude number	$F_l = \frac{V}{\sqrt{g \cdot V^{\frac{1}{3}}}}$	3.8
Length to beam ratio	L/B	3.6
Slenderness ratio	$\frac{L_{WL}}{\nabla^{\frac{1}{3}}}$	4.7
Static load coefficient	$\frac{\nabla}{B^3}$	0.46
Demihull separation ratio	$C_s = \frac{B}{2 \cdot b}$	8.3
Half angle of entrance	i_e	60°
LCG to length ratio measured from the transom	$\frac{LCG}{L}$	0.4
Deadrise angle at amidship	β	17°
Block coefficient	$C_b = \frac{\nabla}{L.B.D}$	0.33

Table 5.2: Adimensional numbers and geometrical parameters of the hull. The adimensional numbers are calculated at the cruise speed, which is 15 m/s. These parameters are the same for the monohull, excepting there are not demihulls.

carried by both foils. The secondary foil, whose job is to provide stability and counteract the moment caused by the main foil lift, is located near the transom and supports the 14% left. Figure 5.3 (a) shows a schematic of this force balance in an airplane. Figure 5.3 (b) shows the arrangement of the foils with the distances relative to the transom. Table 5.3 shows the cruise, foilborne speed of the hydrofoils and the percentage of weight to be carried out by each of them in the model and in the real-scale prototype.

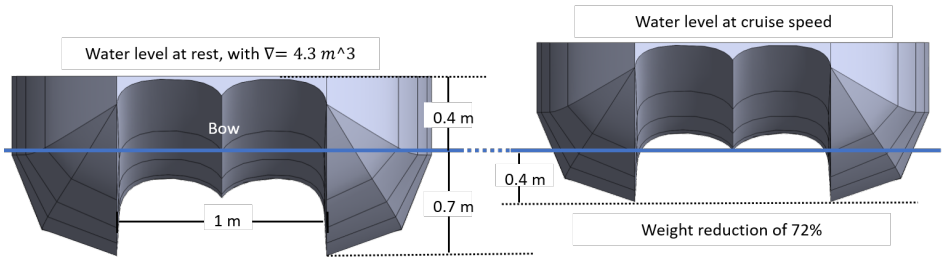

Figure 5.2: Target weight reduction with foils at cruise speed.

Parameter / Variable	Prototype	Model
Estimated weight (kg)	4300	8.5
Tunel width (m)	1	0.13
Cruise speed (m/s)	15	5.3
Foilborne speed (m/s)	7.5	2.7
Weight Reduction objective (%)	72	
Weight supported by the front foil (%)	86	
Supported weight by the rear foil (%)	14	

Table 5.3: Geometric parameters of the prototype and model for hydrofoil design.

The hydrofoil dimensions are limited upwards, downwards and sideways. On consequence, both hydrofoils must fit in a specific area, which is limited by the inner walls of the demihulls; by the water surface, which must be at least 90% of the chord above any of the hydrofoils so that the efficiency of the hydrofoils is not significantly reduced (Vellinga, 2009); and by the keels of the vessel, which must be further below to fulfill the function of protecting the hydrofoils. Figure 5.4 shows these available areas for the design of the front and rear hydrofoils. The rear hydrofoil has a more restricted area because the demihulls have a lower draft when approaching the transom.

The Clarkysm-il is selected for the hydrofoils since this profile matches the recommendations of the literature the best, in comparison to other profiles such as the Eppler E817, the NACA 63-412 and the NACA 4412. The Clarkysm-il has a relative high Cl/Cd within its range of optimum behavior, which is at angles of attack between 0° and 5°. This range is far away from the profile stall angle of attack (15°). In addition, it is a widely experimentally validated profile and is relatively simple to build. Figure 5.5 shows the profile.

Both hydrofoils have positive dihedral and sweep angles. This configuration enhances the transverse stability and helps reducing sudden vertical oscillations due to foil stall. Table 5.4 shows the parameters and input variables and the results for the designed hydrofoils. Figures A.4 and A.5 of

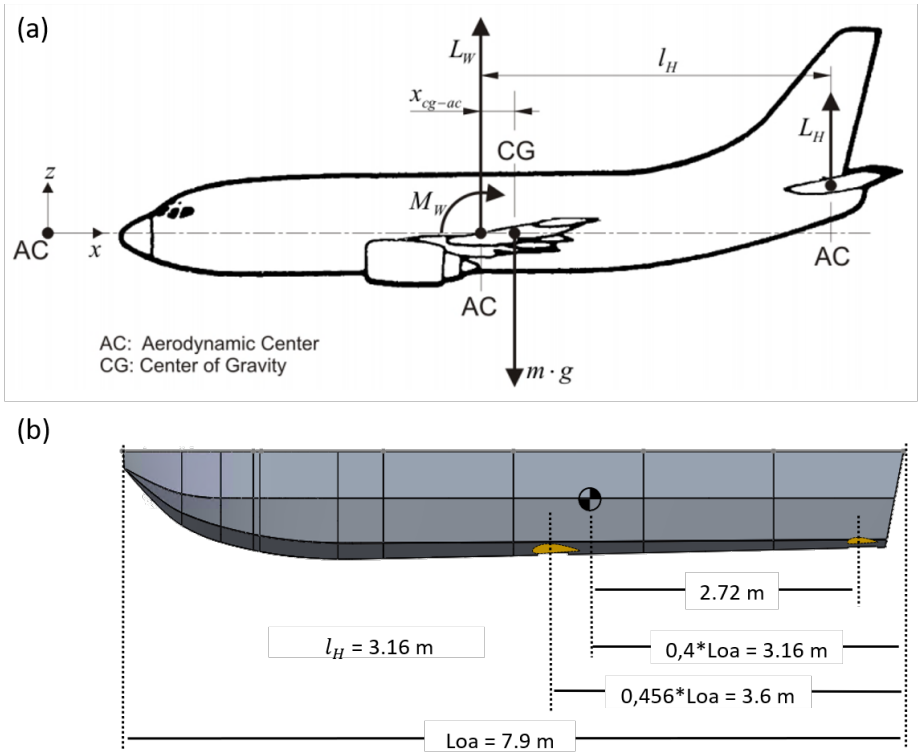

Figure 5.3: (a) Schematic of the location of the main wing and horizontal stabilizers with respect to the center of gravity on an aircraft. Image taken from: `https://www.fzt.haw-hamburg.de/pers/Scholz/HOOU/AircraftDesign_9_EmpennageGeneralDesign.pdf`, (b) Position of the hydrofoils longitudinally on the model.

the appendix A show the plan drawings for both the main and the aft foils.

5.2 Savitsky implementation

5.2.1 Input variables for Savitsky

Table 5.5 shows the input parameters for the monohull and the catamaran. The parameters for the two vessels are similar, given their equal size and weight capacity, excepting that for the catamaran the interference factor and separation ratio are substantially different. It is observed that the interference factor and the separation ratio between half hulls for the monohull are 1 and not 0, which is because there cannot be a zero in the equations and the one does not affect the equation at all. Instead, for the catamaran are $\sqrt{2}$ and 0.5 respectively. For both hull geometries it is assumed that the thrust line passes through the center of gravity of the vessel and that its inclination is zero with respect to the horizontal. Also, it is assumed that the boats are prismatic, due to Savitsky does not take into account variations in the transverse geometry along the boat. The code of this model, which was also

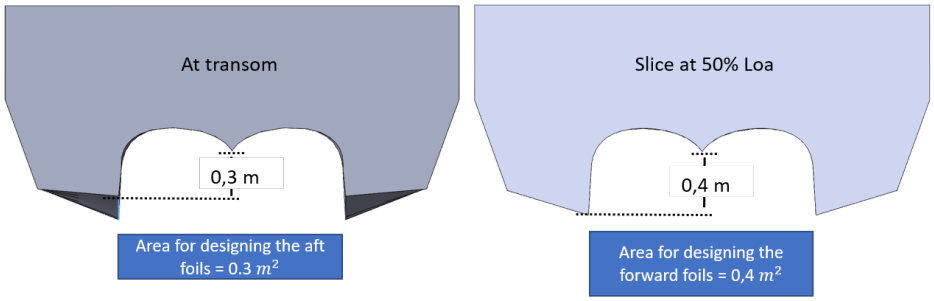

Figure 5.4: Area available for designing the hydrofoils in the model.

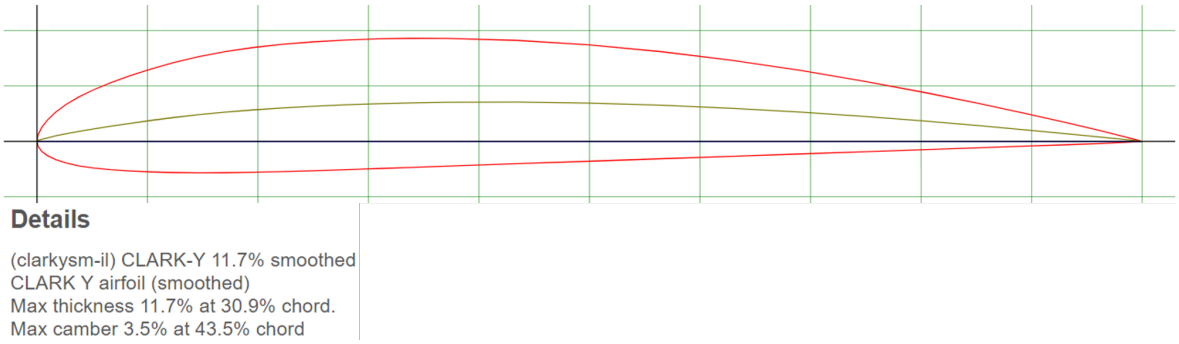

Figure 5.5: Selected profile for both hydrofoils. Source: `http://airfoiltools.com/`.

Parameter / Variable	**Main hydrofoil**	**Aft hydrofoil**
$\rho(\frac{kg}{m^3})$	1000	
$\mu\frac{kg}{m \cdot s}$	1e-3	
Reynolds number at cruise (-)	4.8e6	2.8e6
Profile	Clarkysm-il	
Incidence angle (°)	0	
Taper ratio (-)	1	
Aspect ratio (-)	3.3	
CL @ $\alpha = 0°$	0.781	0.426
CL/CD @ $\alpha = 0°$	130	13
Depth of operation (m)	0.28	0.2
Lift generated (kN)	24	6
Weight reduction objective (%)	70	

Table 5.4: Properties of the hydrofoils for the real-scale prototype

implemented by Giraldo-Pérez et al. (2020), is displayed in the appendix C.

Parameter/variable	**Monohull**	**Catamaran**
Weight (kg)	4310	4310
Mean chine beam (m)	1.84	1.84
Mean deadrise angle (°)	13	17
LCG (m)	3.16	3.16
ρ (kg/m^3)	1000	1000
μ (m^2/s)	1.19e-6	1.19e-6
Perpendicular distance between CG and the action line of the thrust (m)	0	0
Tilt angle of the thrust line(°)	0	0
Interference factor (-)	1	$\sqrt{2}$
Separation ratio between demihulls (-)	1	0.5
Speed range (m/s)	1-18	1-18
Safety factor (-)	1.3	1.3

Table 5.5: Input parameters and variables for Savitsky model.

5.2.2 Selected speeds

Seven speeds are selected in order to build the whole curve of drag vs speed with an acceptable resolution, specially at the speeds where inflections occur in the curve. Figure 5.6 shows the graphical representation of the selected speeds according to Savitsky results. The speeds were selected according to output for the monohull due to it is the baseline geometry.

5.2.3 Selected scale

The selected scale is 1/8 due to limitations in the maximum speed that can be reached with the equipment to be used to tow the model. If the maximum scale to be reached at real scale is 20 m/s, the speed for a scale of 1/8 according to the law of Froude similitude is 7.1 m/s. For obtaining the speeds at which the models were towed, simply divide the intended speeds shown in figure 5.6 by $8^{0.5}$.

5.3 Experimental setup

After an iterative refinement process according to the quality of the collected data, the selected experiment setup is described next.

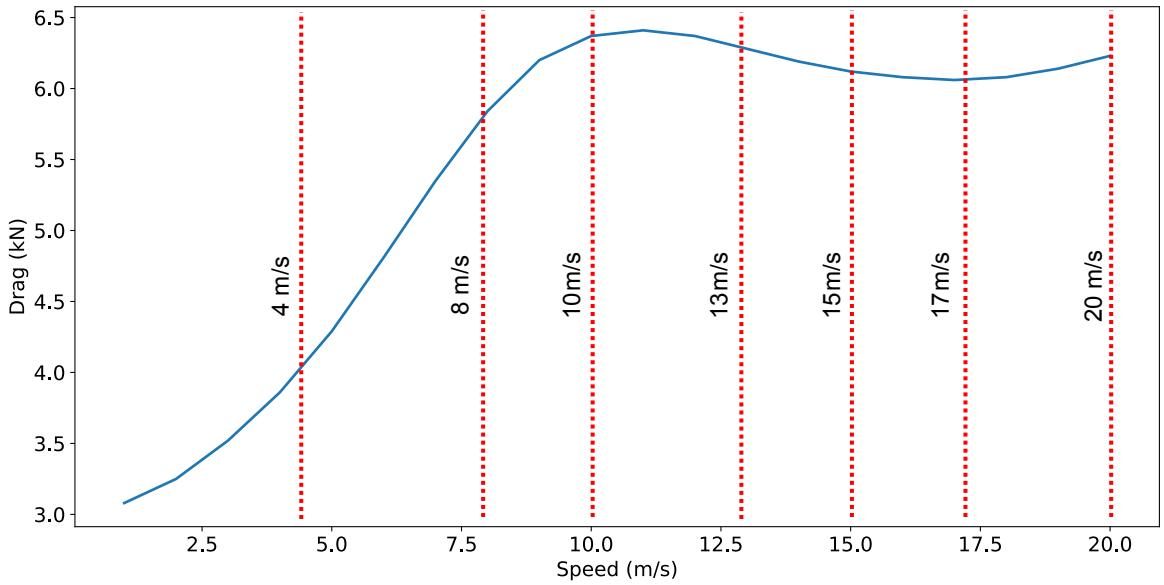

Figure 5.6: Selected speeds for the towing test.

5.3.1 Variables and materials

Figure 5.7 shows the outline of the variables and the sensors and tools to collect each of them. Despite some of the variables were collected separately, they were collected with timestamps for being merged in the post-processing. Out of the variables, only the boat shape is categorical.

According to the scale, a run is considered stable if it lasts at least 5 seconds and if the standard deviation of velocity and force are maximum 0.1 m/s and 0.5 N, respectively, and if its average velocity is more than 0.3 m/s away from the intended velocity for each run. These values are determined as they are less than 2% of the maximum expected values of speed and drag in the experiments. The maximum value expected for the drag is 30 N as the maximum value the load cell supports is 60 Newtons.

The boat is towed in a lake 100 meters long with a test bench that is fixed to the ground and whose traction is generated by a Golden Motor Magicpie BLT-800 electric engine. A rim is connected to the engine through its axis. The rim rolls up a nylon, which in turn is attached to the models center of gravity. This tension generated in the nylon is transmitted by a pulley system which is arranged in such a way that this tension can be measured with a load cell. In this pulley system, a fixed pulley and a guide ring are placed in such a way the nylon touched 180° of the main pulley, in order for the force over the cell to be 2 times the tension in the nylon. The rotational speed of the rim is measured with an encoder. This encoder measures the rpm of the rim, which can be converted to the speed of the boat. Figure 5.8 shows a CAD of the test bench and a diagram of the pulley system to transmit the force to the load cell.

The trim is monitored with a Pololux inertial measurement unit sensor Mini IMU-9 v5 inside the

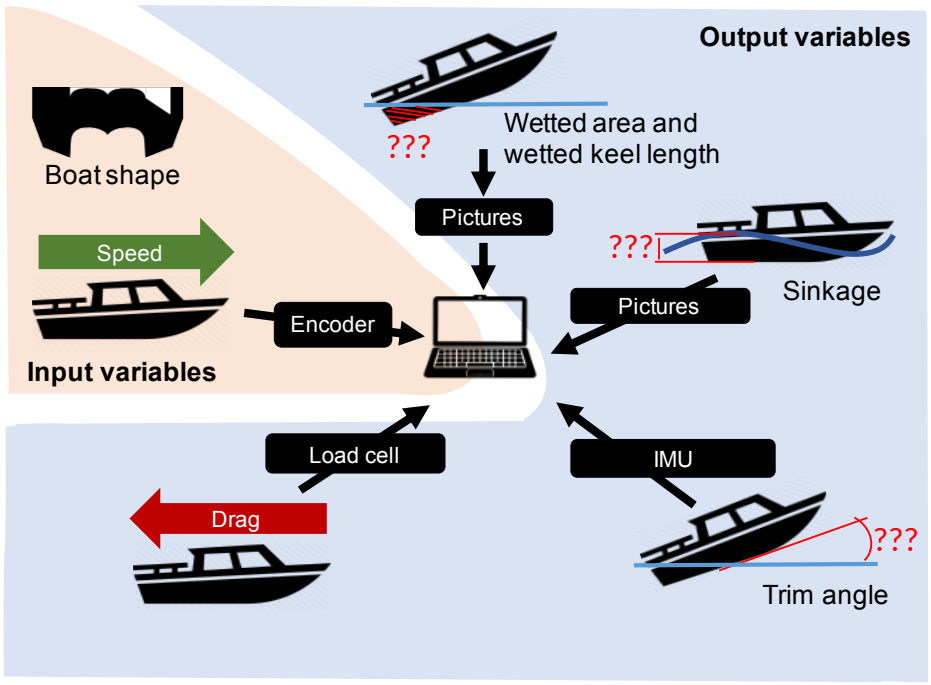

Figure 5.7: Outline of the collected variables. One arrow represent direct collection of the variable in the computer. Two arrows represent the variable is collected separately, and then sent to the computer.

boat. Other variables describing the position of the boat like the wetted area, the sinkage and the wetted keel length are measured by recording videos of the boat. The IMU is positioned in the center of gravity of the models in order to measure principally the trim angle (pitch) of the models. The videos are taken from the ground, from one side of the lake in order to capture the position of the boat with respect to the water surface with the aid of waterlines that were marked in the hulls. This allows to obtain the wetted surface, the trim angle and the sinkage of the boat, and complement the measurements made with the IMU. The layout of the experiment is presented in the Figure 5.9.

For the construction of the models, the ITTC recommended procedure 75-01-01-01 was followed (International Towing Tank, 2002). The models were manufactured in polylactic acid (PLA) by additive manufacturing. Each model was manufactured in 6 parts to be later assembled mechanically with threaded bars and screws. Then, the surface imperfections were polished with polyurethane putty, polyurethane base and finally polyurethane paint, ensuring a suitable surface finish. The scaling procedure of the boat was done with the number of Froude. The characteristics of the models are shown in the Table 5.6 . Figure 5.10 shows the built models of the (a) monohull, (b) catamaran and (c) hysucat.

The complementary weights within the model were carefully positioned in order to keep the center of gravity in 40% of the boat length measured from the transom. For the case of the hysucat, the foils

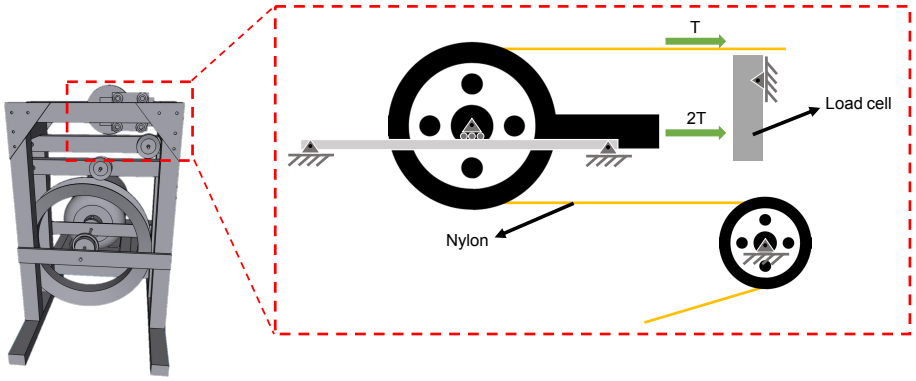

Figure 5.8: CAD of the test bench and diagram of the pulley system and the load cell.

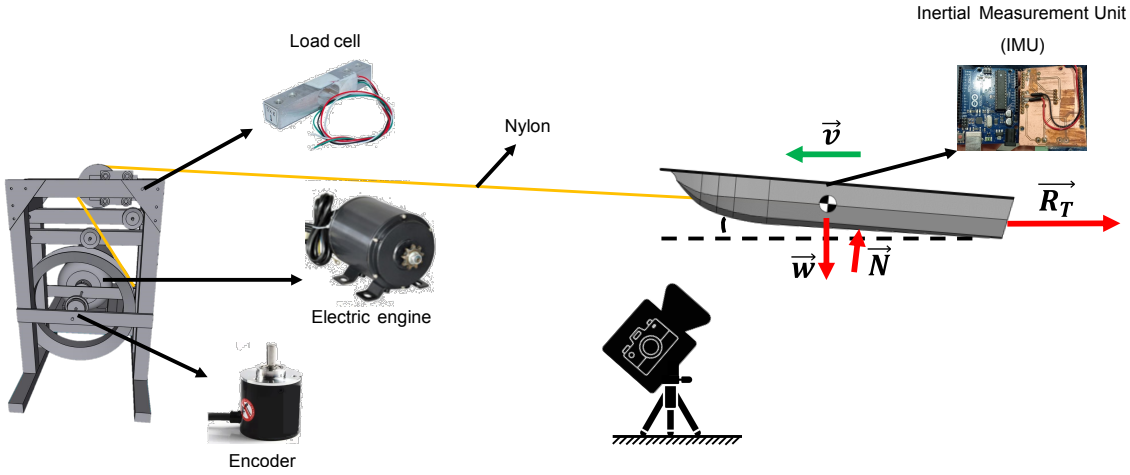

Figure 5.9: Diagram of the experimental setup.

Parameter/variable	**Monohull**	**Catamaran**
Scale	1/8	1/8
Weight (kg)	8.5	8.5
LCG/LOA (-)	0.4	0.4
LOA (m)	1	1
Beam (m)	0.3	0.27
Height (m)	0.14	0.12
Cruise speed (m/s)	5.5	5.5

Table 5.6: Characteristics of the scale models.

were manufactured in aluminum and were machined in a computerized numeric control machine. Both the boats and the foils were sanded in order to smooth the surface. This was especially important

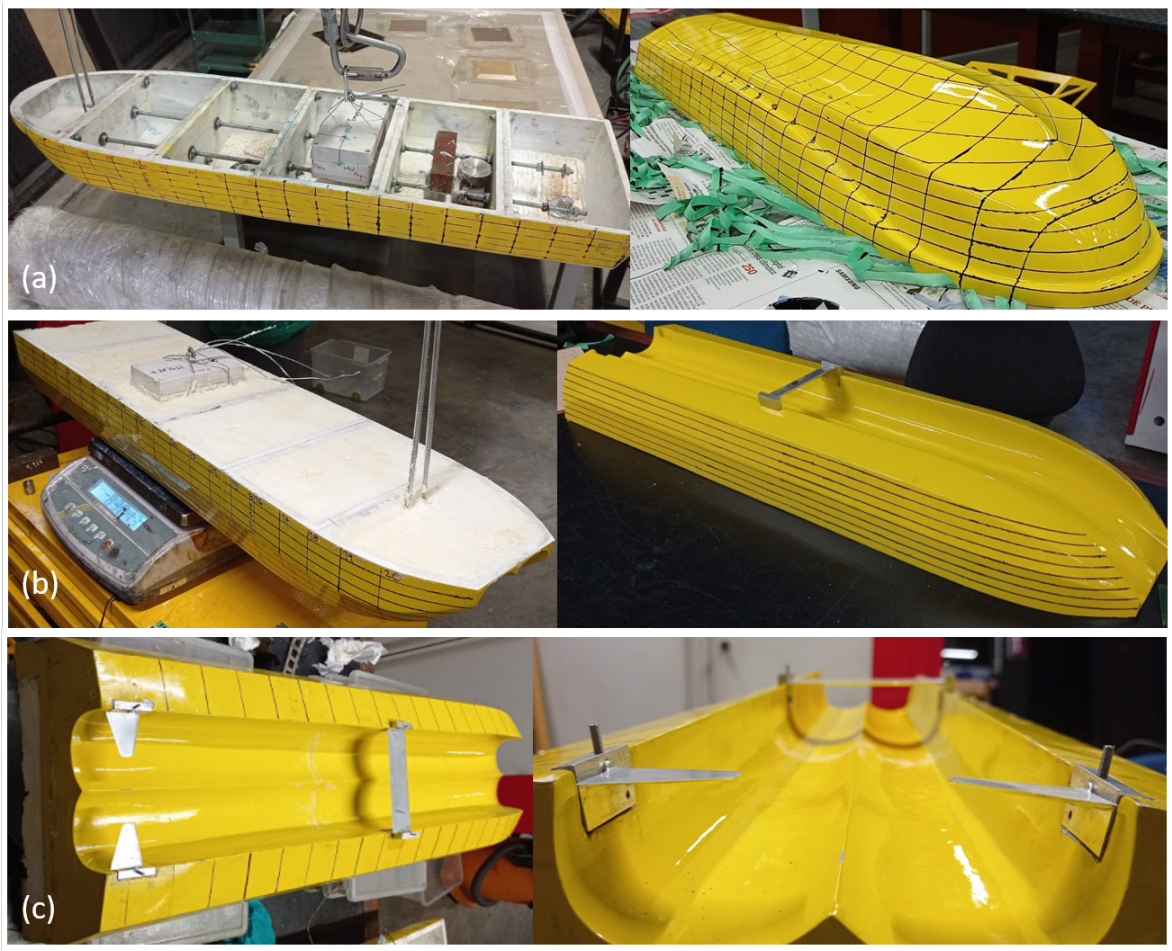

Figure 5.10: Manufacture of the models for the experimental tests. (a) Monohull, (b) Catamaran, (c) Hysucat.

for the hydrofoils, since any roughness on the surface facilitates the detachment of the flow from the surface, which generates premature turbulence.

5.4 Experimental and statistical results

For the speed, drag and trim, at least 3 repetitions per treatment could be measured, excepting for some cases for the trim in which the IMU losts its connection with the computer, so the data could not be recorded. The fact that not the same repetitions could be measured for treatments at the same speeds, constitutes an unbalanced experiment. This can be handled by the tests of multiple comparisons and the tests for the ANOVA assumptions as long as there are more than two points for the treatment containing the least repetitions.

The raw drag and trim angle vs speed data derived from the experiment are shown in Figures 5.11 and 5.12, respectively. The data cleaning was performed by choosing the time frames for each

run where the vessel was stable, according to what was defined in the previous chapter.

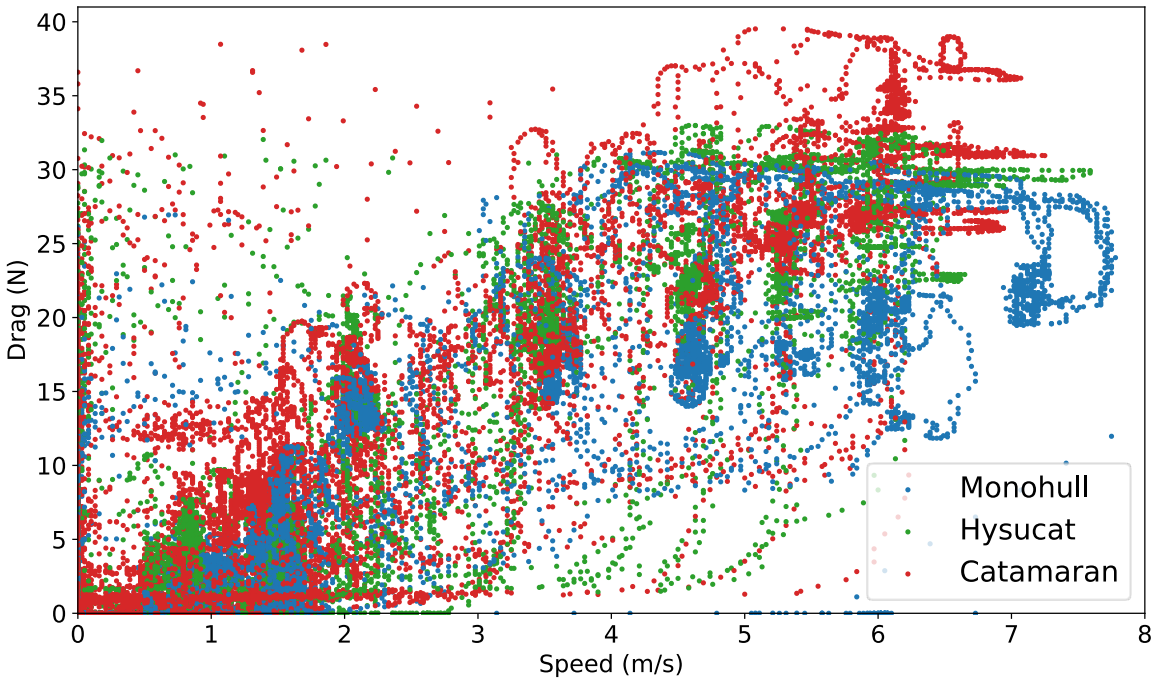

Figure 5.11: Raw results of drag vs. speed for the three scale models.

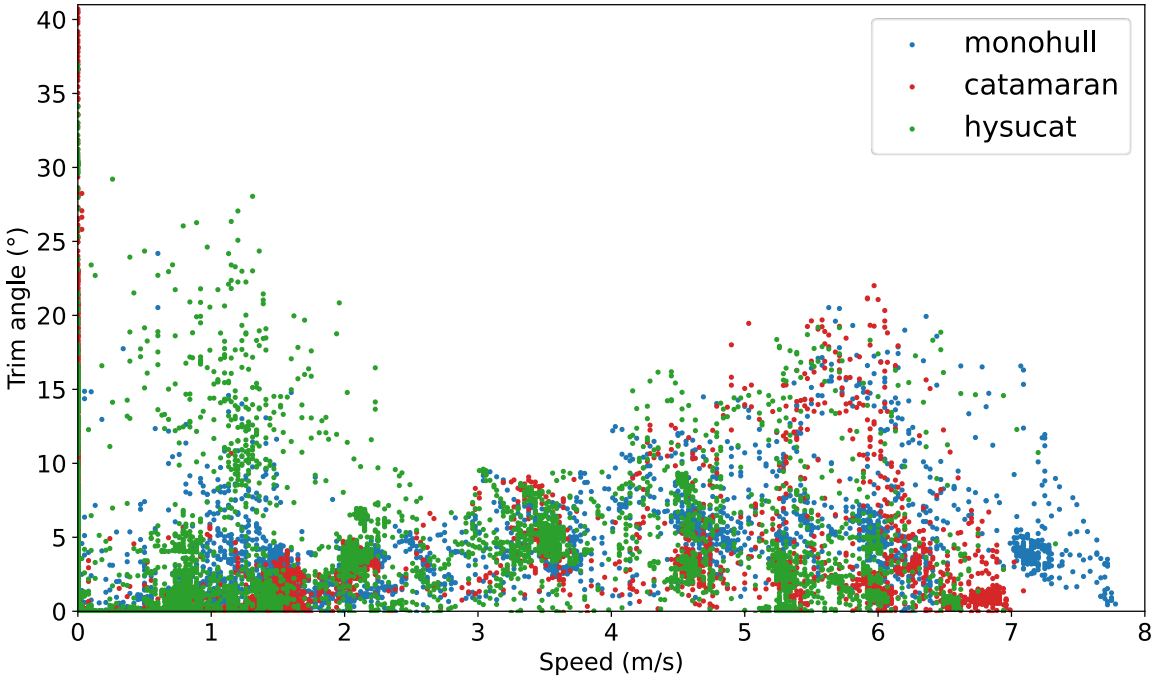

Figure 5.12: Raw results of trim angle (pitch) vs. speed for the three scale models.

5.4.1 Data cleaning

Figure 5.13 shows graphically the cleaning process for a run of the monohull boat at an intended speed of 6 m/s. There, it can be seen that much of the data during the run is discarded and only the part where the two curves reach a plateau is taken.

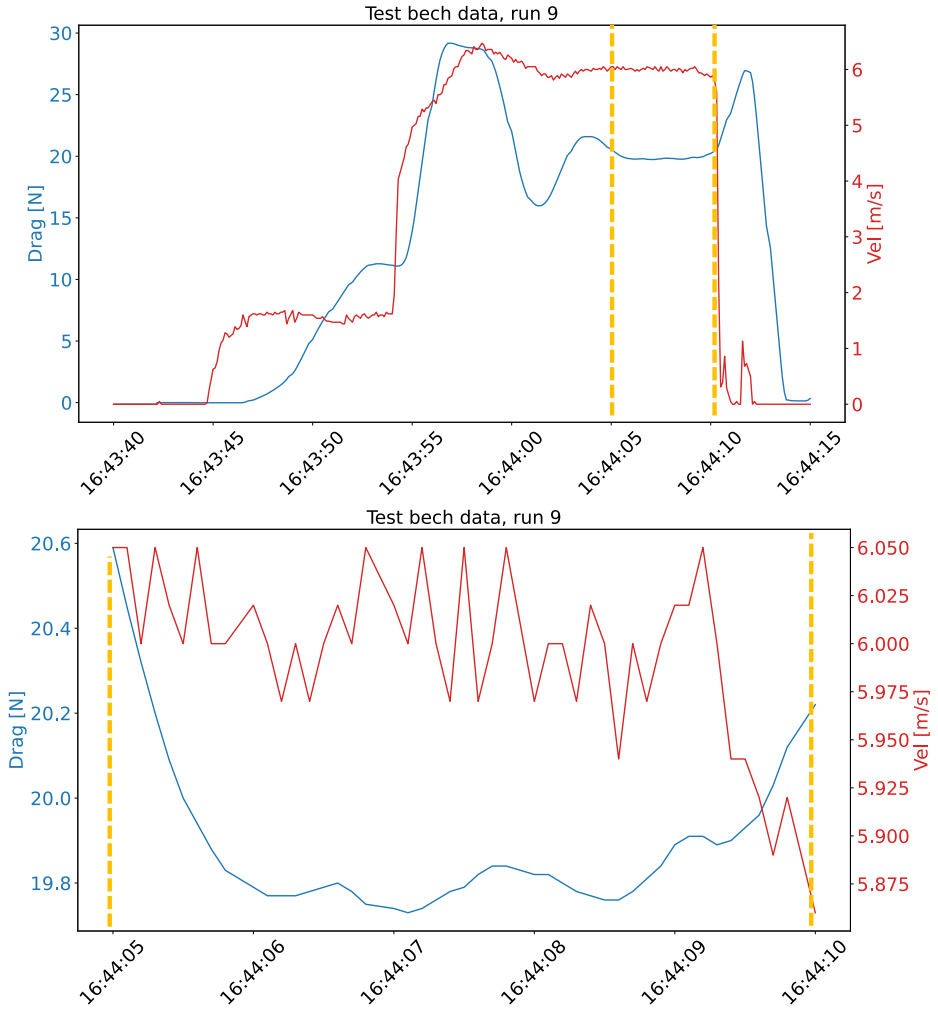

Figure 5.13: Filtering of the data for a run with the monohull for an intended speed of 6 m/s.

Figures 5.14 and 5.15 illustrate the results of performing this procedure for all the runs and the scaling up the results to the real scale, for the drag and the trim angle, respectively.

Figure 5.16 shows the distributions for speed, drag and trim angle for all the runs at real scale at a intended speed of 15 m/s. It can be observed that not all the runs have a distribution similar to a normal distribution. Some of them present multimodal distributions or very flattened normal distributions with outliers. The second case occurs more often for the trim angle (pitch) and is apparently correlated to high oscillations in the speed, which are detected by the IMU, but not by the load cell. Recall that the IMU was located in the boat, while the load cell was on the ground, far

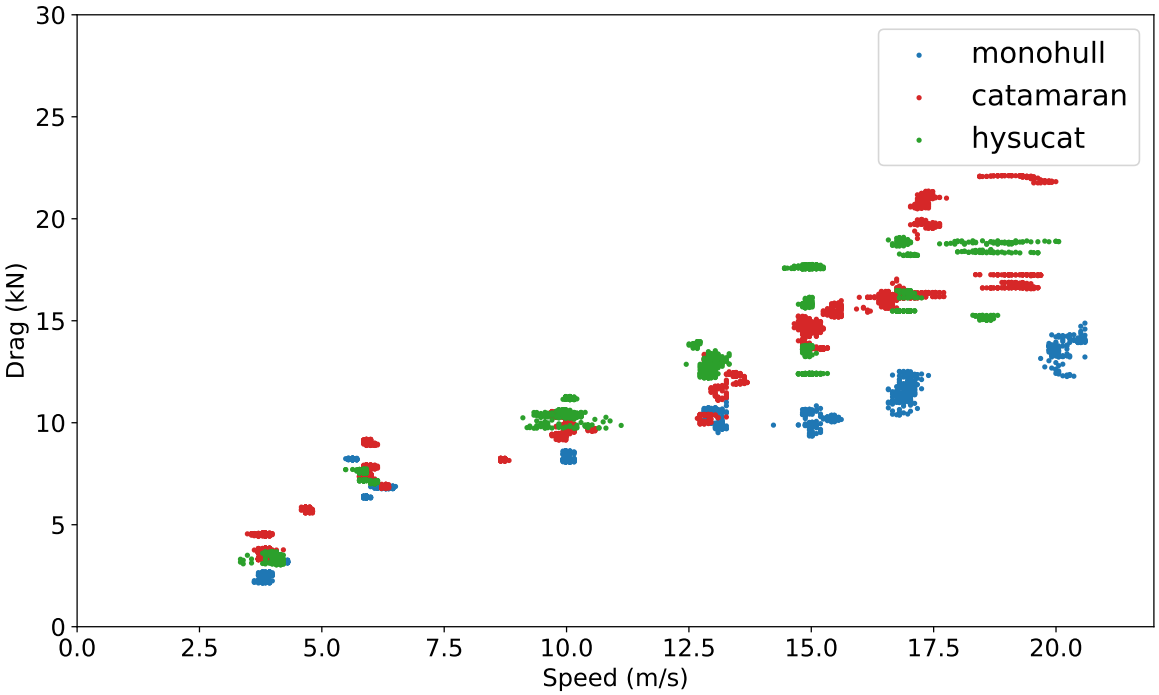

Figure 5.14: Filtered drag vs. speed results for the three hulls. Real-scale results.

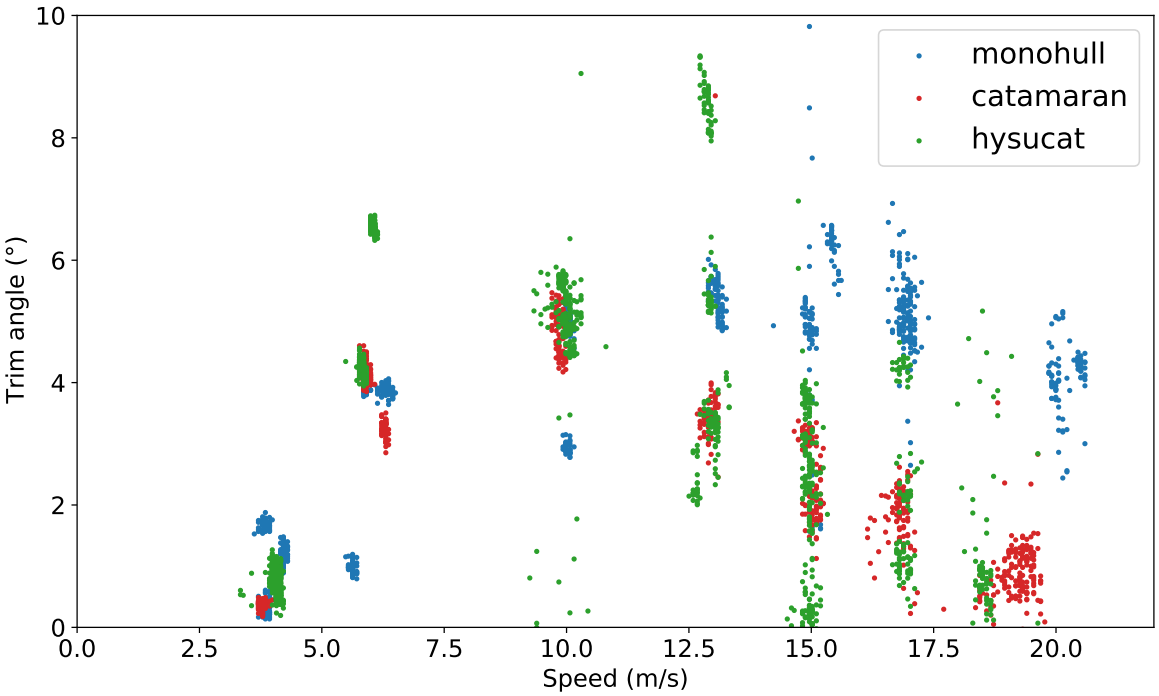

Figure 5.15: Filtered trim angle vs. speed results for the three hulls. Real-scale results.

away from the boat so both sensors were subjected to different sources of variation.

This behavior is also presented for the other six speeds (See from figure B.1 to B.6 in appendix

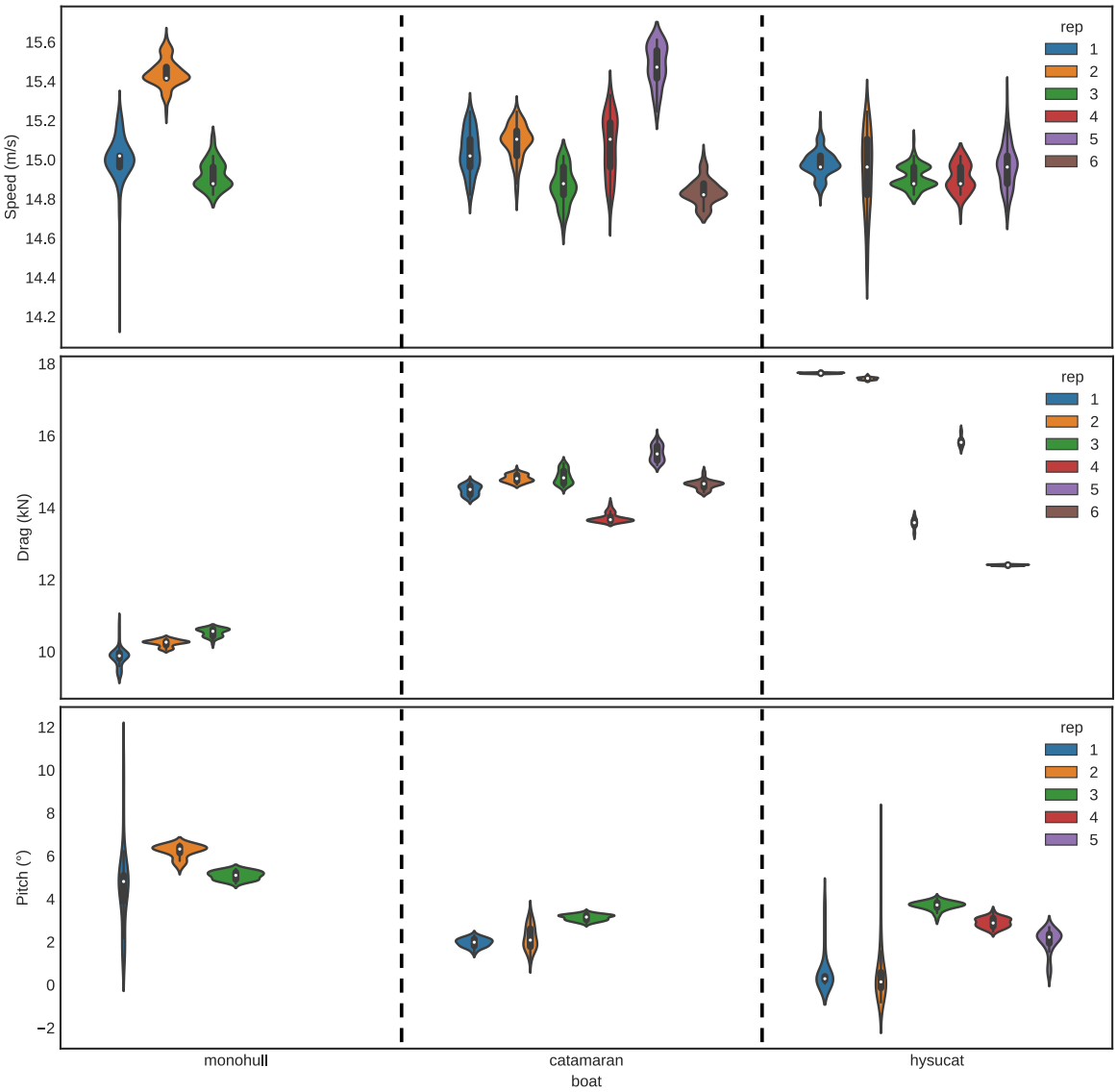

Figure 5.16: Violin plots for speed, drag and trim angle (pitch) for the three boats at a intended speed of 15 m/s.

B). When increasing the speed, the variation is higher for all the variables, but this behavior is more accentuated for the trim angle. This behavior can also be observed in the Figure 5.15, and was expected to occur beforehand due to the electric engine and the test bench from which the boat was towed tend to be more unstable because of the loads and vibrations they are exposed to. Even though this high dispersion is presented, most of the distributions are approximately symmetrical and their means lie near from each other for the same treatment at the same speed in most of the cases.

Runs for the intended speed of 20 m/s are particular as it can be seen in Figures 5.14 and B.6. Due to a restriction in the maximum power of the electric engine with which the models were towed, the measured speed presents very high oscillations for the catamaran and hysucat. The Figure B.6

shows that runs for catamaran and hysucat do not fulfill the criteria for discarding runs explained in the previous chapter. The mean of the measured runs are farther away than 0.2 m/s (or 0.6 m/s at real scale) than the intended speed of 20 m/s. That may give an advantage to those two models (or treatments) with respect to the monohull due to the drag is expected to be underestimated. However, ANOVA and multiple comparison tests are carried out bearing this in mind. The means for all the distributions are used for carrying out the ANOVA and multiple comparisons tests for the drag and the trim angle, assuming the speeds to which the runs where carried out are the intended speeds, not the measured speeds.

5.4.2 ANOVA and multiple comparison tests for drag and trim

Tables 5.7 and 5.8 show a summary of the statistics for all the ANOVAs (and their respective assumptions) carried out for trim and drag at the intended speeds, respectively. It can be observed that, according to the p-values smaller than 0.05, the drag changes according to the hull shape starting from 10 m/s up to 20 m/s. The same occurs for trim, but starting from 15 m/s. The complete ANOVA tables and the charts for visualizing the residuals behavior for all the intended speeds are located in the Appendix D.

According to the Table D.1, which shows the desired criteria to meet in the ANOVAs and their assumptions, some criteria was violated according to some statistics, but this is frequently contradicted by other statistic used for checking the same ANOVA assumption or by the corresponding chart. The most frequently violated assumption is the homoscedasticity or equality of variances between treatments. For example, homoscedasticity is violated for drag and trim for 17 m/s according to Barlett test, but Levenne test shows the opposite. The respective charts for these cases show effectively that the variance is different depending on the treatment.

The only case where is it demonstrated a definitive violation of the homoscedasticity assumption is for the case of the drag at 15 m/s, where both tests and the chart show enough information for rejecting the null hypothesis. This difference in variances of the residuals between the treatments implies that the treatments have a significant effect on the variability of the output variable, which in turn may be due to the different hydrodynamic behaviors between the hulls. This assumption violation is perhaps being accentuated due to the fact that few experimental runs were carried out for some treatment levels or hull shapes, especially for the monohull and the hysucat, which may be affecting the apparent dispersion on each treatment (Gutiérrez Pulido and Salazar, 2004).

In the cases where the p-values of the tests of normality and independence of errors are smaller that 0.05, the corresponding QQ-plot or the histogram of the residuals show that there is not necessarily a violation of the normality assumption. Something similar occurs for the assumption of independence of errors.

		Drag		Trim Angle	
Speed (m/s)	**Test name**	**Statistic**	**p value**	**Statistic**	**p value**
4	Shapiro	-	0.08	-	0.52
	Barlett	-	0.07	-	(Not enough data)
	Levene	-	0.49	-	0.44
	Durbin-Watson	1.97	-	2.71	-
	ANOVA	-	0.052	-	0.51
6	Shapiro	-	0.44	-	0.74
	Barlett	-	0.36	-	0.68
	Levene	-	0.49	-	0.09
	Durbin-Watson	2.83	-	1.83	-
	ANOVA	-	0.43	-	0.29
10	Shapiro	-	0.19	-	0.003
	Barlett	-	0.52	-	0.17
	Levene	-	0.7	-	0.77
	Durbin-Watson	2.06	-	2.27	-
	ANOVA	-	0	-	0.86
13	Shapiro	-	0.79	-	0.08
	Barlett	-	0.46	-	0.17
	Levene	-	0.56	-	0.54
	Durbin-Watson	2.31	-	2.16	-
	ANOVA	-	0.01	-	0.89
15	Shapiro	-	0.33	-	0.73
	Barlett	-	0.007	-	0.5
	Levene	-	0.02	-	0.3
	Durbin-Watson	2.07	-	2.14	-
	ANOVA	-	0.001	-	0.007

Table 5.7: Summary of the statistics and p-values from the ANOVAs carried out and their respective assumptions for drag and trim angle for intended speeds from 4 to 15 m/s. Only p-values are presented here, excepting for Durbin-Watson, whose statistic is presented instead of the p-value.

Figures 5.17 and 5.18 show the confidence intervals for the mean of the drag for the three hulls for all the intended speeds.

Contrary to what had been observed with ANOVAs p-values for the drag, in the Table 5.7, for 4 m/s, the Tukey-HSD test shows that there is a difference between the treatments. This contradiction between the ANOVA and the Tukey-HSD test may be due to a low statistical power, especially for the monohull and the hysucat, whose number of repeats are tree, while for the catamaran there are six. ANOVA and Tukey-HSD tables in the Figure D.2 show that the p-values are very close to 0.05, so

		Drag		Trim Angle	
Speed (m/s)	**Test name**	**Statistic**	**p value**	**Statistic**	**p value**
17	Shapiro	-	0.052	-	0.26
	Barlett	-	0.01	-	0.03
	Levene	-	0.34	-	0.15
	Durbin-Watson	1.28	-	2.6	-
	ANOVA	-	0	-	0
20	Shapiro	-	0.53	-	0.93
	Barlett	-	0.1	-	0.31
	Levene	-	0.45	-	0.01
	Durbin-Watson	2.61	-	1.81	-
	ANOVA	-	0.03	-	0

Table 5.8: Summary of the statistics and p-values from the ANOVAs carried out and their respective assumptions for drag and trim angle for intended speeds for 17 and 20 m/s.

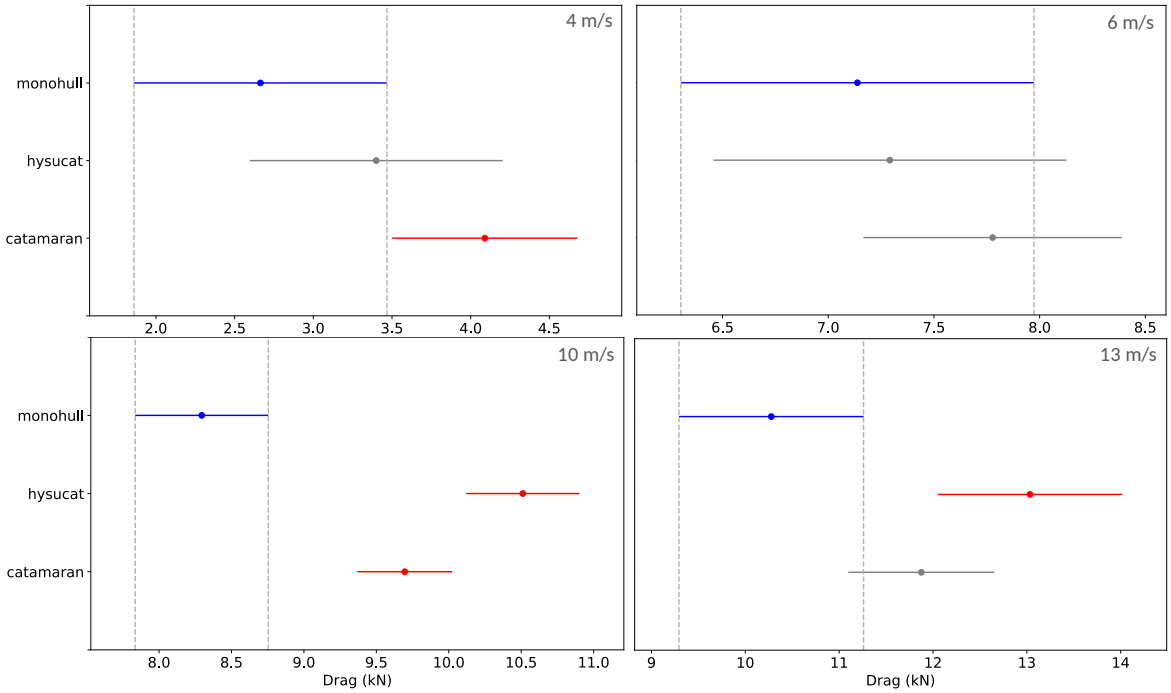

Figure 5.17: Confidence intervals for the mean according to Tukey-HSD test for the drag for the three hulls. Intended speeds from 4 to 13 m/s. The blue line is for the baseline treatment or hull shape. A gray line means no statistical difference with the baseline treatment and the red line mean the opposite.

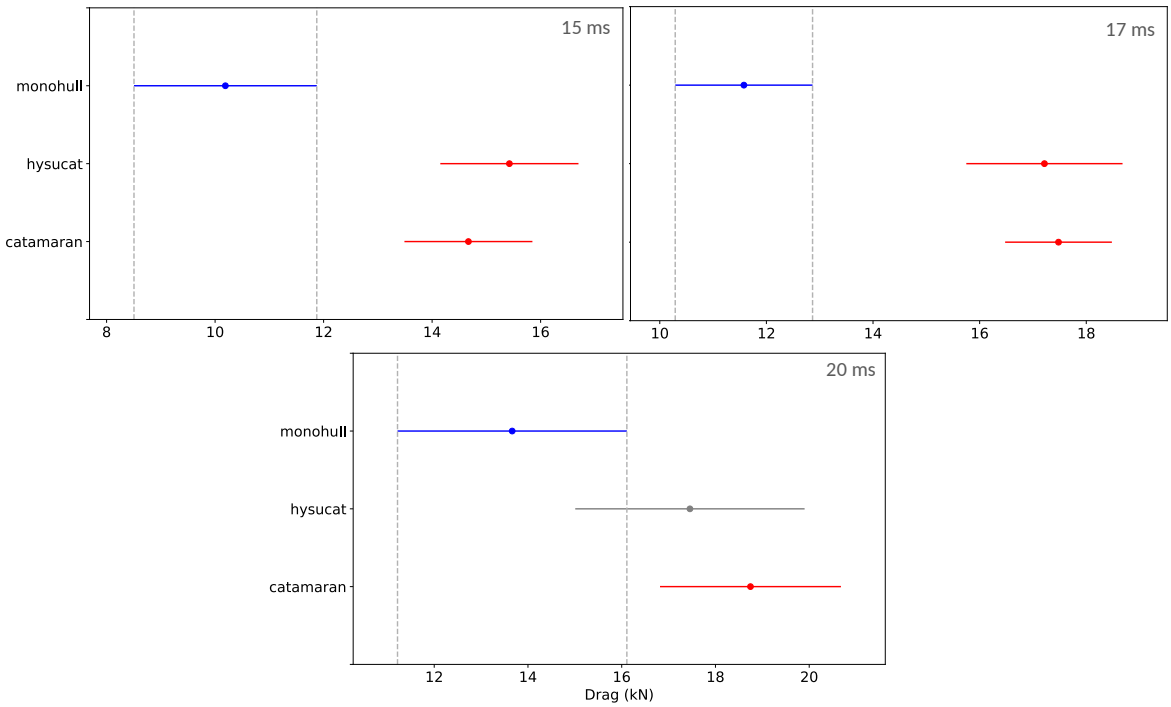

Figure 5.18: Confidence intervals for the mean according to Tukey-HSD test for the drag for the three hulls. Intended speeds from 15 to 20 m/s.

the most conservative is to assume there are not differences at all for the drag between the treatments at the speed.

For a significance of 5%, the monohull statistically presents less drag than the catamaran an the hysucat for speeds of 10 m/s and higher, excepting for 20 m/s in which the monohull is statistically equal to the hysucat. This result for 20 m/s may not be completely correct, due to the fact that the measured speeds reached by the hysucat and the catamaran were lower than for the monohull as mentioned at the end of subsection 5.4.1.

The catamaran and the hysucat drags are statistically always the same, excepting for a speed of 10 m/s, in which the drag of the catamaran is about 1 kN lower. This shows that the hydrofoils brought no drag reduction at any speed different than 10 m/s that could be detected with the present designed experiment. This result is surprising for speeds of more than 10 m/s, in which the hysucat enters in planing regime and the hydrofoils are supposed to generate enough lift to make the boat partially emerge from the water surface.

The mean differences of drag between the monohull and both the catamaran and the hysucat according to the Tukey-HSD test ranges from 1 kN at speeds of 10 m/s to 5 kN at speeds of 20 m/s, which corresponds to 12% and 36% higher average drags in comparison to the average drag of the monohull at those corresponding speeds. This shows that the monohull has better planing capabilities in terms of hydrodynamic drag than the catamaran and the hysucat. This allows to reject the first

null hypothesis stated in subsection 4.4.2, Equation (4.1), (catamaran-monohull) for speeds over 10 m/s, but does not allow to reject the null hypothesis in Equation (4.3) (hysucat-monohull).

Figures 5.19 and 5.20 show that, according to the ANOVAs (see tables 5.7 and 5.8), the trim angle starts being statistically significantly different (higher) for the monohull for speeds greater than 13 m/s.

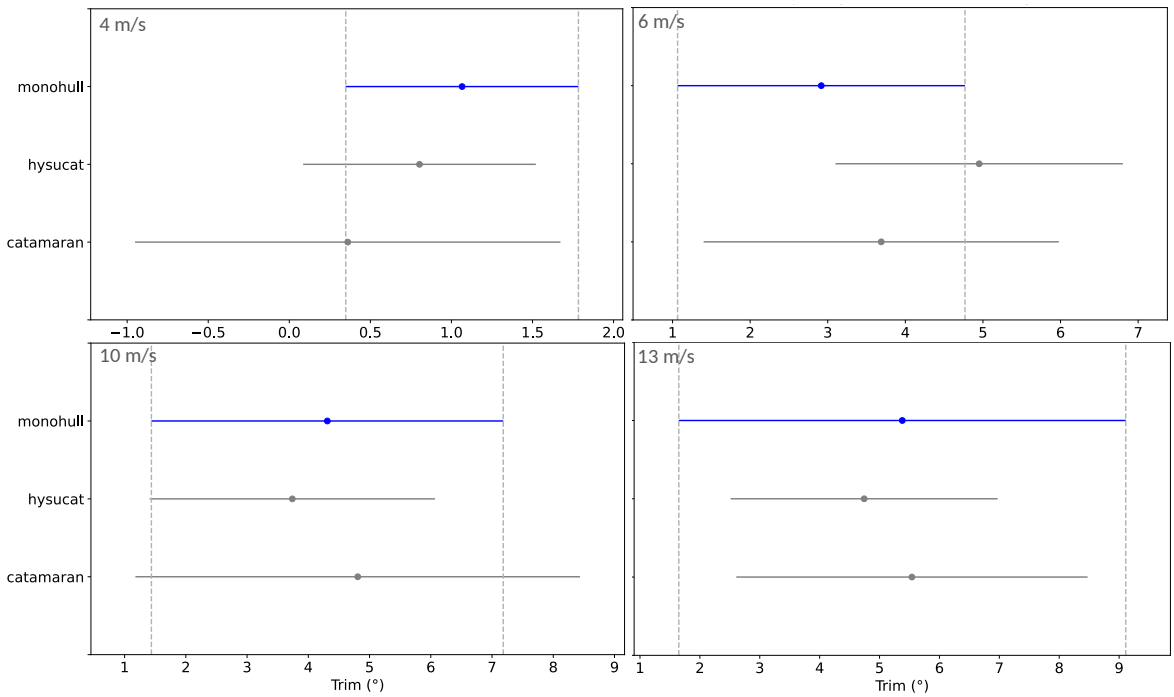

Figure 5.19: Confidence intervals for the mean according to Tukey-HSD test for the trim angle for the three hulls. Intended speeds from 4 to 13 m/s.

The trim angles for the catamaran and the hysucat are statistically the same for all the speeds, which shows that the hydrofoils did not cause a change in the travel position of the catamaran, not even at planing speeds. Interestingly, the widest intervals of the mean for the trim angle are presented for the three boats at speeds of 10 and 13 m/s even though they are not the highest speeds. This does not allow to find different statistical groups despite for the drag differences can be identified starting from 10 m/s.

The means difference between the monohull and both the hysucat and catamaran ranges according to the Tukey-HSD tests from about 3 to 3.5°. This indicates that the monohull travels more inclined at planing speeds in a range of average trim angles between 4 and 6.5°, which is the recommended range by Savitsky et al. (1964). This allows to reject both null hypothesis for the positional variables, stated in subsection 4.4.2, Equations (4.5) (catamaran-monohull) and (4.7) (hysucat-monohull) for speeds over 15 m/s. However, rejecting the second null hypothesis is due to the base geometry is a catamaran, not to the hydrofoils installed.

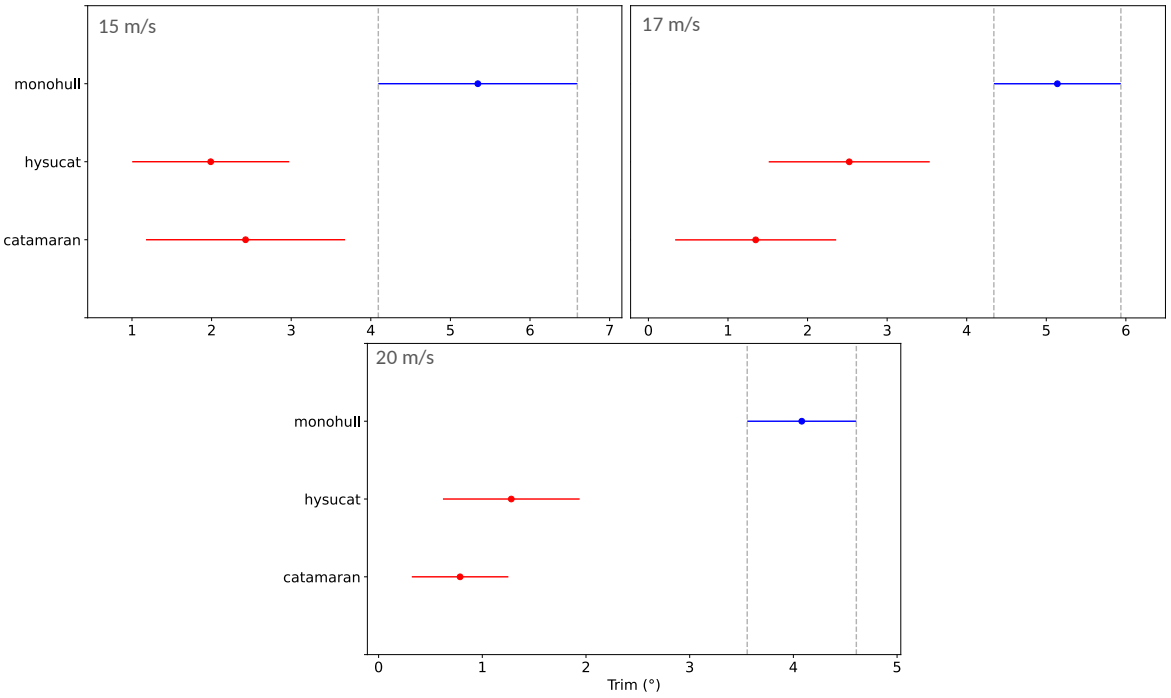

Figure 5.20: Confidence intervals for the mean according to Tukey-HSD test for the trim angle for the three hulls. Intended speeds from 15 to 20 m/s.

Appendix D contains detailed results of the Tukey-HSD tests carried out for the drag and trim angle for all the speeds.

5.4.3 Regression analysis for drag and trim

A polynomial linear regression analysis is performed for the drag and the trim angle, versus the speed. This helps in comparing the hydrodynamic behavior between the three boats according to experimental results and also to compare against the results obtained with the Savitsky model. When carrying out comparisons between the experimental results in the regression analysis, it is important to take into account the speeds from which the output variables start being statistically different between treatments according to the results in the previous subsection.

Figure 5.21 shows the linear regression analysis carried out for the drag with the mean values for all the runs. As expected, the regression lines for the catamaran and the hysucat are very similar for all the speeds. It can be noted that the drag for the monohull starts growing at a slower rate than the drag for the other two hulls at speeds beyond 10 m/s, which is near the transition threshold between the preplaning and planing regime.

The experimental results give much higher values than those predicted by the Savitsky method, except for speeds around 4 m/s where the values are similar. This difference between the Savitsky and experimental results grows as the speed increases. For the monohull, the relative error ranges from

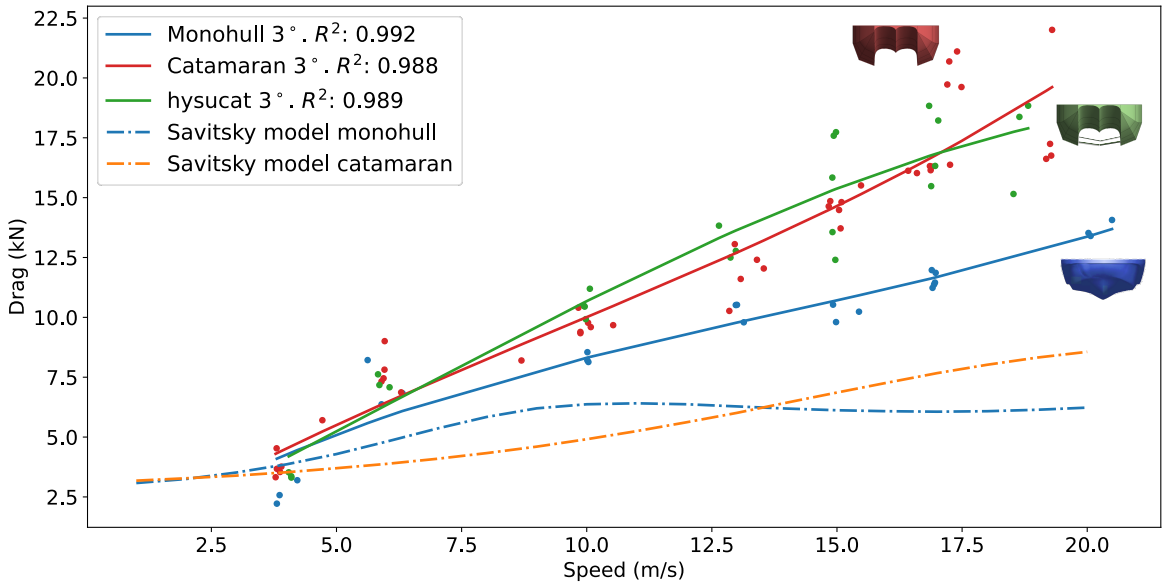

Figure 5.21: Averaged drag vs. speed results for the three full-scale prototypes.

14% to 133%. For the case of the catamaran, the relative error ranges from 29% to 217%. Assuming the Savitsky model was properly implemented, this shows there was some error sources which affected the experiment, giving as a result, increased values of hydrodynamic resistance.

Figure 5.22 shows the linear regression analysis carried out for the trim angle with the mean values for all the runs. The trim angle for the catamaran and hysucat is almost identical for all the speeds. The trim angle of the monohull starts diverging from the other two boats at a speed of 10 m/s, giving support to the affirmations made in the multiple comparison tests for the trim. At planing speeds, both the catamaran and hysucat travel almost horizontally, with trim angles under 3.5°, while the monohull travels more inclined with trim angles between 4 and 5°.

Similarly for the case of the drag, trim angles derived from the regression analysis also present high deviations from the results of Savistky model. For the monohull, there is 60% of relative error at lower speeds. These errors are lowered to around 18% at speeds over 12 m/s. For the case of the catamaran, the relative error is the maximum at 20 m/s with a value of 100%; and the least at 10 m/s with a value of 22%. It is worth noting that even the shapes of the experimental and Savitsky curves for the catamaran are very different from each other, even with apparently opposite behaviors in some cases.

In contrast to the high coefficients of determination obtained for the drag for the catamaran and the hysucat, the coefficients of determination for the trim angle for these two are much lower with values of 0.787 and 0.726 respectively, which is due to the much higher dispersion of the data points in comparison to the monohull.

According to the regression analysis, the polynomials giving the highest coefficients of determina-

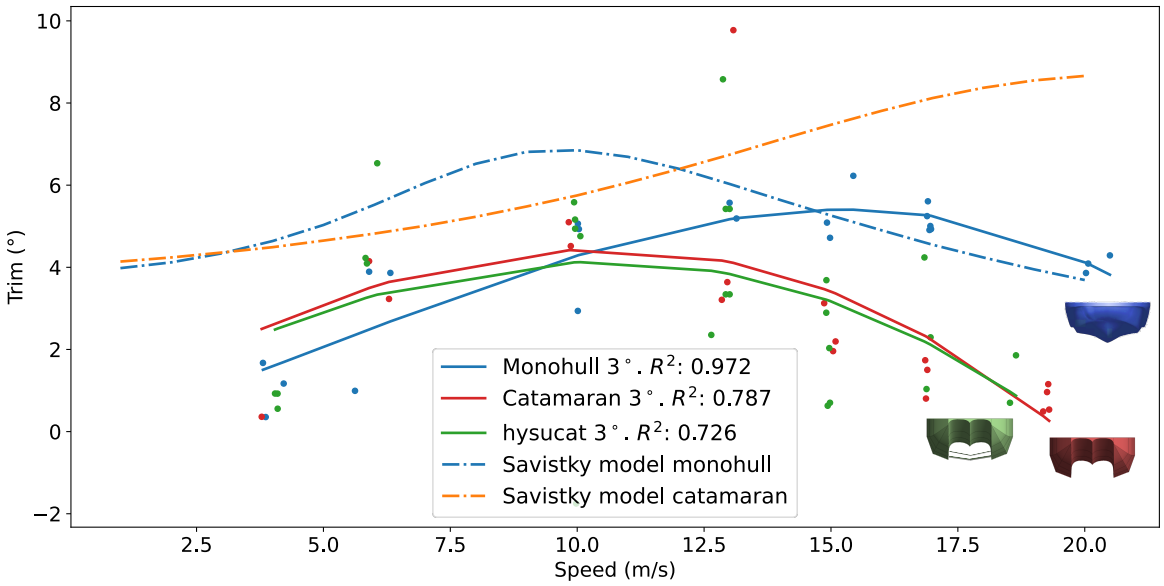

Figure 5.22: Averaged trim vs. speed results for the filtered values of the three full-scale prototypes.

tion for both drag and trim are degree three. The polynomials are of the type:

$$Y = \beta_0 + \beta_1 X_1 + \beta_2 {X_1}^2 + \beta_3 {X_1}^3 \tag{5.1}$$

Table 5.9 shows the coefficient of determination and the value of each of these coefficients with their respective p-value, which results from implementing a hypothesis test, where it is evaluated whether the absence of the coefficient causes any effect in the equation. A p-value value of under 0.05 implies that the absence of the coefficient does cause a change in the equation and is therefore important to describe the phenomenon. A p-value over this number does not necessarily mean the opposite, but it may indicate there is a low statistical power due to lack of data.

It can be observed that most of the coefficients present p-values over 0.05. However, if the regression is carried out for the drag without averaging for each run, all the p-values are reduced to almost zero as can be seen in the Table 5.10, which means that there is a lack of data for the case where the runs are averaged.

Figure 5.21 shows a plot for the experimental results without averaging and their respective regression curves, along with Savitsky curves. The regression analysis carried out for the not-averaged data is only for illustration purposes and should not be taken as a valid result due to, as was previously mentioned, the data points inside an experimental run are not independent data, but are pseudoreplicates.

	Drag			Trim angle		
Hull shape	**r2**	**coef.**	**p val.**	**r2**	**coef.**	**p val.**
Monohull	0.992	0	-	0.972	0	-
		1.2809	0		0.3099	0.031
		-0.093	0.017		0.0289	0.14
		0.0014	0.081		-0.0017	0.017
Catamaran	0.988	0	-	0.787	0	-
		1.277	0		0.7664	0.091
		-0.0428	0.18		-0.0253	0.676
		0.0015	0.196		-0.0007	0.731
Hysucat	0.989	0	-	0.726	0	-
		0.965	0.002		0.7278	0.083
		0.0227	0.592		-0.0258	0.679
		-0.0012	0.43		-0.0006	0.805

Table 5.9: Results of the regression analysis for the experimental results of drag and trim angle.

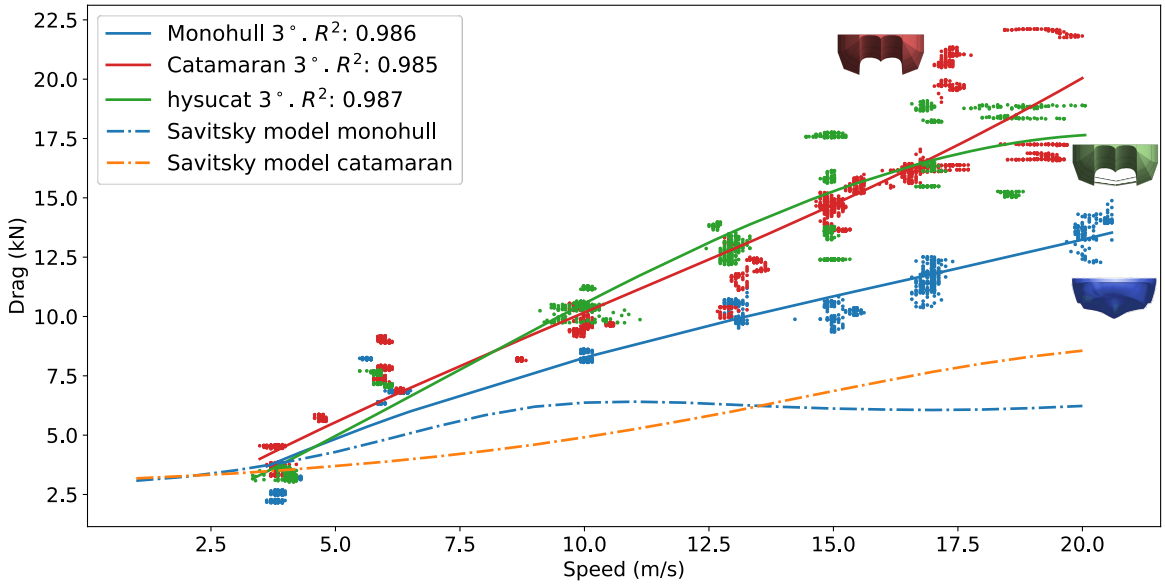

Figure 5.23: Drag vs. speed results for the three full-scale prototypes.

5.4.4 Results for positional variables

Due to some limitations of equipment with which the videos were recorded in the experimental setup, only one measurement per speed and boat shape could be taken for the sinkage, wetted area and

	Drag (kN)		
Hull shape	**r2**	**coef.**	**p val.**
Monohull	0.986	0	-
		1.1551	0
		-0.0410	0
		0.0008	0
Catamaran	0.985	0	-
		1.2597	0
		-0.0357	0
		0.0011	0
Hysucat	0.987	0	-
		0.8277	0
		0.0427	0
		-0.0020	0

Table 5.10: Results of the regression analysis for the experimental results of drag and trim angle. Runs without averaging.

wetted keel length of the models.

Figure 5.24 shows side photos for the three models at cruising speed, which is at the intended speed of 5.3 m/s for the scale models. This is equivalent to 15 m/s in the full-scale prototypes. There, it is observed that the monohull emerges completely from the water at the front, thanks to the fact that it travels with a higher backward inclination. This higher trim angle in comparison to the other two models was mentioned in the previous two subsections. Additionally, it can be observed that in the case of the monohull, the water is deflected towards the sides, while for the catamaran and hysucat the water spray covers almost all the sides of the models.

Figure 5.25 shows the experimental sinkage for the three hulls and the sinkage of the monohull and catamaran. This, according to Savitsky model, and according to its definition in the Figure 2.5. Here, the monohull and the hysucat seem to have a similar behavior, with differences of around 10 cms at displacement and preplaning speeds. The curve for the catamaran follows a different shape for most of the speeds. The three hulls have in common their sinkage is reduced around a 40% due to the hydrodynamic lift caused at planing speeds.

This is the opposite to what Savitsky model shows for the catamaran, which says its sinkage should slightly increase as the speed increases. The differences for the catamaran between the experiments

Figure 5.24: Lateral photograph of the three models at cruising speed (5.3 m/s).

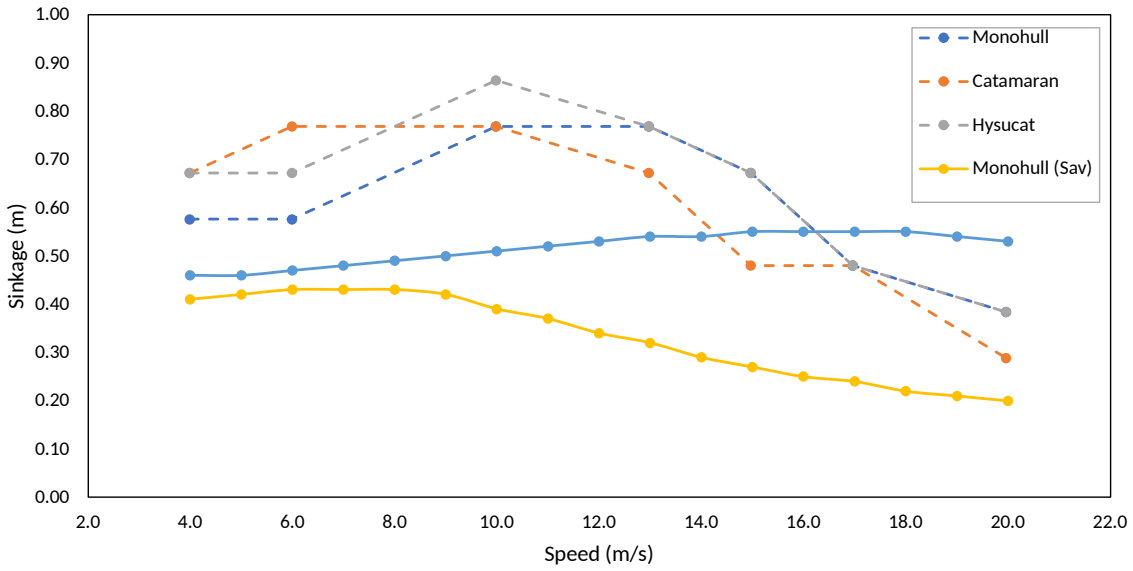

Figure 5.25: Sinkage vs speed for the three boats.

and Savitsky ranges from 10% at the cruise speed to 40% at the highest speeds and 54% at the lowest speeds. For the case of the monohull, the differences range between 20% at the highest speeds to 70% at the lowest speeds and 92% at 10 m/s.

For scaling up the drag force from the scale models to the full-scale prototypes it was necessary to measure the wetted areas and wetted keel lenghts of the models. Figure 5.26 depicts the wetted areas

at cruise speed for the CAD models of the full-scale monohull and catamaran. Appendix E contains the side pictures for the three boats and the CADs illustrating their wetted areas.

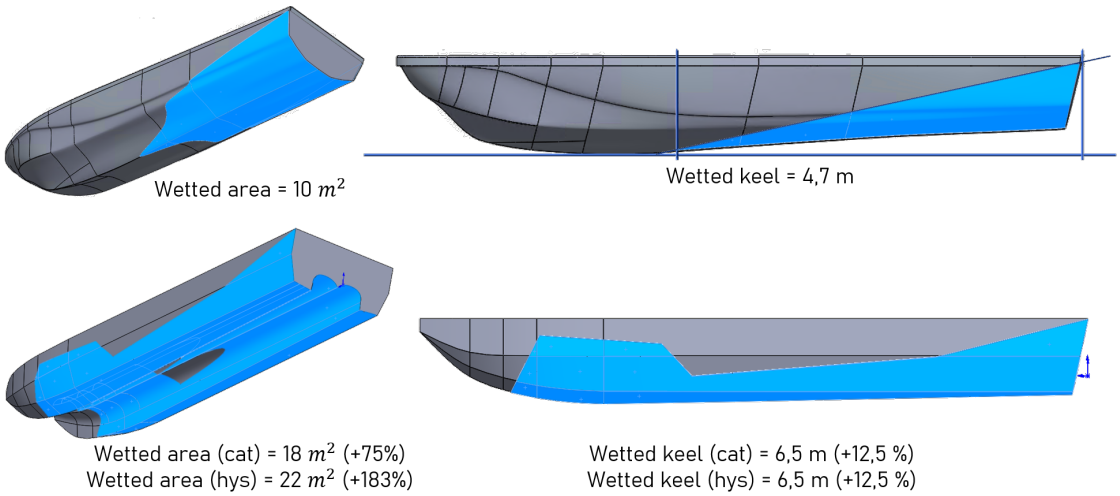

Figure 5.26: CAD representation of the wetted areas for the three vessels. Only one image is included for the catamaran and hysucat, because the shape of the wetted area is relatively similar. 'cat' and 'hys' stand for catamaran and hysucat respectively.

Figure 5.27 summarizes the results for wetted area for the three hulls.

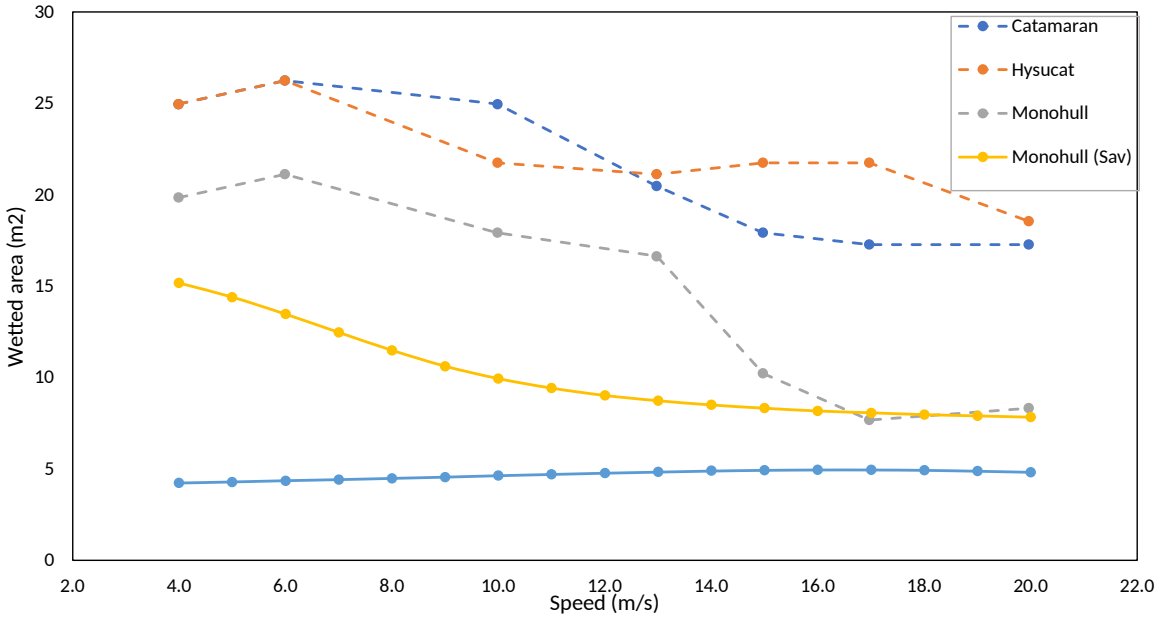

Figure 5.27: Wetted area vs speed for the three models.

The wetted area for the hysucat and the catamaran is almost the same for all the speeds, while the area for the monohull is greatly reduced beyond planing speeds. The monohull has in average 18% less wetted area than the other two hulls at displacement and preplaning speeds. At planing speeds

beyond 12 m/s, the catamaran and hysucat have in average twice of the wetted area of the monohull, which is near the 40% mentioned by Yun et al. (2018) in their book.

With respect to Savitsky, experimental wetted areas are very different, excepting for the monohull at speeds beyond 15 m/s. The differences for the catamaran are between 85% and 75%, while for the monohull range between 5% at 17 m/s to 32% at the lowest speeds and 75% at 10 m/s.

Similarly to what happens for drag and trim, the wetted keel length of the monohull starts being very different beyond 10 m/s in comparison with the other two boats due to it starts decreasing significantly, while for the catamaran and the hysucat it stays almost constant. The catamaran and the hysucat travel almost horizontally, which makes the wetted keel length to be almost equal to the total length of the boat for all the speeds. In contrast, the monohull reaches at planing speeds a wetted keel length almost half of its total length, as it is observed in the Figure 5.28.

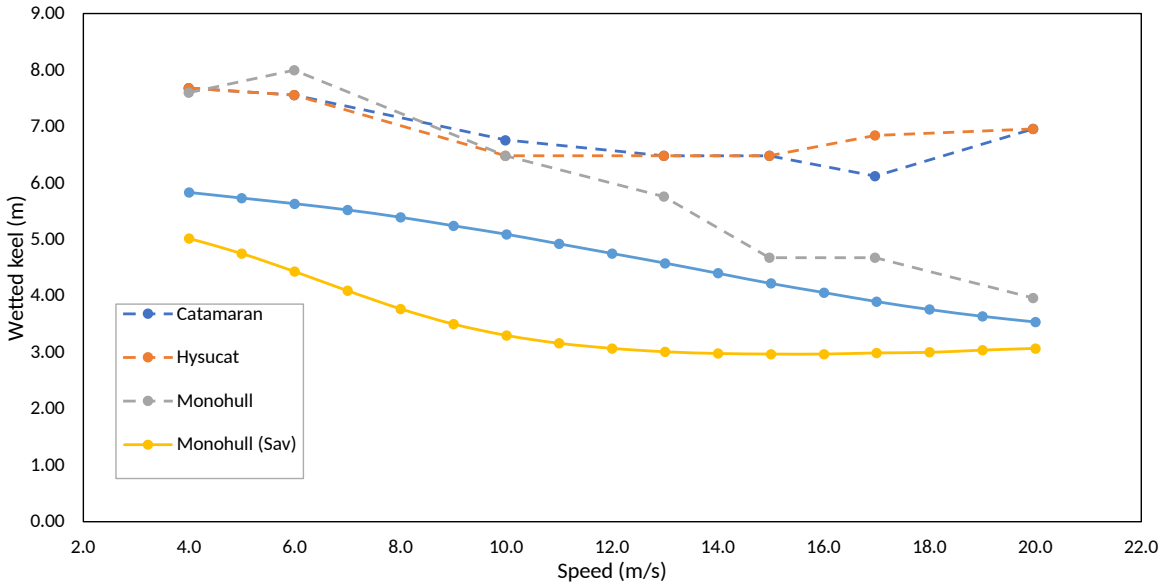

Figure 5.28: Wetted keel length vs speed for the three boats.

This significant reduction in wetted area and wetted keel length due to the higher trim angle at planing speeds in the case of the monohull, partially explains that the drag force for the monohull is increased at a lower rate in comparison to the other boats at planing speeds.

The larger wetted area can be attributed to the fact that the water has contact at all times with the inner walls of the demihulls and the top of the tunnel. This contact with the top of the tunnel is an undesirable effect, since from the conceptual design it was planned that this area would not have contact with water at cruising speed due to the high drag it could add up. This would be achieved implementing the hydrofoils. Additionally, the monohull has hard chines combined with spray deflectors that cause a separation of the flow from the hull and guide it to the sides. This prevents downward hull suction from being caused (No Frills Sailing, 2021) and prevents the sides of

the boat of being in contact with water.

In contrast, the catamaran and hysucat, by not having sharp corners but rounded chines, allow the water to follow the contour by deflecting the water upwards, as it is presented in the Figure 5.29.

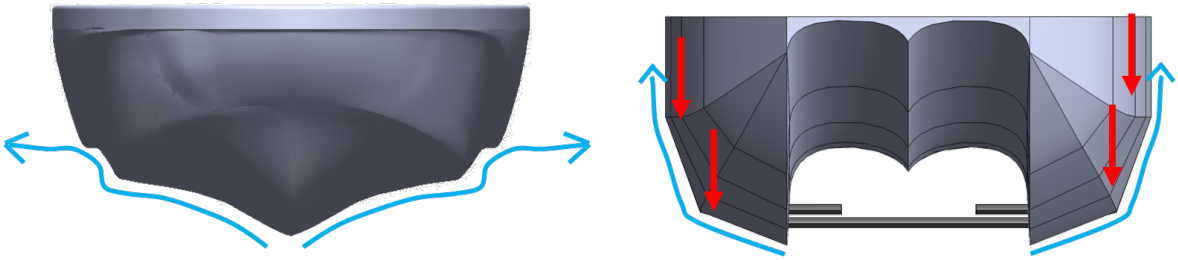

Figure 5.29: Graphic representation of the flow deflection sideways for the monohull and upwards for the catamaran and the hysucat.

This deflection may be causing a resultant downward force. Possibly, this causes the hulls to be sucked in the same direction, eliminating the hydrofoil effect in the case of the hysucat. Additionally, this upward deflection of the flow causes almost the entire lateral area of the catamaran to remain wet according to the Figure 5.24.

This large additional wetted area for the catamaran and hysucat compared to the monohull may be the cause of the large difference in consumption between these vessels. One way to reduce this gap could be by implementing spray deflectors (Russell, 2015) on the catamaran and varying the area and angle of attack of the hydrofoils, looking for the vessel to further reduce its sinkage at high speeds. These solutions may reduce the drag of the catamaran and hysucat, but it is uncertain how much this reduction may be.

It could also be though that the catamaran and hysucat are travelling at pre-planing regimes instead of planing, which is causing the higher increasing of the drag/speed rate beyond 6 m/s in comparison to the monohull as it is seen in the Figure 5.21. However, Froude numbers were calculated from the wetted keels shown in the Figure 5.28, which shows all the three hulls go well beyond the planing threshold, which is around 1 and slightly below 10 m/s for the three hulls. These Froude numbers are presented in the Figure 5.30.

It can also be seen that the monohull reaches higher Froude numbers, due to the fact that it travels with higher trim angles and lower wetted keel lengths at the planing regime.

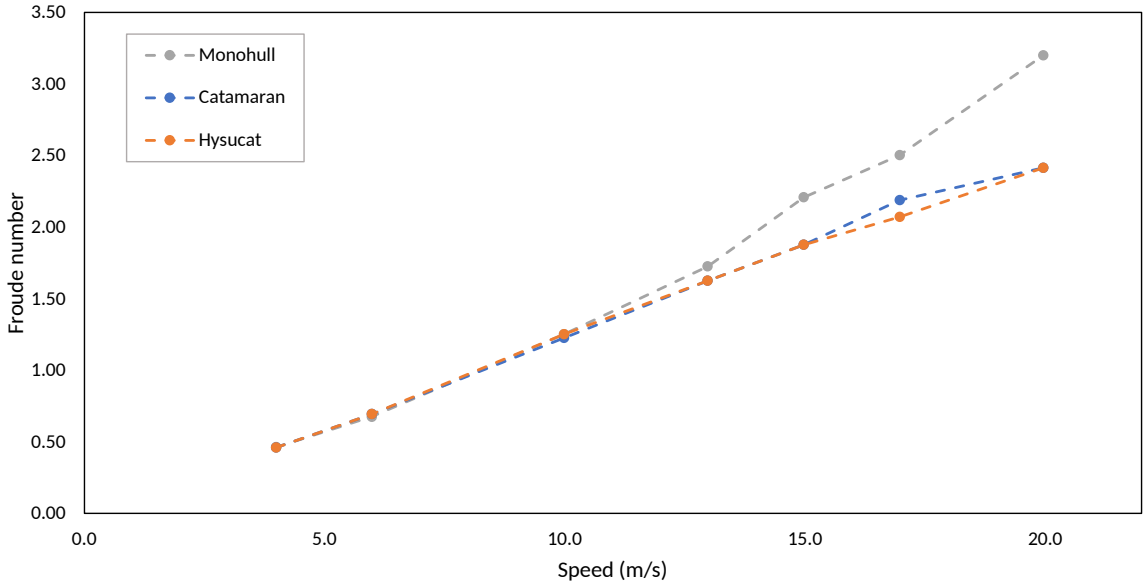

Figure 5.30: Froude number vs speed for the three boats.

Chapter 6

Conclusions

Hydrofoil supported catamarans are presented in this work as a candidate to compete against monohulls in terms of hydrodynamic performance in contexts where installing hydrofoils that increase the draft of the hull are not technically feasible. Although planing boats and hydrofoils have been widely studied during the last 50 years or more mainly through statistical, experimental and numerical approaches, the literature review carried out in this work allows to conclude that no studies carrying the comparison between these geometries with experimental, statistical models or numerical methods have been at least published.

The proposed methodology allows to compare experimentally any hull geometries at different speeds in an objective and unbiased way as long as dimensions, weight and weight distribution are kept as similar as possible for all the geometries. The methodology allows to find statistical differences between the hydrodynamic performance of multiple geometries at the same time, so the reliability on the results heavily depends on the number of repetitions carried out per treatment or hull geometry at each speed. Here, the Savitsky statistical model helps with the design of the experiment and as a baseline for the experimental results. In this work, a comparison between the monohull, catamaran and hysucat is carried out. The geometries were selected according to the context of Colombian rivers and their particular characteristics. Seven intended speeds and a scale of 1/8 of the models in relation to the real scale prototypes were selected. These speeds were selected in order to obtain acceptable resolutions of the curves for the variables vs the speed. Limiting the comparison of the hulls at the same speeds allows to reduce the complexity of the design of experiments to a single-factorial experiment.

For towing the model boats and collecting the data a bench test was developed. The experiment allowed to collect variables such as speed, hydrodynamic drag, trim angle, sinkage, wetted area and wetted keel area. Due to some limitations on some of the instruments, only representative statistical data could be collected for speed, drag and trim angle, for which the respective inferential statistical

analyses are carried out. However, the other variables measured provided valuable information about the dynamic positioning of the boats at the intended speeds. The filtered data show, as expected, normal distributions for most of the runs, especially for the speed and drag. The trim angle, which was collected from the IMU, shows a more sensible response to the instantaneous changes in speed during the runs, specially at speeds over 12 m/s for the real scale. Runs at the maximum intended speed, which is 20 m/s for the real scale, show high variations specially for the speed and the trim angle, which may be due to the limitation of power of the electric engine and the high vibrational loads exerted over the bench test. However, the runs keep a symmetrical behavior that allow to average the results to carry out the ANOVA and multiple comparison tests without incurring in pseudoreplication.

From the ANOVA and multiple comparison tests for the drag and trim it can be observed that there is not statistical difference between the catamaran and the hysucat at any speed, which shows the hydrofoil did not produce any change in the catamaran behavior, not at least for the level of variability presented. In contrast, the average drag for the catamaran and hysucat starts being higher than for the monohull at speeds over 10 m/s, which is the speed of transition between the displacement and planing regimes. The differences in average drag for the catamaran and hysucat in comparison to the monohull starts being 12% higher at 10 m/s in comparison with the monohull and ends up being up to 36% higher at 20 m/s. These differences in average drag between the camataran and the monohull agree to what was found in the literature review. However, the drag reduction objective for the hysucat was not achieved. These results derived from the multiple comparison tests are reinforced by the obtained results with the linear regression analyses.

For the case of the positional variables, the monohull travels with a higher backward inclination at speeds higher than 15 m/s with average trim angles between 4 and 6.5°, which is the optimum according to the literature. In contrast, the catamaran and the hysucat travel almost horizontally with average trim angles between 1.5 and 2.5° at the same speeds. This higher backward inclination for the monohull allow it to have around half of the wetted area at speeds over 15 m/s in comparison to the catamaran and the hysucat. Furthermore, the wetted keel length for the monohull goes down to a 60% of its total length over 15 m/s, while the wetted keel lengths for the catamaran and the hysucat are kept to a 90% the total length of the catamaran/hysucat at speeds over 10 m/s. Other factors that contribute to the higher wetted area for the catamaran and the hysucat are: The inherent feature of the catamarans for having a higher wetted area than the monohulls according to the literature (Even though this should have been reduced by installing the hydrofoils); and the fact that the round chines allows the water sprays to follow the hull contour, which derives in the sides of the catamaran/hysucat hull to be completely wetted as well. This much higher wetted area for the catamaran/hysucat is, according to the theory, one of the main responsibles for the higher drag and general worse hydrodynamic performance in comparison to the monohull at planing speeds.

With respect to the Savitsky results, very high differences were obtained in comparison to the experimental results specially for the drag, with relative errors ranging from 14 to 133% for the monohull and 29 to 217% for the catamaran. For the trim angle, relative errors range from 18 to 60% for the monohull and 22 to 100% for the catamaran. For sinkage, wetted area and wetted keel length no different results are obtained, excepting for wetted area for the monohull at speeds beyond 15 m/s, where absolute errors fall to less than 10%. However, it would be good to increase the number of repetitions carried out for each treatment at each speed for sinkage, wetted area and wetted keel length for having statistical representative results. This heavily depends on the technology available for taking the photographs of the boats from one side. Assuming the Savitsky model was correctly implemented, the high differences of the experimental results in comparison to the Savitsky results show there was some error sources which affected the experiment, giving as a result increased values of hydrodynamic drag and different values in dynamic positioning variables. However, this large discrepancies does not invalidate the experimental results in the sense they are a comparison exercise and do not plan to give ground-truth values for the hydrodynamic performance.

For solving the problem of the water wetting the laterals of the catamaran/hysucat hull, unnecessarily increasing the wetted area of these geometries, it could be installed spray deflectors or hard chines similar to the monohull in order to deflect these water streams towards the laterals. The wetted area could be further decreased by tuning some hydrofoil parameters such as the angle of attach and plan area. These solutions might decrease the hysucat drag at planing speeds, but it is uncertain how much this reduction might be and again, the reduction should be more than 36% for it to be lower than the drag of the monohull.

Some signals of low statistical power due to few runs carried out for each treatment were identified, such as contradictions between the tests to check the fulfillment of the ANOVA assumptions; a disagreement between the ANOVA results and the Tukey-HSD results for one speed; and the p-values of the coefficients for the linear regression being higher than 0.05. Carrying more runs (at least 10 per treatment or hull geometry at each speed) would allow to determine with a much higher statistical confidence whether the hydrofoils do cause a change in the behavior of the catamaran at the expense of increasing the experiment cost and time. Nonetheless, this would not change the fact that the monohull has a much better hydrodynamic performance at planing speeds than the hysucat. For that to happen, the hydrofoils would have to reduce at least in a 36% the catamaran hydrodynamic drag at speeds beyond 10 m/s. Another way to increase the statistical confidence and improve the quality of collected data would be use a more robust test infrastructure that resist the better the vibrational loads and where external factors can be more certainly blocked. The ideal case would be to carry out the experiments in a towing tank certified by the ITTC, but the economic limitations of the project did not allow this.

References

Arcadis Nederland, B. and Jesyca, S. (2015). Plan maestro fluvial de colombia 2015. *Bogotá: Ministerio de Transporte de Colombia*.

Bertin, J. J. and Smith, M. L. (1998). *Aerodynamics for engineers*, volume 5. Prentice Hall New Jersey.

Broglia, R., Jacob, B., Zaghi, S., Stern, F., and Olivieri, A. (2014). Experimental investigation of interference effects for high-speed catamarans. *Ocean Engineering*, 76:75–85.

Bullard, N. (2019). Electric Car Price Tag Shrinks Along With Battery Cost.

Calle, G. M. (2016). Un río difícil. el magdalena: historia ambiental, navegabilidad y desarrollo. *Memorias. Revista Digital de Historia y Arqueología desde el Caribe*, (28):29–60.

Cames, M., Graichen, J., Siemons, A., and Cook, V. (2015). Emission reduction targets for international aviation and shipping. *Policy Department A: Economic and Scientific Policy, European Parliament, B-1047 Brussels*.

Candela speedboat (2018). Candela speedboat: the journey.

Cheemakurthy, H., Tanko, M., and Garme, K. (2017). Urban waterborne public transport systems: An overview of existing operations in world cities. Technical report.

Clement, E. P. and Blount, D. L. (1963). Resistance tests of a systematic series of planing hull forms. *David Taylor Model Basin, Department of the Navy, Research and Development Report, Report 1314, Hydromechanics Laboratory, Washington DC, USA, Published by: The Society of Naval Architects and Marine Engineers, Paper No. 10*.

Comission, T. E. (2017). Work Programme 20182020: 11. *Smart, green and integrated transport, LC-MG-1-11-2019: Structuring R&I towards zero emission waterborne transport*, 27:2018–2020.

Davidson, G., Roberts, T., Friezer, S., Davis, M., Bose, N., Thomas, G., Binns, J., and Verbeek, R. (2011). Maximising efficiency and minimising cost in high speed craft. In *International Conference on Fast Sea Transportation*, volume 11, pages 727–734.

Day, A., Cameron, P., and Nixon, E. (2017). Moderate-cost approaches for hydrodynamic testing of high performance sailing vessels. In *INNOVSAIL International Conference on Innovation in High Performance Sailing Yachts*, pages 173–182.

De Luca, F. and Pensa, C. (2017). The naples warped hard chine hulls systematic series. *Ocean Engineering*, 139:205–236.

Ebbert, C. (2017). Seabubbles, a new hydrofoil taxi for city rivers.

Ekman, F., Ribas, C. N., and Rydelius, F. (2016). Model for predicting resistance and running attitude of high-speed craft equipped with interceptors. *Royal Institute of Technology, Stockholm.*

European Comission (2018). *Statistical pocketbook 2018: EU transport in figures.* European Comission.

European Comission (2020). Inland waterways: What do we want to achieve?

Faison, L. A. (2014). *Design of a high speed planing hull with a cambered step and surface piercing hydrofoils.* PhD thesis, Massachusetts Institute of Technology.

Faltinsen, O. M. (2005). *Hydrodynamics of high-speed marine vehicles.* Cambridge university press.

Fridsma, G. (1969). A systematic study of the rough-water performance of planing boats. Technical report, Stevens Inst Of Tech Hoboken Nj Davidson Lab.

Frisk, D. and Tegehall, L. (2015). Prediction of high-speed planing hull resistance and running attitude-a numerical study using computational fluid dynamics. Master's thesis.

Fu, T., Brucker, K., Mousaviraad, S., Ikeda, C., Lee, E., O'shea, T., Wang, Z., Stern, F., and Judge, C. (2014). An assessment of computational fluid dynamics predictions of the hydrodynamics of high-speed planing craft in calm water and waves. In *30th Symposium on Naval Hydrodynamics*, pages 2–7.

Gerdsen, H. G. and Jabbusch, W. (1987). Foil arrangement for a planning craft. US Patent 4,665,853.

Giraldo-Pérez, E., Gaviria, G., Betancur, E., Osorio-Gómez, G., and Mejía-Gutiérrez, R. (2020). Influence of energy consumption on battery sizing of electric fluvial vessels: a colombian case study. In *2020 Fifteenth International Conference on Ecological Vehicles and Renewable Energies (EVER)*, pages 1–8. IEEE.

Gutiérrez Pulido, H. and Salazar, V. (2004). Análisis y diseño de experimentos.

Higgins, A., Restrepo, J. C., Ortiz, J. C., Pierini, J., and Otero, L. (2016). Suspended sediment transport in the magdalena river (colombia, south america): Hydrologic regime, rating parameters and effective discharge variability. *International Journal of Sediment Research*, 31(1):25–35.

Holtrop, J. and Mennen, G. (1982). An approximate power prediction method. *International Shipbuilding Progress*, 29(335):166–170.

Honaryar, A., Ghiasi, M., Liu, P., and Honaryar, A. (2021). A new phenomenon in interference effect on catamaran dynamic response. *International Journal of Mechanical Sciences*, 190:106041.

Hoppe, K. (2001). Recent applications of hydrofoil-supported-catamarans. *Fast Ferry International*, 36.

Hoppe, K.-G. (1989). *The HYSUCAT development*. Department of Mechanical Engineering, University of Stellenbosch.

Hoppe, K.-G. W. (1986). Catamaran with hydrofoils. US Patent 4,606,291.

Hu, J., Zhang, Y., Wang, P., and Qin, F. (2020). Numerical and experimental study on resistance of asymmetric catamaran with different layouts. *Brodogradnja: Teorija i praksa brodogradnje i pomorske tehnike*, 71(2):91–110.

International Towing Tank (2002). Recommended procedures and guidelines-01-01: Model manufacture ship models.

International Towing Tank (2008). Recommended Procedures and Guidelines 7.5-02-05-01: Testing and Extrapolation Methods High Speed Marine Vessels Resistance Test.

Jean Vaucher (2014). History of ships: Prehistoric craft.

Kandasamy, M., Ooi, S. K., Carrica, P., Stern, F., Campana, E. F., Peri, D., Osborne, P., Cote, J., Macdonald, N., and de Waal, N. (2011). Cfd validation studies for a high-speed foil-assisted semi-planing catamaran. *Journal of marine science and technology*, 16(2):157–167.

Khazaee, R., Rahmansetayesh, M. A., and Hajizadeh, S. (2019). Hydrodynamic evaluation of a planing hull in calm water using rans and savitsky's method. *Ocean Engineering*, 187:106221.

Kim, D. J., Kim, S. Y., You, Y. J., Rhee, K. P., Kim, S. H., and Kim, Y. G. (2013). Design of high-speed planing hulls for the improvement of resistance and seakeeping performance. *International Journal of Naval Architecture and Ocean Engineering*, 5(1):161–177.

Kim, S.-W., Lee, G.-W., and Seo, K.-C. (2018). The comparison on resistance performance and running attitude of asymmetric catamaran changing shape of tunnel stern exit region. In *IOP Conference Series: Materials Science and Engineering*, volume 383, page 012047. IOP Publishing.

L. Blount, D. and L. Fox, D. (1976). Small-Craft Power Prediction. *Marine Technology*, 13:14–45.

Latorre, R. (1997). Ship hull drag reduction using bottom air injection. *Ocean engineering*, 24(2):161–175.

Lee, T.-S. (1982). Interference factor for catamaran planing hulls. *AIAA Journal*, 20(10):1461–1462.

Liu, C. Y. and Wang, C. T. (1979). Interference effect of catamaran planing hulls. *Journal of Hydronautics*, 13(1):31–32.

Mejia-Gutierrez, R., Osorio-Gomez, G., Montoya, J. A., Velásquez-López, A., Restrepo, A. E. D., Laverde, J. V. R., Espíndola, D. T. M., Sierra, J. E., Salgado, B. A. M., López, J., Betancur-Valencia, E., Fernandez-Montoya, M., Correa-Herrera, H., Figueroa, M., Rodríguez, M., Mesa, G. J. E., Oviedo, E. S. G., Giraldo-Perez, E., Rio, S. B. D., Gómez, C. V., Pineda, J. D. M., Correa, S. E., Botero, C. R., Restrepo, L. B., Botero, D. V., álvarez, M. E., Pérez, J. F., García, J. D., Pérez, M. A. Z., Ruíz, L. F., Montoya, M. X. A., Correa, M. O., Bedoya, M. P., C, M. J. F., Silva, S. B., Alzate, L. F., Barrientos, J. D., Mass, E. P., Ramirez, L., Gaviria, J. D., Medina, B., Sierra, J. E., Márquez, J., and González, J. P. (2021). Diseño de detalle - Embarcación Electro-Solar para movilidad fluvial. Technical report, Universidad EAFIT, Medellín.

Mira, J.-D., Valderrama, S., Londoño, M.-J., Giraldo-Pérez, E., Betancur, E., Osorio-Gómez, G., and Mejía-Gutiérrez, R. (2020). Preliminary design tools applied to a solar powered vessel design: a south american river analysis. In *2020 Fifteenth International Conference on Ecological Vehicles and Renewable Energies (EVER)*, pages 1–9. IEEE.

Molland, A. F., Turnock, S. R., and Hudson, D. A. (2017). *Ship resistance and propulsion*. Cambridge university press.

Morabito, M. G. (2011). Experimental investigation of the lift and interference of asymmetric planing catamaran demi-hulls. In *Proceedings of the 11th International Conference on FAST2011.*

Müller-Graf, B. (1989). Resistance and propulsion characteristics of the vws hard chine catamaran hull series 89. *Versuchsanstalt für Wasserbau und Schiffbau, Berlin.*

Najafi, A., Aliakbari, T., and Hashemi, S. A. (2019). Experimental optimization of hydrodynamic performance of catamarans using hydrofoil element. *Proceedings of the Institution of Mechanical Engineers, Part M: Journal of Engineering for the Maritime Environment*, 233(2):488–501.

Najafi, A. and Nowruzi, H. (2019). On hydrodynamic analysis of stepped planing crafts. *Journal of Ocean Engineering and Science*.

No Frills Sailing (2021). Hard chines in sailboat design.

Ozden, M. C. and Demir, E. (2009). The successful design and construction of solar/electric boats nusrat and muavenet: An overview. In *Ever Monaco 2009 Conferences on Ecological Vehicles and Renewable Energies*, pages 27–29. Citeseer.

Restrepo, J. D., Escobar, R., and Tosic, M. (2018). Fluvial fluxes from the magdalena river into cartagena bay, caribbean colombia: Trends, future scenarios, and connections with upstream human impacts. *Geomorphology*, 302:92–105.

Restrepo, J. D., Kettner, A. J., and Syvitski, J. P. (2015). Recent deforestation causes rapid increase in river sediment load in the colombian andes. *Anthropocene*, 10:13–28.

Russell, J. (2015). Spray rails and lifting strakes.

Savitsky, D. et al. (1964). Hydrodynamic design of planing hulls. *Marine Technology and SNAME News*, 1(04):71–95.

Savitsky, D. and Morabito, M. (2010). Surface wave contours associated with the forebody wake of stepped planing hulls. *Marine Technology*, 47(1):1–16.

Seif, M. S. and Amini, E. (2004). Performance comparision between planing monohull and catamaran at high froude numbers.

Sherman, T. and Fisher, P. A. (1975). A study of planing catamaran hull and tunnel interactions. Technical report, MICHIGAN UNIV ANN ARBOR SHIP HYDRODYNAMICS LAB.

Skene, N. L. (1973). *Skene's elements of yacht design, 8th ed.* Dodd, Mead.

solar boat race, T. (2018). A brief history of solar boat racing.

Solar Splash (2012). The 2012 DONG Enery Solar Challenge.

Souto-Iglesias, A., Fernández-Gutiérrez, D., and Pérez-Rojas, L. (2012). Experimental assessment of interference resistance for a series 60 catamaran in free and fixed trim-sinkage conditions. *Ocean Engineering*, 53:38–47.

Sponberg, E. W. (2011). The design ratios. *A Naval Architect's Dozen (or thereabouts). Revised.*

Srinakaew, S. (2017). *A numerical study of resistance components of high-speed catamarans and the scale effects on form factor*. PhD thesis, University of Southampton.

Stopford, M. (2008). *Maritime economics 3e*. Routledge.

Sukas, O. F., Kinaci, O. K., Cakici, F., and Gokce, M. K. (2017). Hydrodynamic assessment of planing hulls using overset grids. *Applied Ocean Research*, 65:35–46.

Thomas, G., Tomic, P., and Tuite, A. (2007). High-speed catamaran or monohull? how do you choose? *Ships and Offshore Structures*, 2(2):137–147.

Tuck, E. O. and Lazauskas, L. (1998). Optimum hull spacing of a family of multihulls. *Ship Technology Research-Schiffstechnik*, 45(4):180.

Union Internationale des Transports Publics (2013). WATERBORNE TRANSPORT, A UNIQUE CONTRIBUTION TO ENHANCING MOBILITY FOR CITIES ON WATER.

Vellinga, R. (2009). *Hydrofoils: Design, Build, Fly*. Peacock Hill Publishing.

Wyman, D. B. (1998). Wyman's Formula.

Yengejeh, M. A., Amiri, M. M., Mehdigholi, H., Seif, M. S., and Yaakob, O. (2016). Numerical study on interference effects and wetted area pattern of asymmetric planing catamarans. *Proceedings of the Institution of Mechanical Engineers, Part M: Journal of Engineering for the Maritime Environment*, 230(2):417–433.

Yousefi, R., Shafaghat, R., and Shakeri, M. (2013). Hydrodynamic analysis techniques for high-speed planing hulls. *Applied Ocean Research*, 42:105–113.

Yousefi, R., Shafaghat, R., and Shakeri, M. (2014). High-speed planing hull drag reduction using tunnels. *Ocean engineering*, 84:54–60.

Yun, L. and Bliault, A. (2012). Hydrofoil Craft. In *High Performance Marine Vessels*, pages 161–202. Springer.

Yun, L., Bliault, A., and Rong, H. Z. (2018). *High Speed Catamarans and Multihulls: Technology, Performance, and Applications*. Springer.

Zaghi, S., Broglia, R., and Di Mascio, A. (2011). Analysis of the interference effects for high-speed catamarans by model tests and numerical simulations. *Ocean Engineering*, 38(17-18):2110–2122.

Appendix A

Sketch drawings of the catamaran hull and the hydrofoils

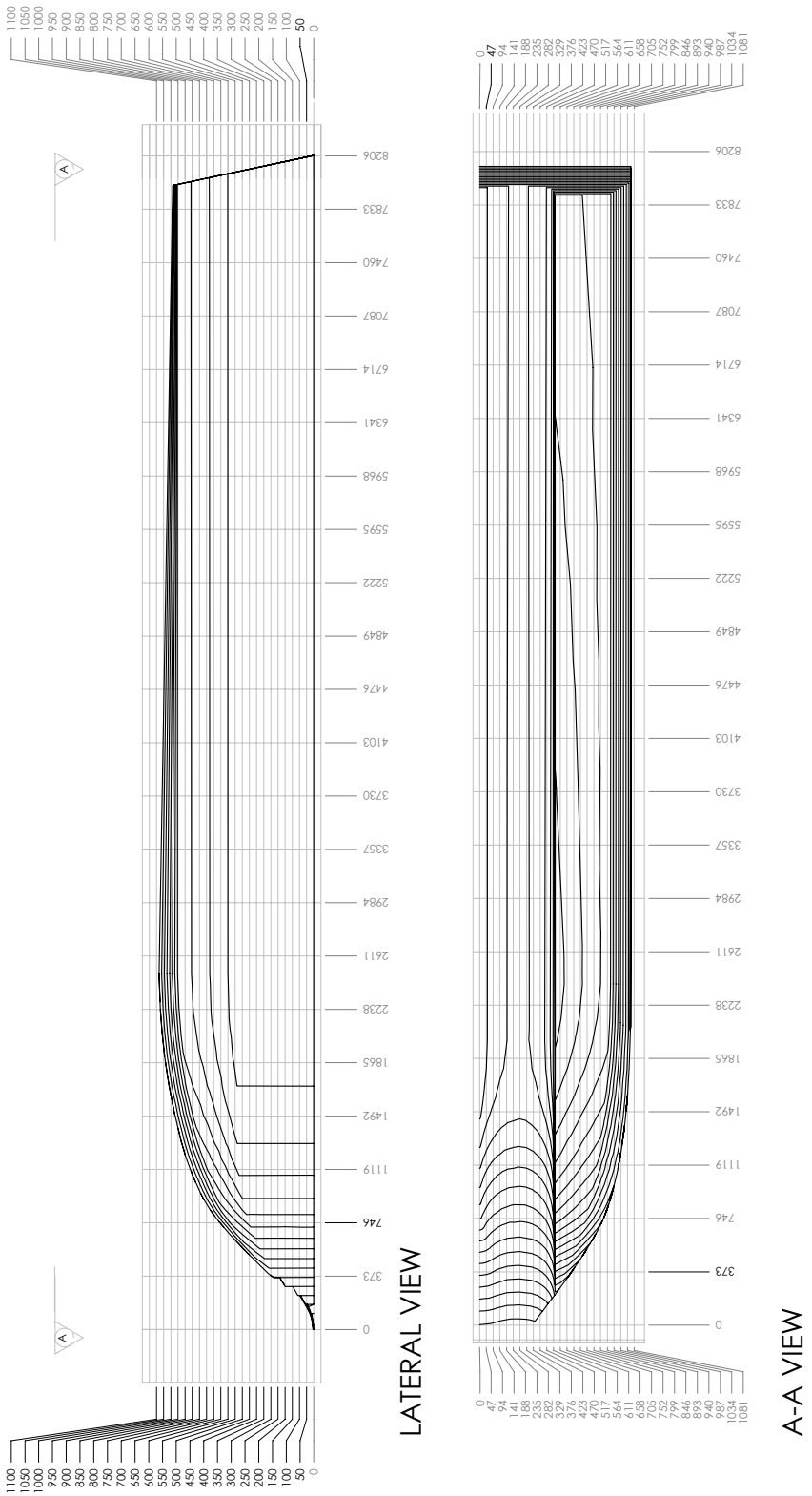

Figure A.1: Catamaran hull longitudinal Body plans.

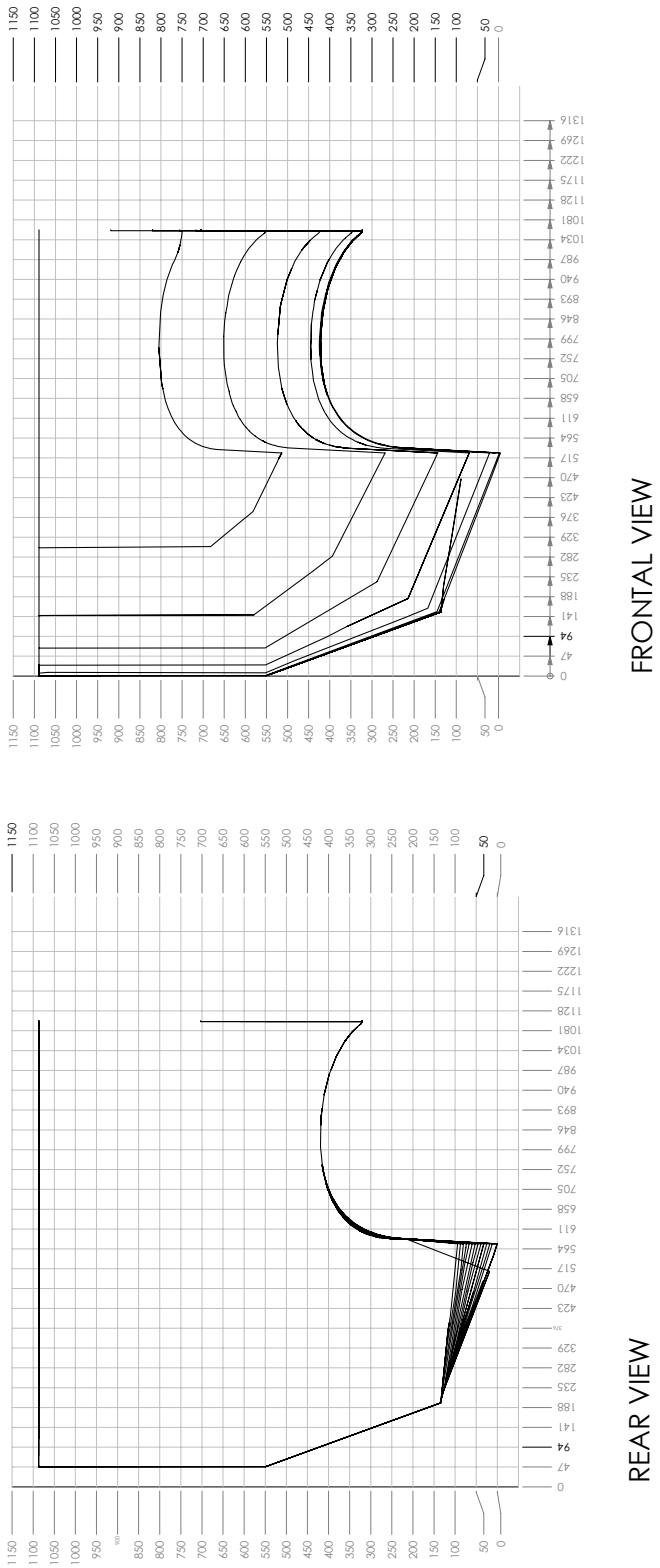

Figure A.2: Catamaran hull frontal and rear body plans.

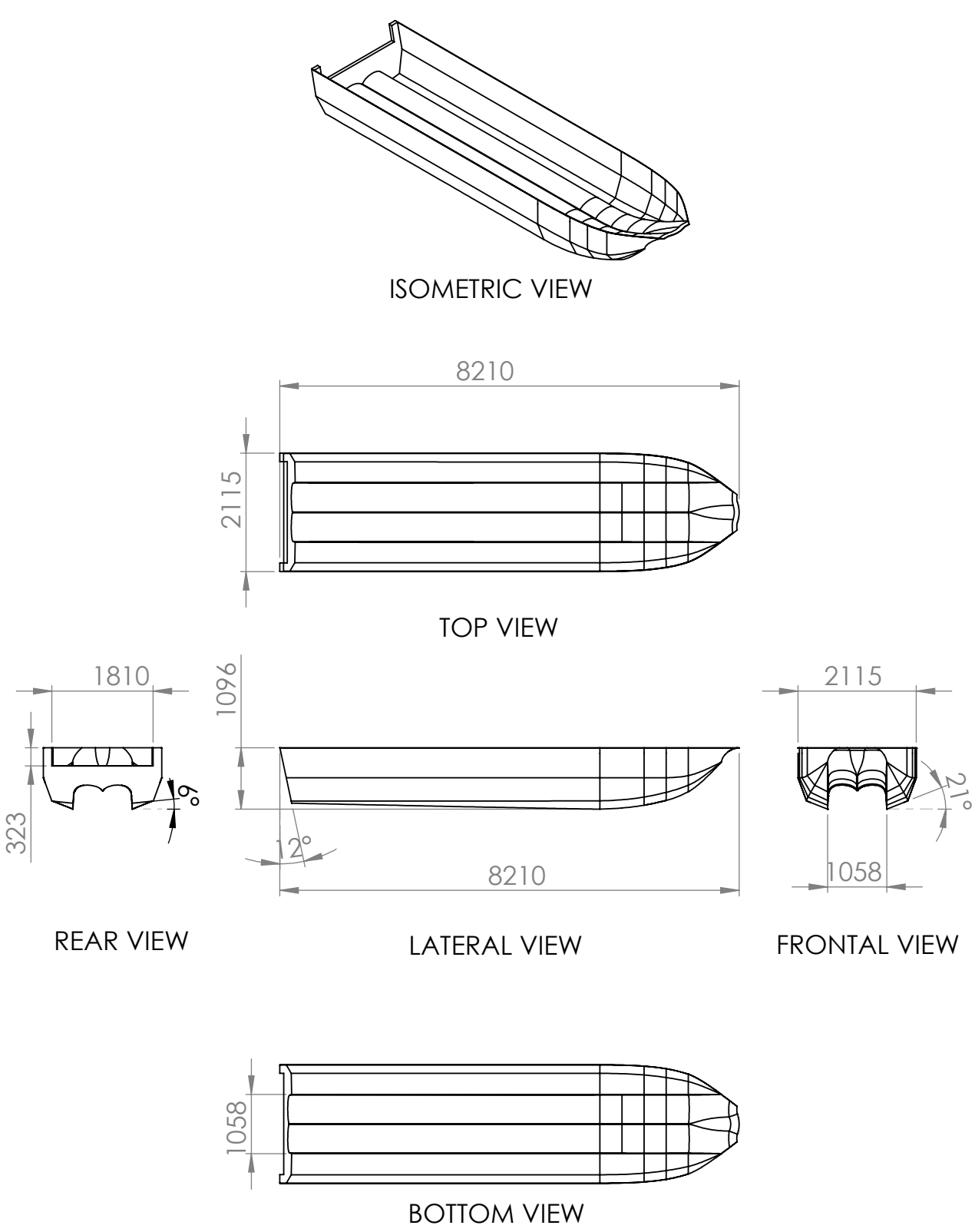

Figure A.3: Catamaran hull sketch drawings.

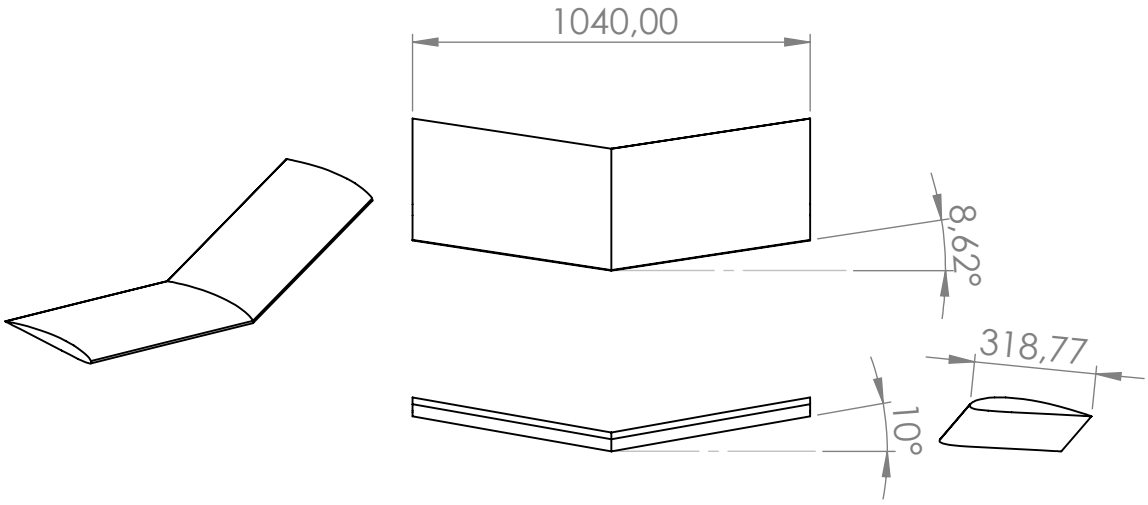

Figure A.4: Main hydrofoil sketch drawings.

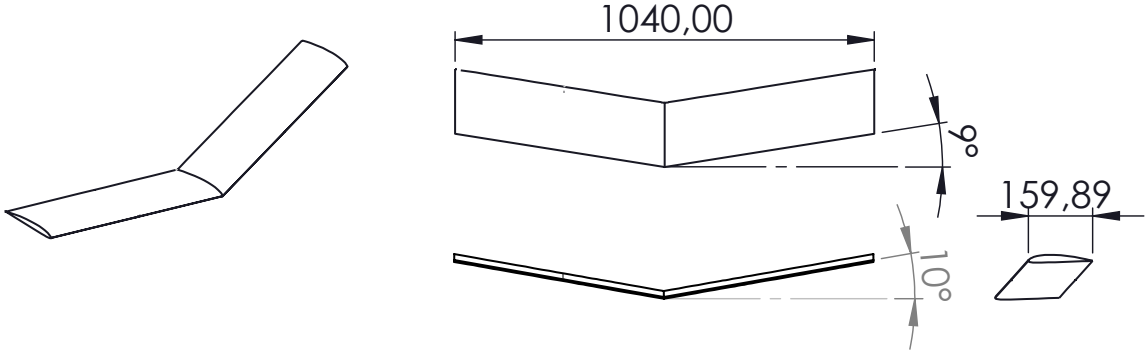

Figure A.5: Rear hydrofoil sketch drawings.

Appendix B

Visualizations of the collected data

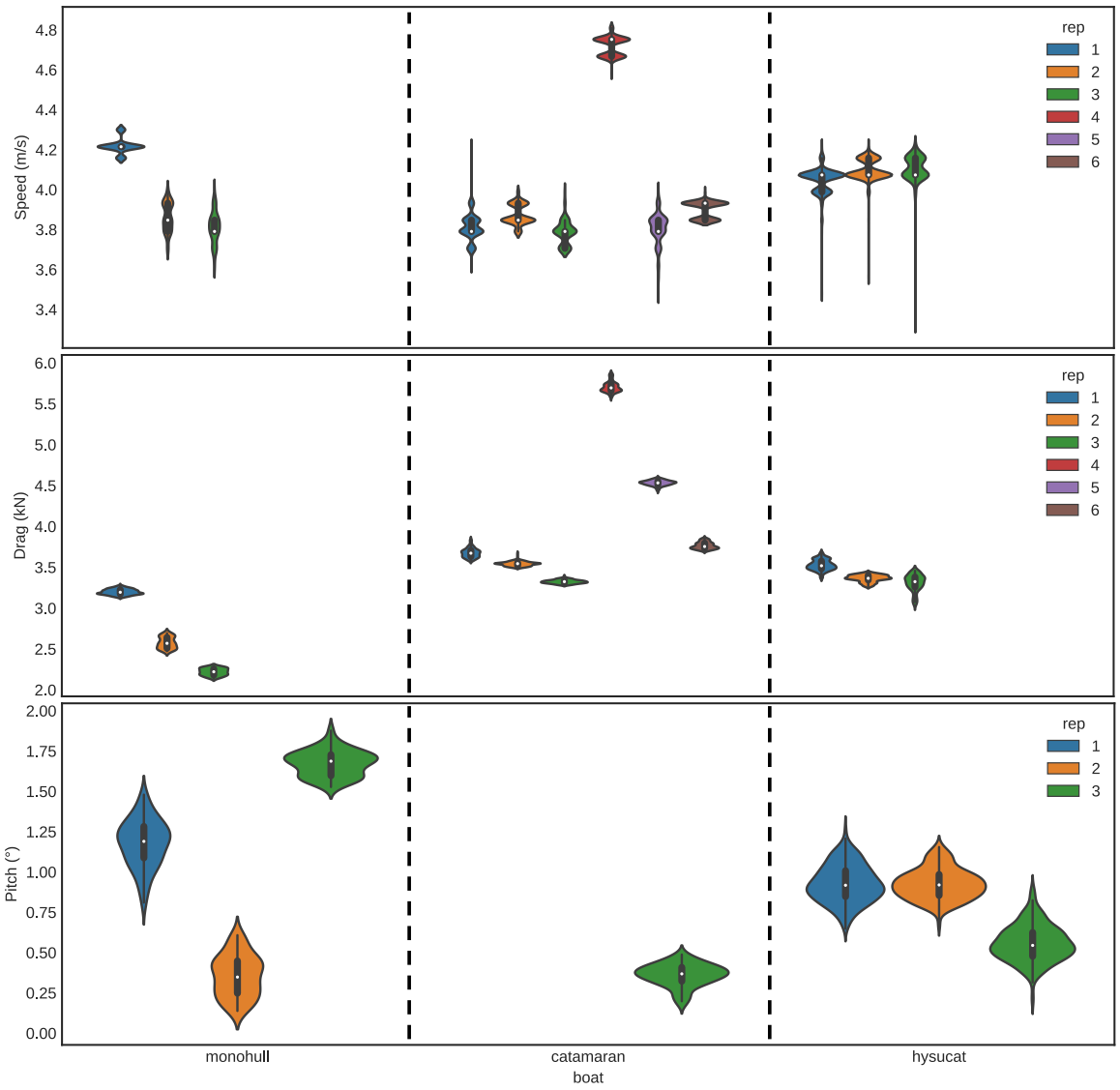

Figure B.1: Violin plots for speed, drag and trim angle (pitch) for the three boats at a intended speed of 4 m/s.

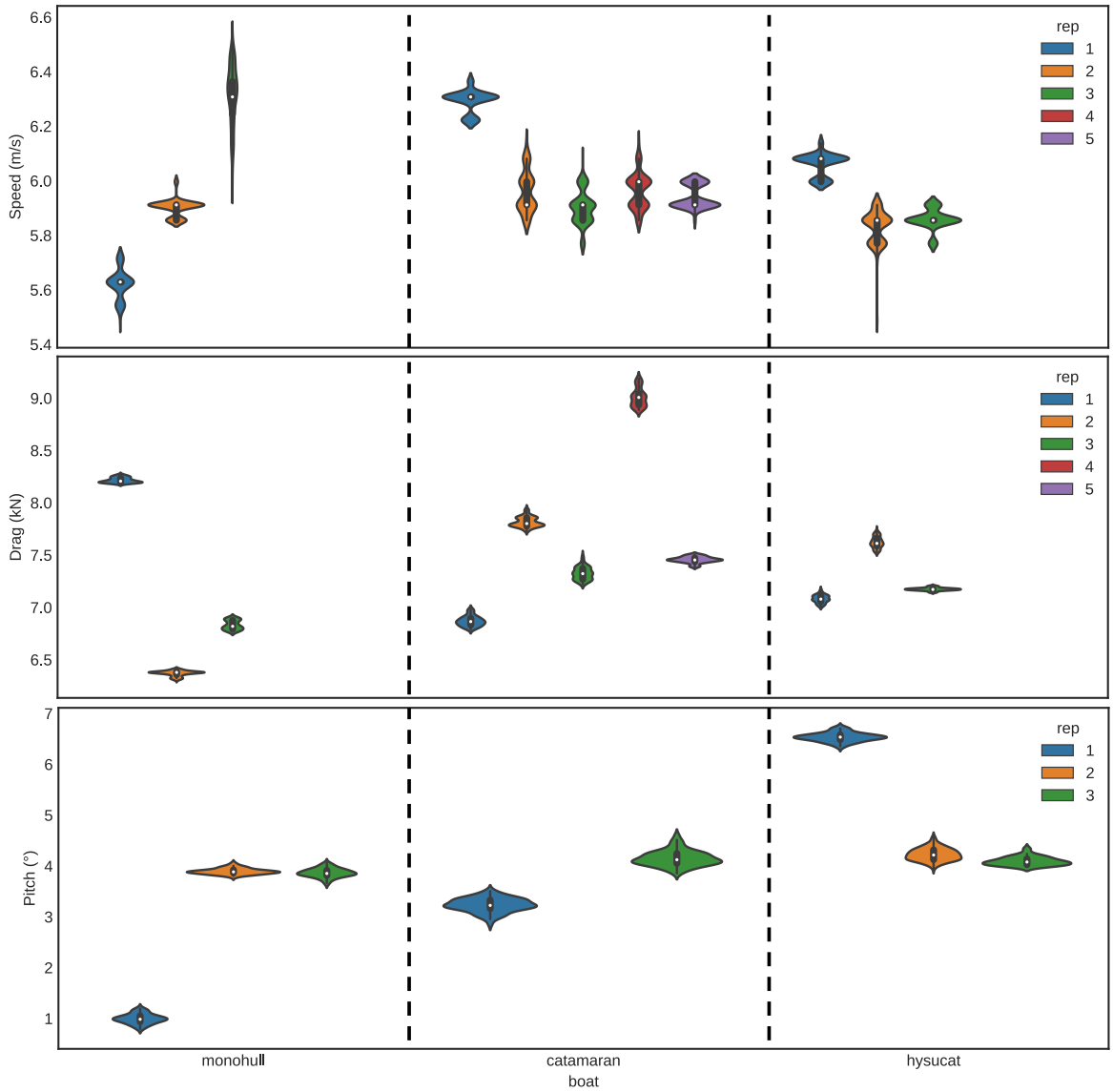

Figure B.2: Violin plots for speed, drag and trim angle (pitch) for the three boats at a intended speed of 6 m/s.

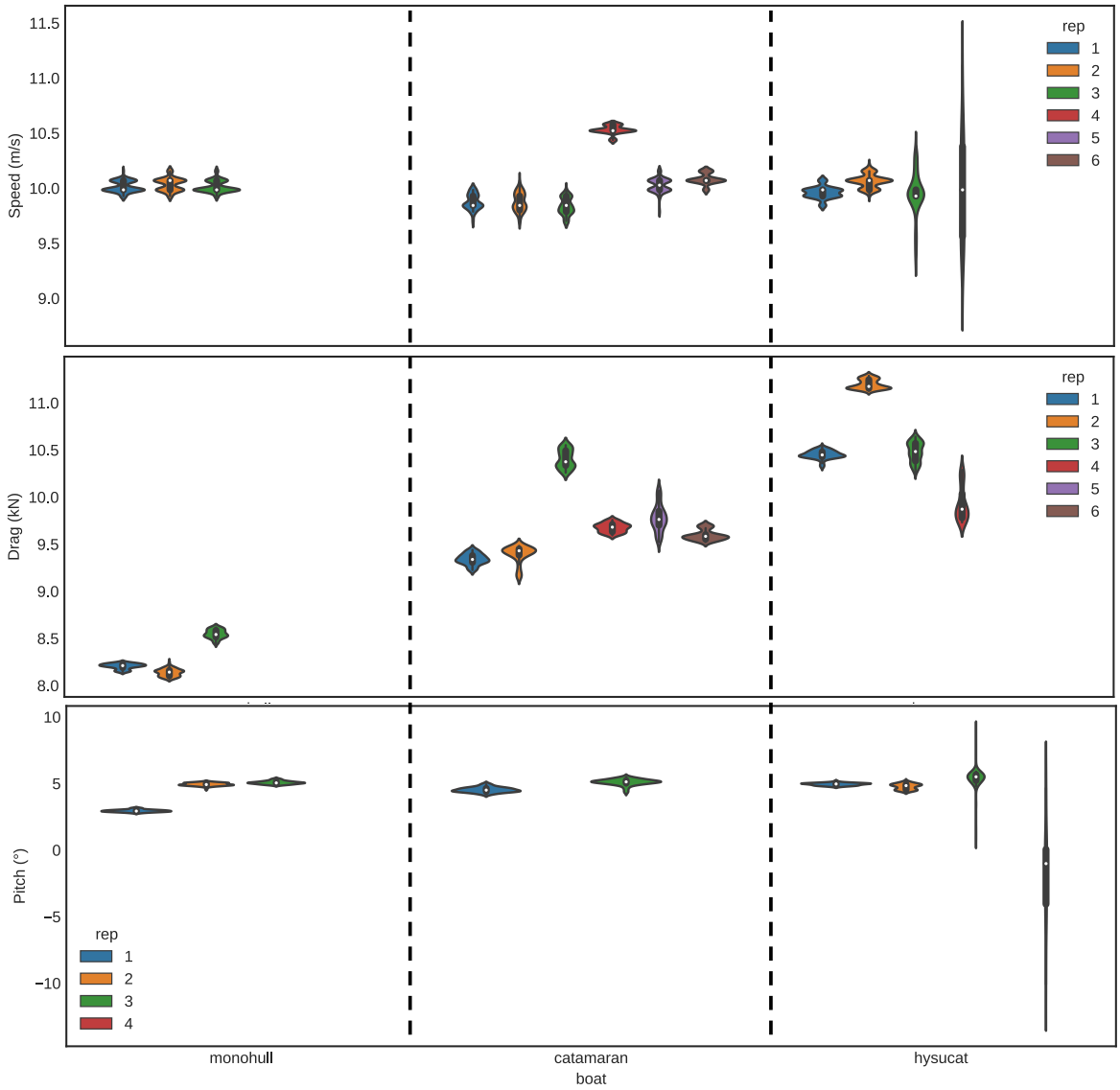

Figure B.3: Violin plots for speed, drag and trim angle (pitch) for the three boats at a intended speed of 10 m/s.

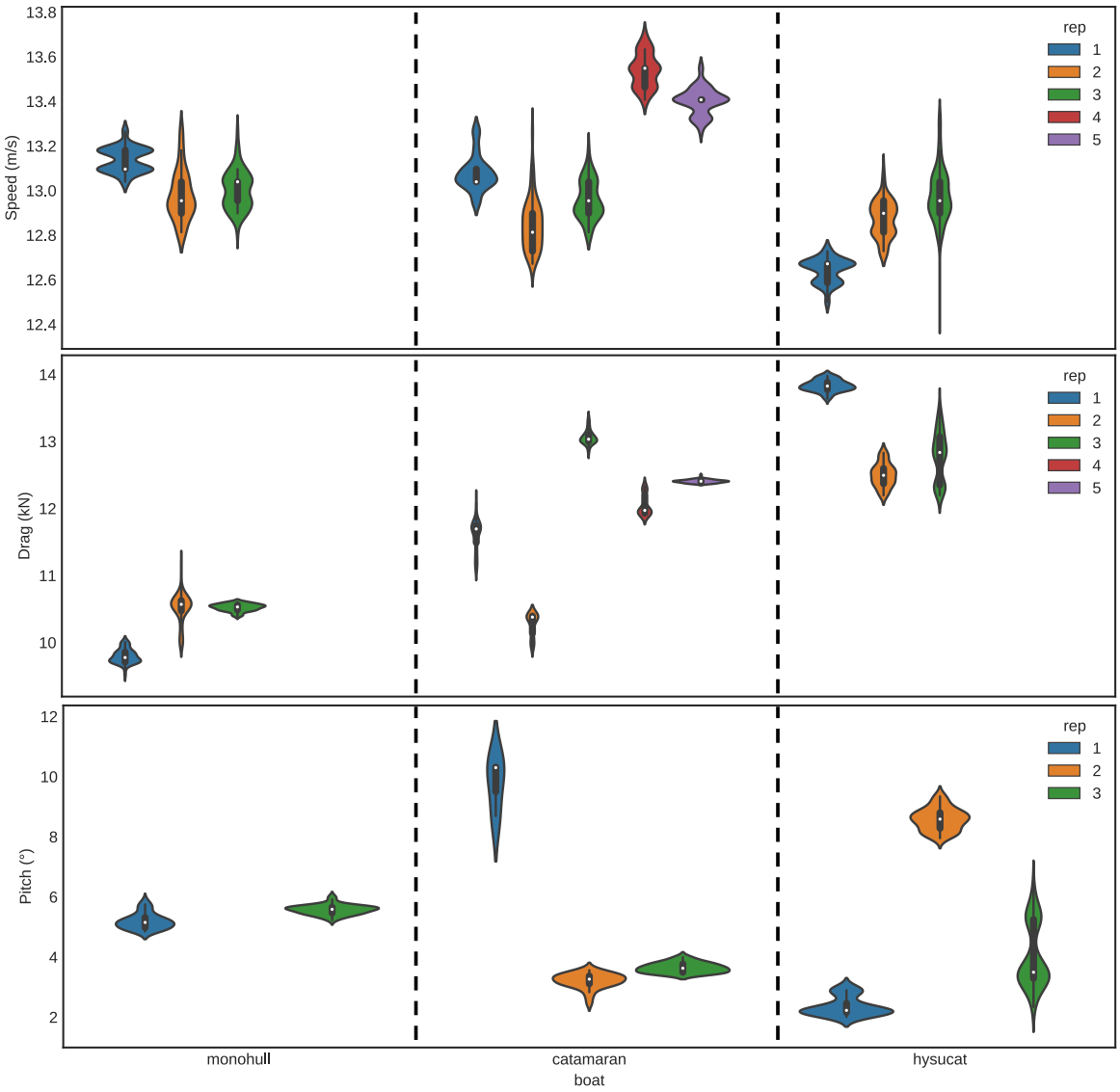

Figure B.4: Violin plots for speed, drag and trim angle (pitch) for the three boats at a intended speed of 13 m/s.

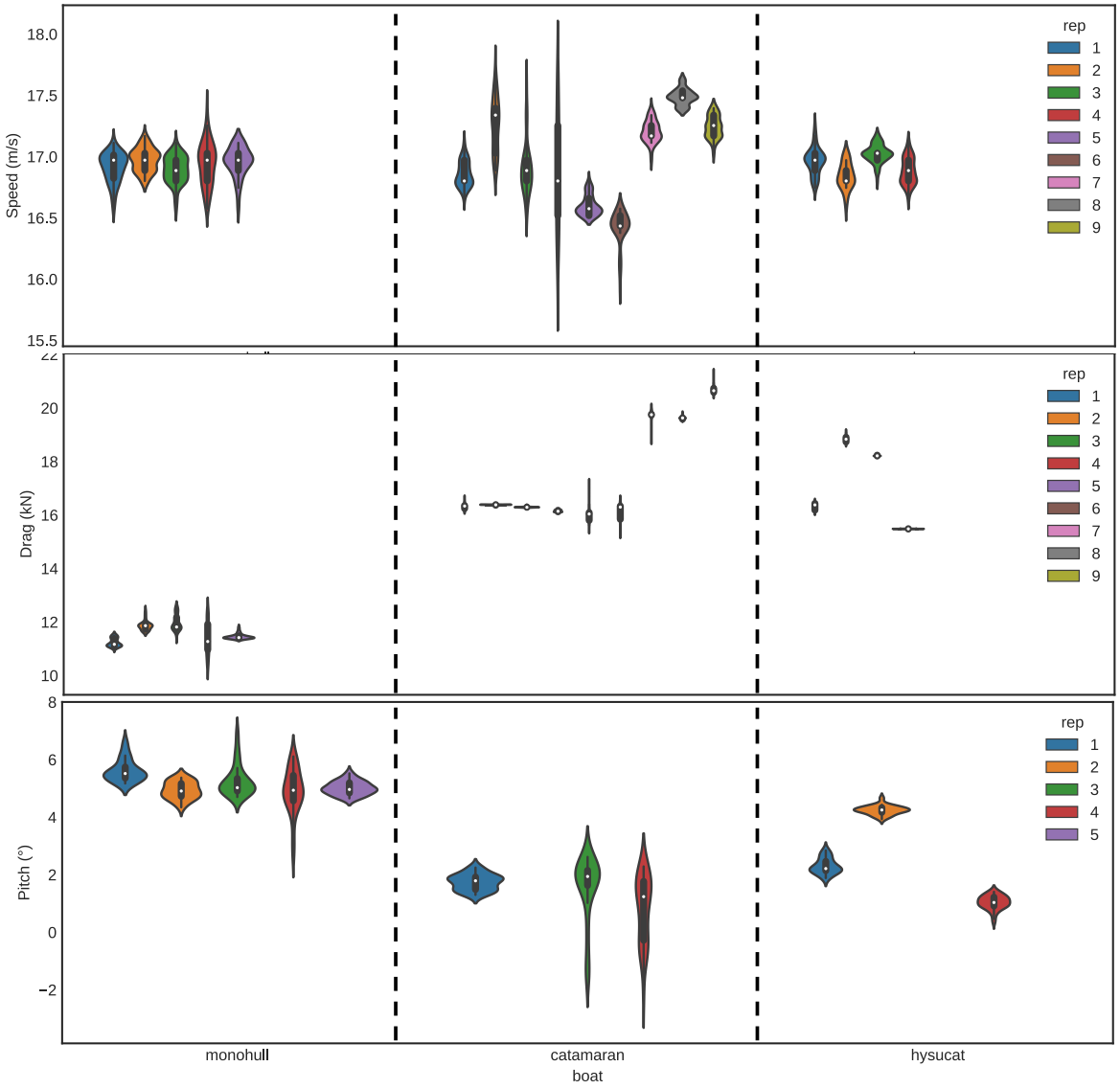

Figure B.5: Violin plots for speed, drag and trim angle (pitch) for the three boats at a intended speed of 17 m/s.

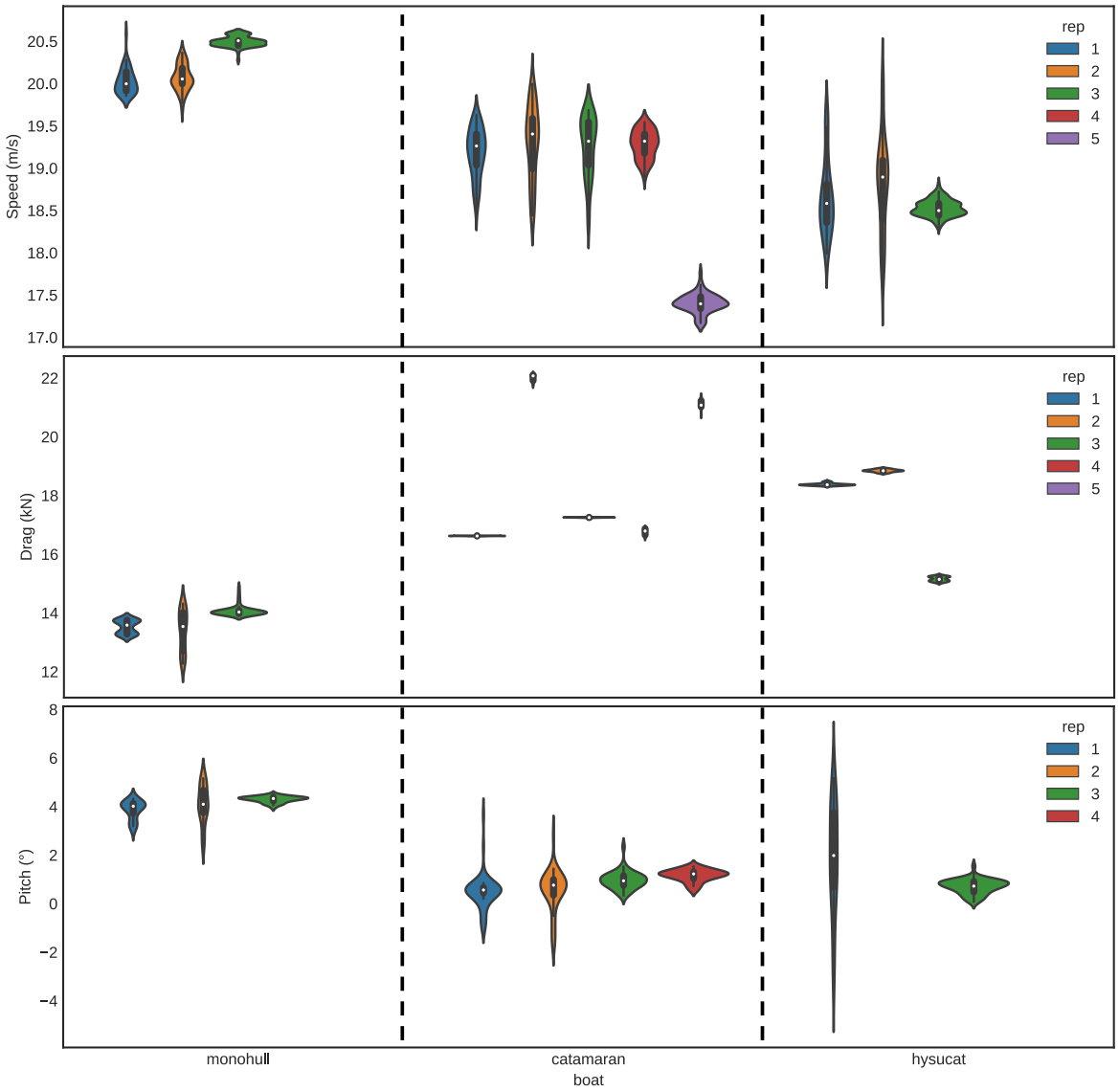

Figure B.6: Violin plots for speed, drag and trim angle (pitch) for the three boats at a intended speed of 6 m/s.

Appendix C

Script of Savitsky model

Authors of the code: Erick Giraldo, Esteban Betancur

Language: Python 3.0

C.1 Main code

```
import numpy as np
from scipy.optimize import fsolve

def Drag_Sav(mass, b, beta, l_cg, rho, nu, f, eps, v, r, A,
    eta_T = 0.95, eta_D = 0.7, eta_eng = 0.96):
    """
    Function for calculating drag, power and boat position according to
    Savistsky method.
    Savistsky originally calculates the effective power.

    Source of model: Daniel Savistsky, 1964,
        'Hydrodynamic design of planing hulls'.
    Source with an easier explanation: Molland,
        'Ship resistance and propulsion', page 216.
    Source for catamarans adaptation: 1979,
        'Interference effect of catamaran planing hulls'.

    Input arguments:
```

```
    mass: Boat mass (kg)
    b: Mean chine beam (m)
    beta: Deadrise angle (degrees)
    l_cg: Longitudinal center of gravity (m)
    rho: water density (kg/m3)
    nu: Kinematic viscosity of water (-)
    v: Boat speed (m/s)
    f: Perpendicular distance from thrust line to CG (m)
    eps: Thrust line angle with respect to keel (Degrees). if f and eps are
        zero, thrust line passes through cg and parallel to keel
    A: Interference factor due to demihulls [-]. 1 for a monohull
    r: Separation ratio due to demihulls [-]. 1 for a monohull
    eta_T: Transmission efficiency [0-1] (-)
    eta_D: Quasi-propulsive coefficient [0-1] (-)

Output arguments:
    tao: Angle of trim (Degrees)
    d: Draft of the keel at transom (m)
    T: Trust. Calculated with the effective power. (kN)
    inst_kw: Installer power (kW)
    R_t: Total resistance (kN)
    S: Wetted area (m2)
    lk: Wetted keel length (m)
    lm: Mean keel wetted length (m)
    lp: Distance from keel-transom to longitudinal center of pressure (m)

"""
c_v = v/np.sqrt(9.81*b) # Coefficient of  viscous resistance.
c_lbeta = mass*9.81 / (0.5*rho*b**2*v**2) # Lift coefficient of
    # a warped surface.

Eq1 = lambda c_l0 : c_lbeta - c_l0 + 0.0065*beta*c_l0**0.6 # equation for
    #calculating c_l0.
c_l0_initial_guess = 0.5
c_l0 = fsolve(Eq1, c_l0_initial_guess)[0] # Lift coefficient o a
```

```
 # flat surface


# Iterative calculation
tao = 0
delta_M = -1

while delta_M<=0.0:

    tao += 1e-2
    Eq2 = lambda lamb : c_l0 - \
    (tao**1.1*r**(3/2))*((0.012*lamb**0.5)/A +\
        0.0055*lamb**(2.5)*A/((c_v**2)*r)) # Equation for calculating
            # lambda.
    lamb = fsolve(Eq2, 1)[0]
    lm = lamb*b
    lp = lm * (0.75 - 1/(5.21*((c_v/lamb)**2)*(r/A**2) + 2.39))

    re = v*lm/nu
    cf = 0.075/(np.log10(re)-2)**2    # coefficient of frictional
        # resistance

    if A == 1 and r == 1:  # If the boat is a monohull, then...
        S = lm*b/(np.cos(np.deg2rad(beta))) # wetted surface area for
            # a monohull
    else:   # If these values are different from 1, then it is a catamaran
        S = b**2*((r/np.cos(np.deg2rad(beta))) +\
        2*lamb*np.tan(np.deg2rad(tao)))

    Df = 0.5*rho*S*v**2*cf # drag due to frictional resistance

    T = (mass*9.81*np.sin(np.deg2rad(tao))+Df)/\
    1000*np.cos(np.deg2rad(eps))  # thrust [kN]
    N = mass*9.81*np.cos(np.deg2rad(tao))/1000\
    - T*np.sin(np.deg2rad(eps))
```

```
        PT_L =  l_cg * np.sin(np.deg2rad(eps)) + f # perpendicular vertical
            # distance from point p from where moments
            # are calculated to thrust line

        delta_M = -N*lp + mass*9.81*l_cg/1000 -\
            T*PT_L*(np.cos(np.deg2rad(eps)) + \
            np.sin(np.deg2rad(eps))*np.cos(np.deg2rad(90-eps)))

    lk = (1/2) * ( (b/np.pi)*\
        (np.tan(np.deg2rad(beta))/np.tan(np.deg2rad(tao    ))) + lm )
            # Wetted keel length.
            # lk results from combining equations 3 and 5 from "hydrodynamic
            # design of planing hulls" by savistky.

    d = lk*np.sin(np.deg2rad(tao)) # Draft of the keel at transom
        kCG = VCG*np.cos(tao) + np.sin(tao)*\
            ( l_cg-v_cg*np.tan(tao))# [m] Vertical
                # distance from keel-transom intersection to CG.
                #Equation found trough geometric calculations.

    R_t = T*np.cos(np.deg2rad(tao+eps)) # total drag [kN]
    P_e = R_t*v # effective power [kW]

    inst_kw = P_e * (1/eta_D) * (1/eta_T) * (1/eta_eng)  # installed power [kW]

    # print(lm, lk, lamb)

    return([tao, d, T, inst_kw, R_t, S, lk, lm, lp])

def speedIterSav(mass, b, beta, l_cg, rho, nu, f, eps, speeds, r, A, SF):
    ''' Function for calculating savitsky variables at different speeds

    Input variables
    ---------------
      mass, b, beta, l_cg, rho, nu, f, eps, r and A are the same variables
```

```
    defined in the Savitsky function
  speeds: range of speeds to be the function evaluated in
  SF: Safety factor for accounting for several other resistance factors,
      like waves, wind gusts, etc. Some sources mention that it should be
      1.2

Output variables
---------------
  results_sav_df: Dataframe containing the variables from Savitsky

'''

# Calculating results in the range of speeds
results_sav = [sd.Drag_Sav(mass, b, beta, l_cg, rho, nu, f, eps, v, r, A)\
                     for v in speeds]
results_sav_df = pd.DataFrame(results_sav).round(2)
results_sav_df.columns = ['Tao', 'd', 'T', 'inst_kw', 'R_t', 'S', 'lk', 'lm',
    'lp']
results_sav_df.index = speeds
results_sav_df.index.name = 'Speed'

results_sav_df[['inst_kw', 'R_t', 'Tao']] = \
results_sav_df[['inst_kw', 'R_t', 'T']] * SF

return results_sav_df.round(2)
```

C.2 Inputs for the monohull

```
SF = 1    # Safety factor. Extracted from the iterative battery weight

mass = 4500 #mass: Boat mass (kg) In the experiments, the scaled mass
            # was slightly higher than 8.7 kg
b =  1.7 #b: Mean chine beam (m).
beta = 10.9 #beta: Deadrise angle (Ã°)
```

```
loa = 7.91
l_cg = loa*0.4 #l_cg: Longitudinal center of gravity (m)
rho = 1000 #rho: water density (kg/m3)
nu = 1.19e-6 #nu: Kinematic viscosity of water (m2/s)
A = 1   # interference factor [-]. 1 for a monohull
r = 1   # Separation ratio [-]. 1 for a monohull
f = 0 # perpendicular distance from cg to thrust line (m)
eps = 0 # angle of thrust line measured from keel (Â°)

speeds = range(1,21)

emp13px_resultsSav = speedIterSav(mass, b, beta, l_cg, rho, nu, f, eps, speeds,
                r, A, SF)
```

C.3 Inputs for the catamaran

```
# parameters for iterative sizing

SF = 1 # Safety factor. Extracted from the iterative battery weight

#Parameters for the catamaran

mass = 4500 #mass: Boat mass (kg)
b =  1.84 #b: Mean chine beam (m)
beta = 17 #beta: Deadrise angle at amidship (Â°)
loa = 7.9
l_cg = loa*0.4 #l_cg: Longitudinal center of gravity (m)
rho = 1000 #rho: water density (kg/m3)
nu = 1.19e-6 #nu: Kinematic viscosity of water (m2/s)
f = 0 # perpendicular distance from cg to thrust line (m)
eps = 0 # angle of thrust line measured from keel (Â°)
A = np.sqrt(2)   # interference factor [-]. np.sqrt(2) for a camaran with
                        # flat internal faces (asymmetric demihulls) with a
                        # r smaller than 0.55 according to authors of savitsky
```

```
                        # for planing catamarans.
r = 0.43   # Separation ratio [-]. b1/b where b1 is the beam of both demihulls
            # and b is the total beam (not chine beam but full beam.)

speeds = range(1,21)

CAT1IT7_13px_resultsSav = speedIterSav(mass, b, beta, l_cg, rho, nu, f, eps, speeds,
                                r, A, SF)
```

Appendix D

ANOVA assumptions and results

Table D.1 shows the statistics evaluated for asserting the compliance of the ANOVA assumptions. Sections D.1 and D.2 contain the assumptions evaluated for each speed for drag and trim respectively, in addition to some charts for evaluating the residuals behavior for each treatment.

Test name	H_0	**Criteria to meet**
Shapiro	Normal distribution of residuals	p >0.5
Barlett	Homogeinity of variances	p >0.5
Levene		p >0.5
Durbin-Watson	Independence of errors	1.5 <D <2.5
ANOVA	There is not an effect of the treatments in the variance on the output variable	p <0.5

Table D.1: Desired criteria to meet in the ANOVA assumptions and in the ANOVA.

D.1 ANOVA results for drag

Test name	**Statistic**	**p value**
Shapiro	-	0.08
Barlett	-	0.07
Levene	-	0.49
Durbin-Watson	1.97	-

Table D.2: Tests statistics for the ANOVA assumptions for the drag at a speed of 4 m/s.

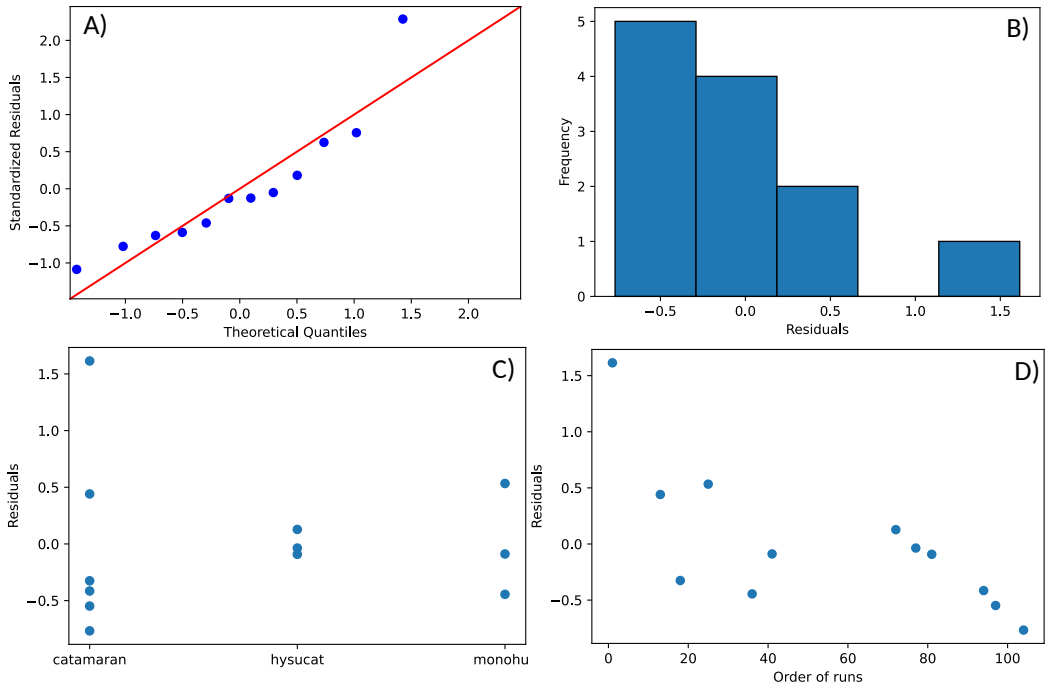

Figure D.1: Charts of the residuals behavior for the drag at a speed of 4 m/s. a) QQ plot. Points should lie near the red line in order for the normality assumption to be fulfilled. b) Histogram of the residuals. c) Variance plot of the residuals. For the similarity of the variance of the treatments assumption to be fulfilled, the amplitude of the residuals should be similar in all the treatments. d) Residuals vs order of runs. If the independence of errors assumption is fulfilled, the points should be distributed randomly around a horizontal line.

a)

	sum_sq	df	F	PR(>F)
C(boat)	4.167873	2.0	4.18359	0.051917
Residual	4.483094	9.0	NaN	NaN

b)

	group1	group2	Diff	Lower	Upper	q-value	p-value
0	catamaran	hysucat	0.689990	-0.702222	2.082203	1.955264	0.390062
1	catamaran	monohull	1.425488	0.033276	2.817701	4.039485	0.045055
2	hysucat	monohull	0.735498	-0.872090	2.343086	1.804989	0.443369

Figure D.2: Results for the drag at a speed of 4 m/s. a) ANOVA table. b) Tukey-hsd test.

Test name	**Statistic**	**p value**
Shapiro	-	0.44
Barlett	-	0.36
Levene	-	0.49
Durbin-Watson	2.83	-

Table D.3: Tests statistics for the ANOVA assumptions for the drag at a speed of 6 m/s.

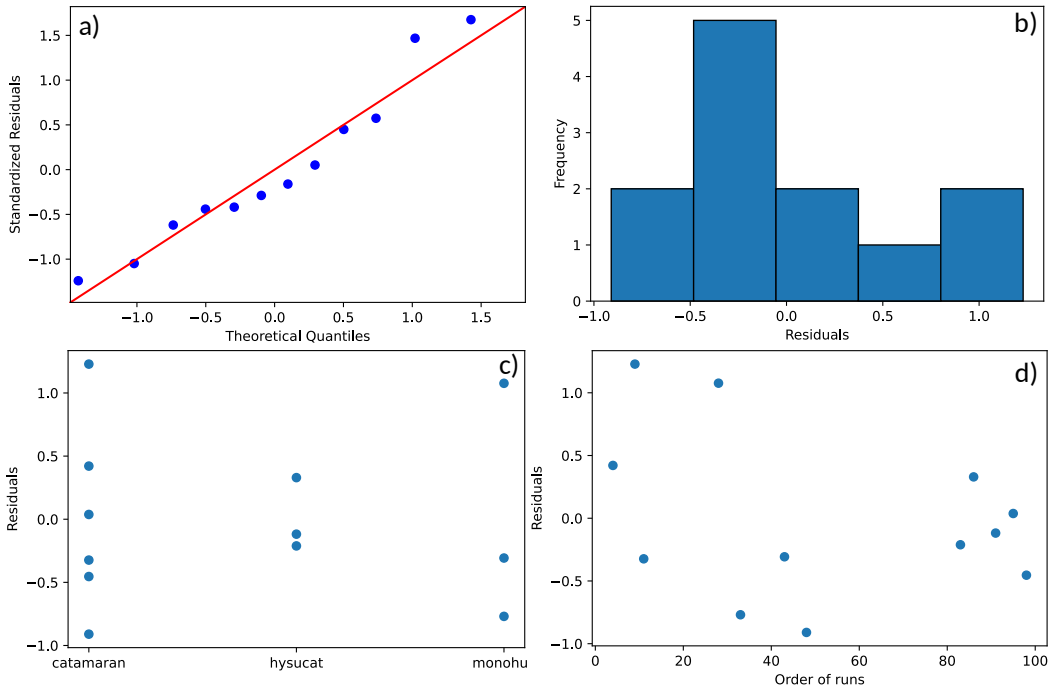

Figure D.3: Charts of the residuals behavior for the drag at a speed of 6 m/s. a) QQ plot. b) Histogram of the residuals. c) Variance plot of the residuals. d) Residuals vs order of runs.

a)

	sum_sq	df	F	PR(>F)
C(boat)	0.986521	2.0	0.917205	0.433978
Residual	4.840077	9.0	NaN	NaN

b)

	group1	group2	Diff	Lower	Upper	q-value	p-value
0	catamaran	hysucat	0.486346	-0.960235	1.932926	1.326387	0.626915
1	catamaran	monohull	0.639821	-0.806760	2.086402	1.744953	0.465538
2	hysucat	monohull	0.153476	-1.516892	1.823843	0.362489	0.900000

Figure D.4: Results for the drag at a speed of 6 m/s. a) ANOVA table. b) Tukey-hsd test.

Test name	**Statistic**	**p value**
Shapiro	-	0.19
Barlett	-	0.52
Levene	-	0.7
Durbin-Watson	2.06	-

Table D.4: Tests statistics for the ANOVA assumptions for the drag at a speed of 10 m/s.

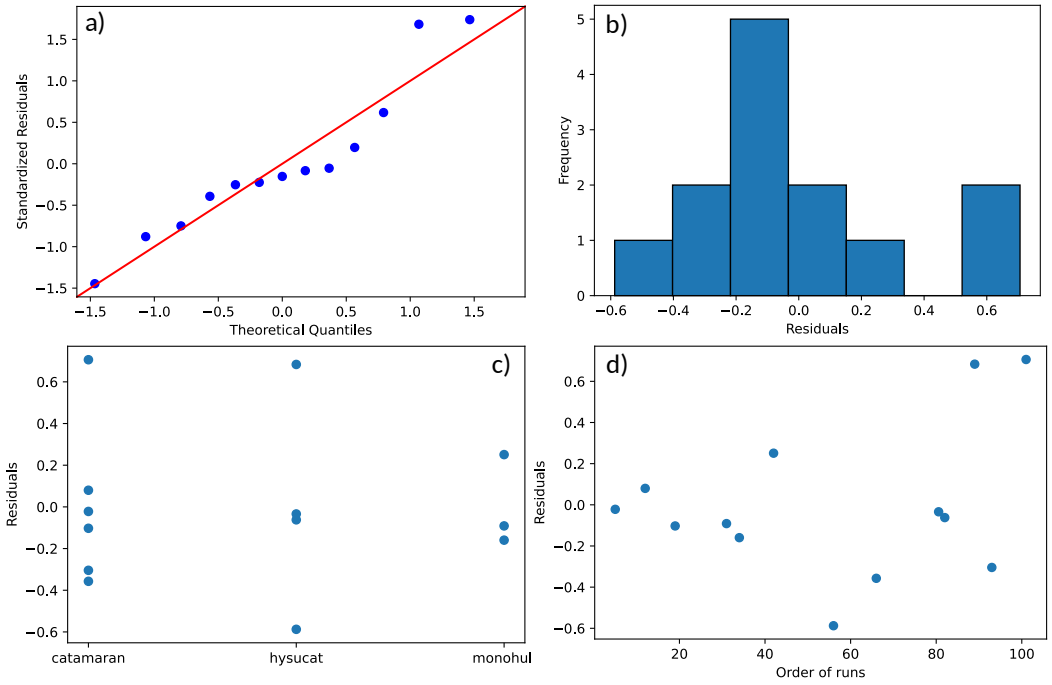

Figure D.5: Charts of the residuals behavior for the drag at a speed of 10 m/s. a) QQ plot. b) Histogram of the residuals. c) Variance plot of the residuals. d) Residuals vs order of runs.

a)

	sum_sq	df	F	PR(>F)
C(boat)	8.479327	2.0	25.691939	0.000115
Residual	1.650192	10.0	NaN	NaN

b)

	group1	group2	Diff	Lower	Upper	q-value	p-value
0	catamaran	hysucat	0.815283	0.096938	1.533628	4.397055	0.027242
1	catamaran	monohull	1.401052	0.614145	2.187960	6.897903	0.001683
2	hysucat	monohull	2.216336	1.366378	3.066293	10.102407	0.001000

Figure D.6: Results for the drag at a speed of 10 m/s. a) ANOVA table. b) Tukey-hsd test.

Test name	**Statistic**	**p value**
Shapiro	-	0.79
Barlett	-	0.46
Levene	-	0.56
Durbin-Watson	2.32	-

Table D.5: Tests statistics for the ANOVA assumptions for the drag at a speed of 13 m/s.

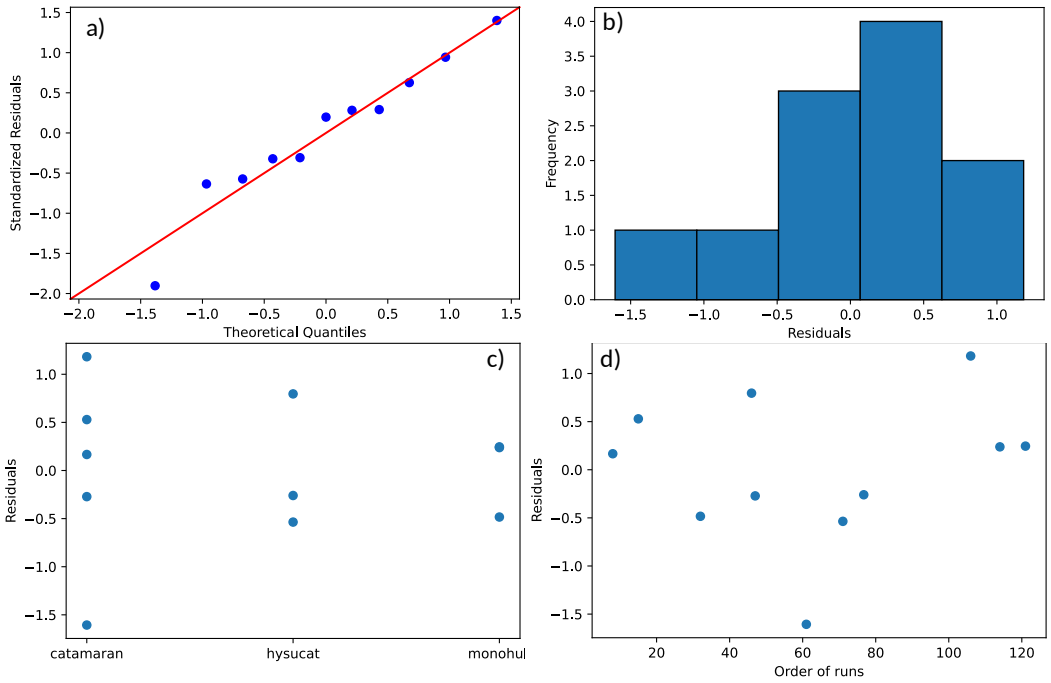

Figure D.7: Charts of the residuals behavior for the drag at a speed of 13 m/s. a) QQ plot. b) Histogram of the residuals. c) Variance plot of the residuals. d) Residuals vs order of runs.

a)

	sum_sq	df	F	PR(>F)
C(boat)	11.538222	2.0	8.099366	0.011945
Residual	5.698334	8.0	NaN	NaN

b)

	group1	group2	Diff	Lower	Upper	q-value	p-value
0	catamaran	hysucat	1.158817	-0.600824	2.918458	2.658897	0.205709
1	catamaran	monohull	1.598750	-0.160891	3.358391	3.668320	0.073452
2	hysucat	monohull	2.757567	0.790228	4.724906	5.659235	0.009722

Figure D.8: Results for the drag at a speed of 13 m/s. a) ANOVA table. b) Tukey-hsd test.

Test name	Statistic	p value
Shapiro	-	0.33
Barlett	-	0.007
Levene	-	0.02
Durbin-Watson	2.07	-

Table D.6: Tests statistics for the ANOVA assumptions for the drag at a speed of 15 m/s.

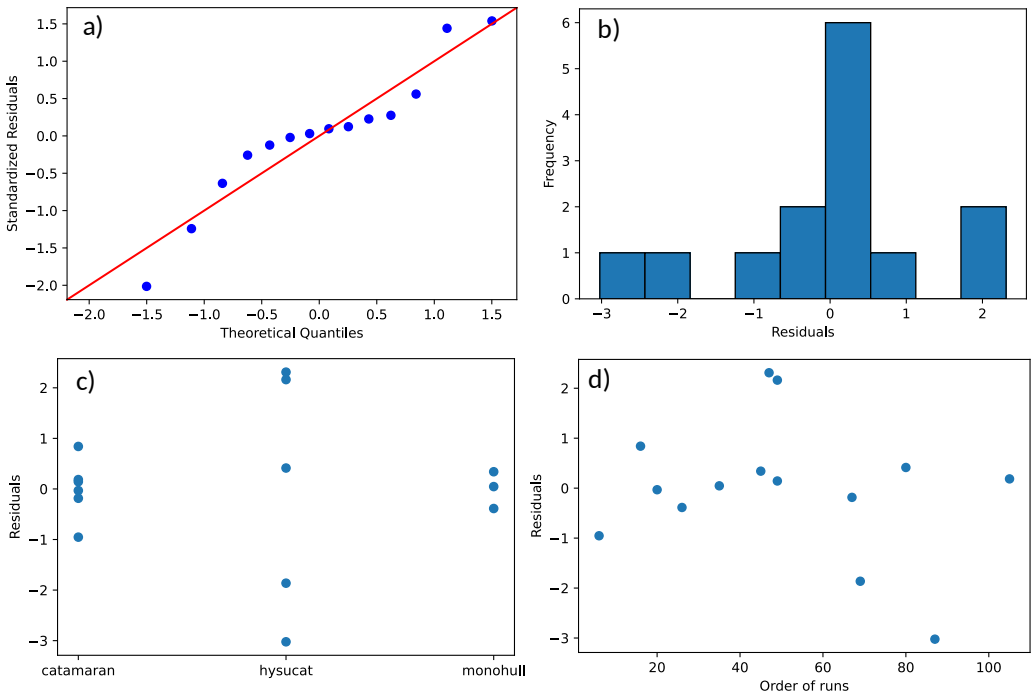

Figure D.9: Charts of the residuals behavior for the drag at a speed of 15 m/s. a) QQ plot. b) Histogram of the residuals. c) Variance plot of the residuals. d) Residuals vs order of runs.

a)

	sum_sq	df	F	PR(>F)
C(boat)	56.385779	2.0	12.521957	0.001462
Residual	24.766240	11.0	NaN	NaN

b)

	group1	group2	Diff	Lower	Upper	q-value	p-value
0	catamaran	hysucat	0.755300	-1.697306	3.207905	1.175614	0.684204
1	catamaran	monohull	4.479667	1.615640	7.343693	5.970930	0.003733
2	hysucat	monohull	5.234966	2.277013	8.192920	6.756097	0.001517

Figure D.10: Results for the drag at a speed of 15 m/s. a) ANOVA table. b) Tukey-hsd test.

Test name	**Statistic**	**p value**
Shapiro	-	0.052
Barlett	-	0.01
Levene	-	0.34
Durbin-Watson	1.28	-

Table D.7: Tests statistics for the ANOVA assumptions for the drag at a speed of 17 m/s.

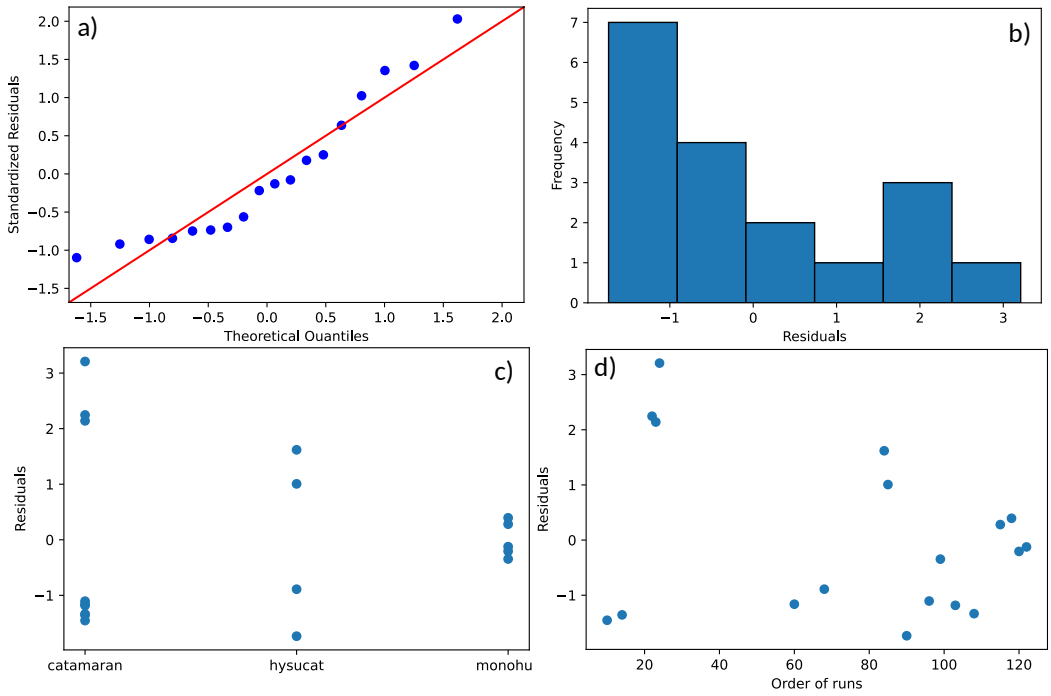

Figure D.11: Charts of the residuals behavior for the drag at a speed of 17 m/s. a) QQ plot. b) Histogram of the residuals. c) Variance plot of the residuals. d) Residuals vs order of runs.

a)

	sum_sq	df	F	PR(>F)
C(boat)	122.514535	2.0	24.515385	0.000019
Residual	37.480913	15.0	NaN	NaN

b)

	group1	group2	Diff	Lower	Upper	q-value	p-value
0	catamaran	hysucat	0.264063	-2.202320	2.730446	0.393136	0.900
1	catamaran	monohull	5.901356	3.612082	8.190630	9.465631	0.001
2	hysucat	monohull	5.637293	2.884039	8.390547	7.518304	0.001

Figure D.12: Results for the drag at a speed of 17 m/s. a) ANOVA table. b) Tukey-hsd test.

Test name	**Statistic**	**p value**
Shapiro	-	0.53
Barlett	-	0.1
Levene	-	0.45
Durbin-Watson	2.61	-

Table D.8: Tests statistics for the ANOVA assumptions for the drag at a speed of 20 m/s.

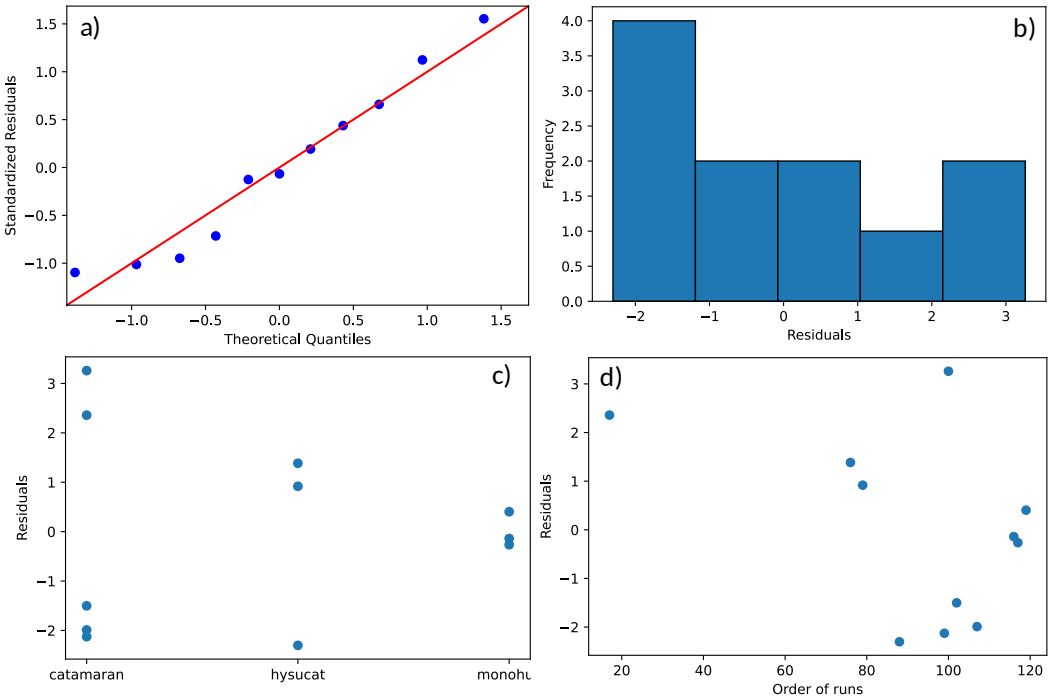

Figure D.13: Charts of the residuals behavior for the drag at a speed of 20 m/s. a) QQ plot. b) Histogram of the residuals. c) Variance plot of the residuals. d) Residuals vs order of runs.

a)

	sum_sq	df	F	PR(>F)
C(boat)	49.277926	2.0	5.592291	0.030238
Residual	35.247042	8.0	NaN	NaN

b)

	group1	group2	Diff	Lower	Upper	q-value	p-value
0	catamaran	hysucat	1.291736	-3.084609	5.668081	1.191717	0.678684
1	catamaran	monohull	5.083507	0.707163	9.459852	4.689891	0.025504
2	hysucat	monohull	3.791771	-1.101131	8.684674	3.128862	0.128284

Figure D.14: Results for the drag at a speed of 20 m/s. a) ANOVA table. b) Tukey-hsd test.

D.2 ANOVA results for trim

Test name	Statistic	p value
Shapiro	-	0.52
Barlett	-	(Not enough data)
Levene	-	0.44
Durbin-Watson	2.71	-

Table D.9: Tests statistics for the ANOVA assumptions for the trim angle at a speed of 4 m/s.

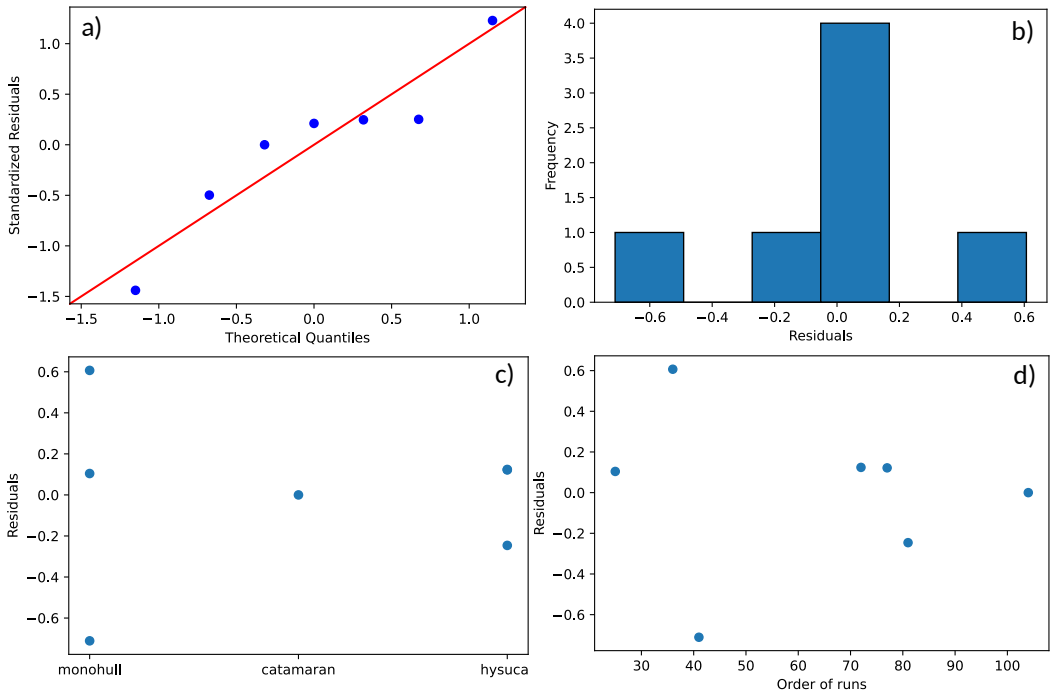

Figure D.15: Charts of the residuals behavior for the trim angle at a speed of 4 m/s. a) QQ plot. b) Histogram of the residuals. c) Variance plot of the residuals. d) Residuals vs order of runs.

a)

	sum_sq	df	F	PR(>F)
C(boat)	0.38563	2.0	0.790605	0.513645
Residual	0.97553	4.0	NaN	NaN

b)

	group1	group2	Diff	Lower	Upper	q-value	p-value
0	monohull	catamaran	0.705085	-1.324397	2.734567	1.748624	0.496584
1	monohull	hysucat	0.262584	-1.172477	1.697644	0.920955	0.791815
2	catamaran	hysucat	0.442501	-1.586981	2.471983	1.097411	0.728817

Figure D.16: Results for the trim angle at a speed of 4 m/s. a) ANOVA table. b) Tukey-hsd test.

Test name	**Statistic**	**p value**
Shapiro	-	0.74
Barlett	-	0.68
Levene	-	0.09
Durbin-Watson	1.83	-

Table D.10: Tests statistics for the ANOVA assumptions for the trim angle at a speed of 6 m/s.

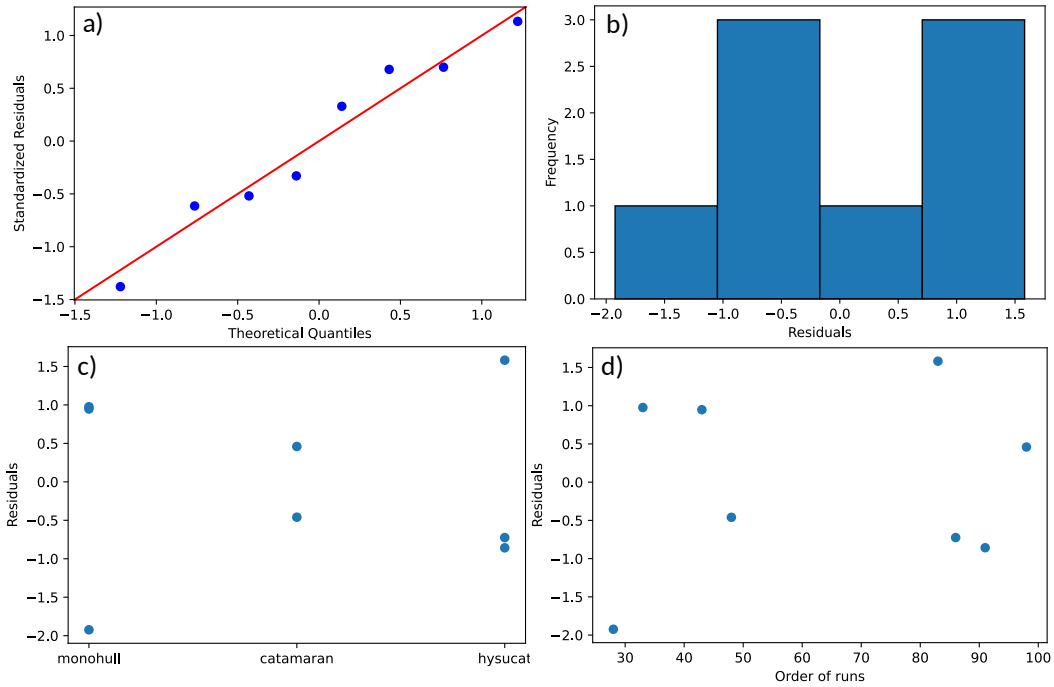

Figure D.17: Charts of the residuals behavior for the trim angle at a speed of 6 m/s. a) QQ plot. b) Histogram of the residuals. c) Variance plot of the residuals. d) Residuals vs order of runs.

a)

	sum_sq	df	F	PR(>F)
C(boat)	6.300242	2.0	1.617506	0.287253
Residual	9.737588	5.0	NaN	NaN

b)

	group1	group2	Diff	Lower	Upper	q-value	p-value
0	monohull	catamaran	0.772933	-3.367320	4.913187	0.858039	0.811151
1	monohull	hysucat	2.034797	-1.668358	5.737952	2.525463	0.265181
2	catamaran	hysucat	1.261864	-2.878390	5.402117	1.400804	0.612245

Figure D.18: Results for the trim angle at a speed of 6 m/s. a) ANOVA table. b) Tukey-hsd test.

Test name	**Statistic**	**p value**
Shapiro	-	0.003
Barlett	-	0.17
Levene	-	0.77
Durbin-Watson	2.27	-

Table D.11: Tests statistics for the ANOVA assumptions for the trim angle at a speed of 10 m/s.

Test name	**Statistic**	**p value**
Shapiro	-	0.08
Barlett	-	0.17
Levene	-	0.55
Durbin-Watson	2.16	-

Table D.12: Tests statistics for the ANOVA assumptions for the trim angle at a speed of 13 m/s.

Test name	**Statistic**	**p value**
Shapiro	-	0.73
Barlett	-	0.5
Levene	-	0.3
Durbin-Watson	2.14	-

Table D.13: Tests statistics for the ANOVA assumptions for the trim angle at a speed of 15 m/s.

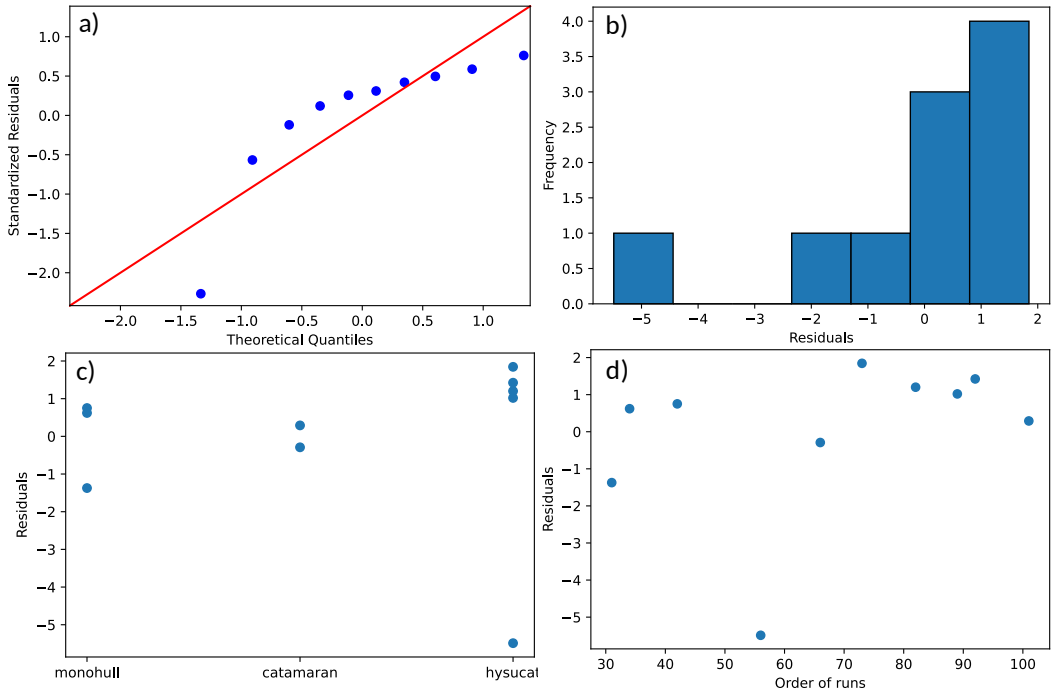

Figure D.19: Charts of the residuals behavior for the trim angle at a speed of 10 m/s. a) QQ plot. b) Histogram of the residuals. c) Variance plot of the residuals. d) Residuals vs order of runs.

a)

	sum_sq	df	F	PR(>F)
C(boat)	1.780361	2.0	0.151811	0.861905
Residual	41.046229	7.0	NaN	NaN

b)

	group1	group2	Diff	Lower	Upper	q-value	p-value
0	monohull	catamaran	0.496617	-6.006825	7.000058	0.317716	0.900000
1	monohull	hysucat	0.571913	-4.630840	5.774667	0.457360	0.900000
2	catamaran	hysucat	1.068530	-4.891973	7.029033	0.745873	0.849358

Figure D.20: Results for the trim angle at a speed of 10 m/s. a) ANOVA table. b) Tukey-hsd test.

Test name	**Statistic**	**p value**
Shapiro	-	0.26
Barlett	-	0.03
Levene	-	0.15
Durbin-Watson	2.6	-

Table D.14: Tests statistics for the ANOVA assumptions for the trim angle at a speed of 17 m/s.

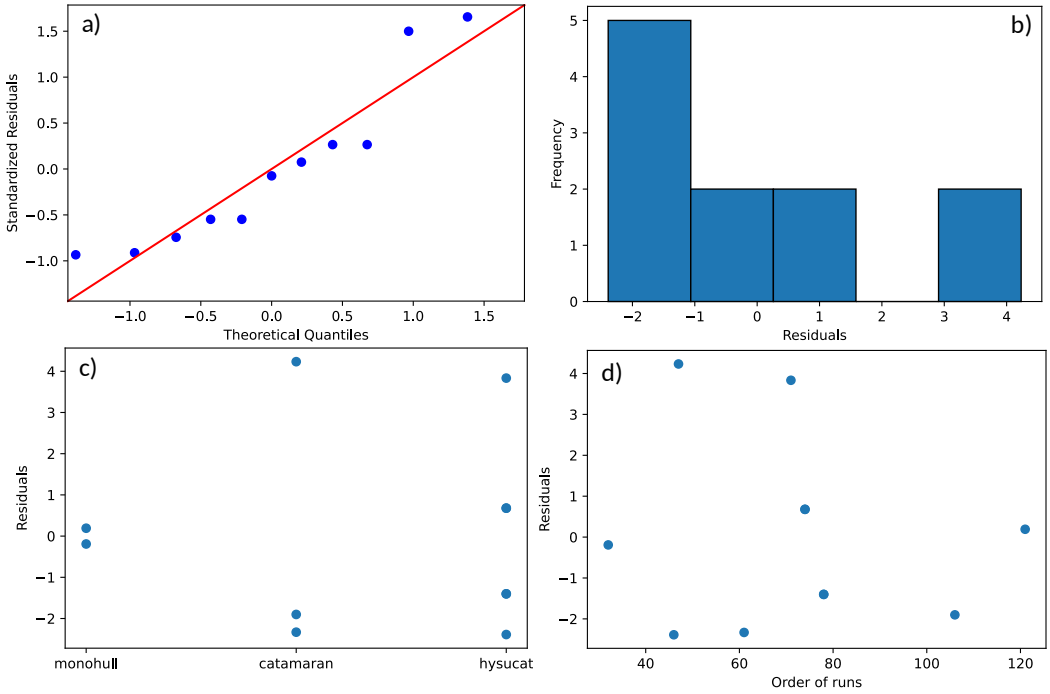

Figure D.21: Charts of the residuals behavior for the trim angle at a speed of 13 m/s. a) QQ plot. b) Histogram of the residuals. c) Variance plot of the residuals. d) Residuals vs order of runs.

a)

	sum_sq	df	F	PR(>F)
C(boat)	1.497129	2.0	0.114504	0.893244
Residual	52.299640	8.0	NaN	NaN

b)

	group1	group2	Diff	Lower	Upper	q-value	p-value
0	monohull	catamaran	0.161058	-6.502551	6.824668	0.097585	0.900000
1	monohull	hysucat	0.636532	-5.323582	6.596646	0.431198	0.900000
2	catamaran	hysucat	0.797590	-4.364020	5.959200	0.623886	0.894619

Figure D.22: Results for the trim angle at a speed of 13 m/s. a) ANOVA table. b) Tukey-hsd test.

Test name	**Statistic**	**p value**
Shapiro	-	0.93
Barlett	-	0.31
Levene	-	0.01
Durbin-Watson	1.81	-

Table D.15: Tests statistics for the ANOVA assumptions for the trim angle at a speed of 20 m/s.

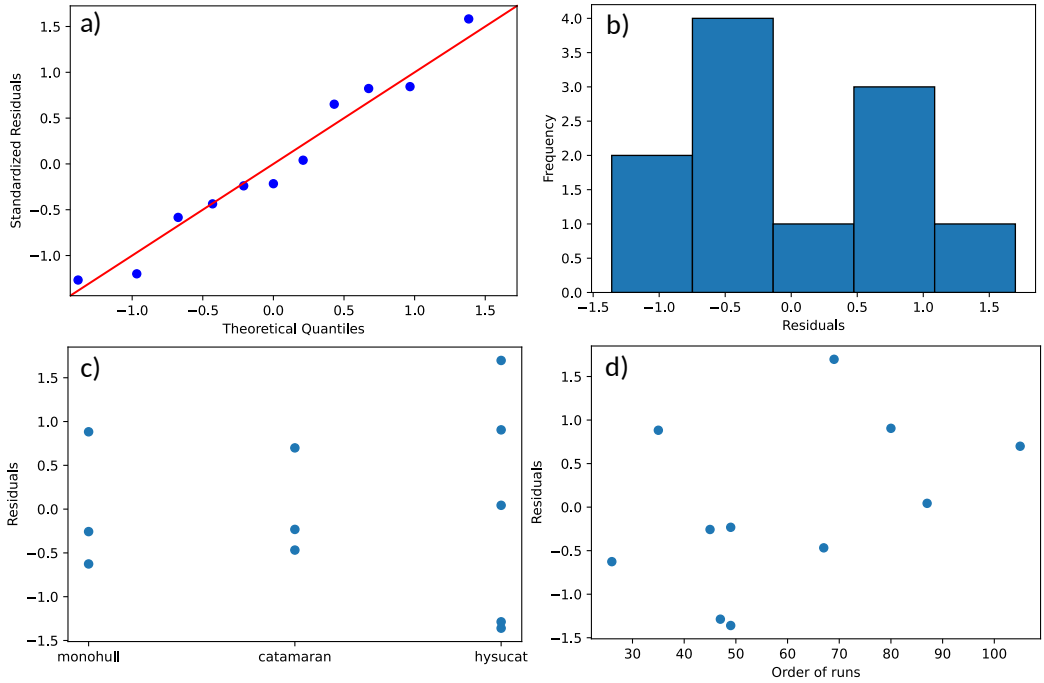

Figure D.23: Charts of the residuals behavior for the trim angle at a speed of 15 m/s. a) QQ plot. b) Histogram of the residuals. c) Variance plot of the residuals. d) Residuals vs order of runs.

a)

	sum_sq	df	F	PR(>F)
C(boat)	22.581784	2.0	9.812604	0.007033
Residual	9.205216	8.0	NaN	NaN

b)

	group1	group2	Diff	Lower	Upper	q-value	p-value
0	monohull	catamaran	2.917894	0.417421	5.418367	4.711488	0.024951
1	monohull	hysucat	3.355583	1.119092	5.592075	6.057755	0.006647
2	catamaran	hysucat	0.437690	-1.798802	2.674181	0.790150	0.831392

Figure D.24: Results for the trim angle at a speed of 15 m/s. a) ANOVA table. b) Tukey-hsd test.

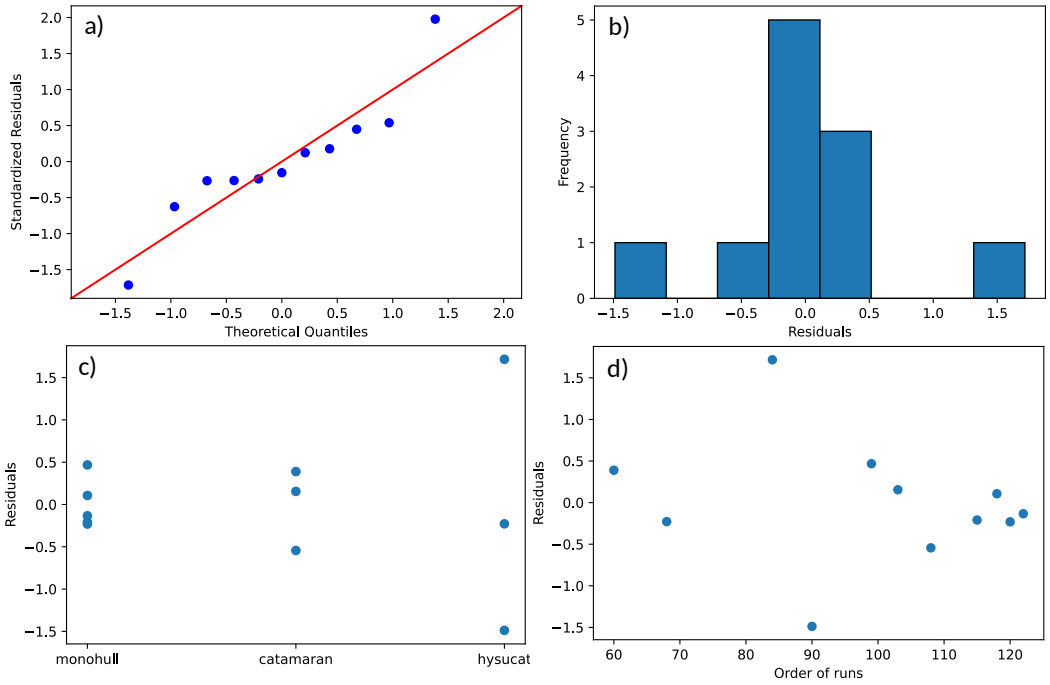

Figure D.25: Charts of the residuals behavior for the trim angle at a speed of 17 m/s. a) QQ plot. b) Histogram of the residuals. c) Variance plot of the residuals. d) Residuals vs order of runs.

a)

	sum_sq	df	F	PR(>F)
C(boat)	30.061204	2.0	19.946294	0.000779
Residual	6.028429	8.0	NaN	NaN

b)

	group1	group2	Diff	Lower	Upper	q-value	p-value
0	monohull	catamaran	3.791283	1.981392	5.601173	8.457553	0.001000
1	monohull	hysucat	2.615694	0.805803	4.425584	5.835062	0.008210
2	catamaran	hysucat	1.175589	-0.847930	3.199108	2.345627	0.277766

Figure D.26: Results for the trim angle at a speed of 17 m/s. a) ANOVA table. b) Tukey-hsd test.

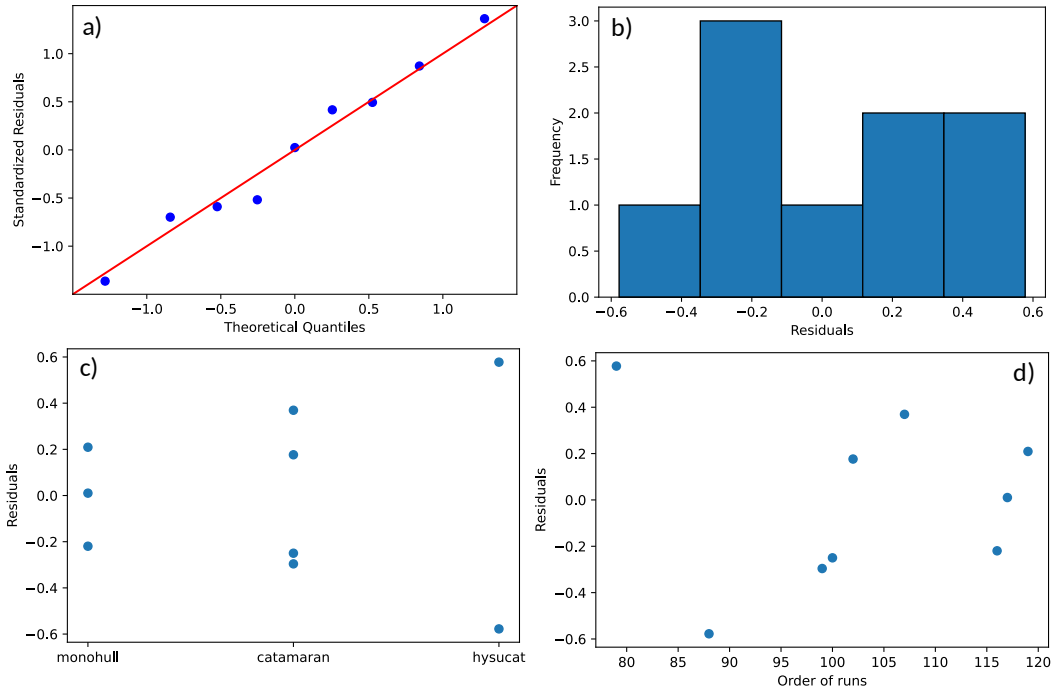

Figure D.27: Charts of the residuals behavior for the trim angle at a speed of 20 m/s. a) QQ plot. b) Histogram of the residuals. c) Variance plot of the residuals. d) Residuals vs order of runs.

a)

	sum_sq	df	F	PR(>F)
C(boat)	19.926171	2.0	55.50956	0.000135
Residual	1.076905	6.0	NaN	NaN

b)

	group1	group2	Diff	Lower	Upper	q-value	p-value
0	monohull	catamaran	3.295176	2.303525	4.286827	14.401979	0.001000
1	monohull	hysucat	2.801391	1.616141	3.986640	10.243922	0.001000
2	catamaran	hysucat	0.493785	-0.630641	1.618211	1.903309	0.424443

Figure D.28: Results for the trim angle at a speed of 20 m/s. a) ANOVA table. b) Tukey-hsd test.

Appendix E

Side photos of the boats and wetted areas

E.1 Monohull

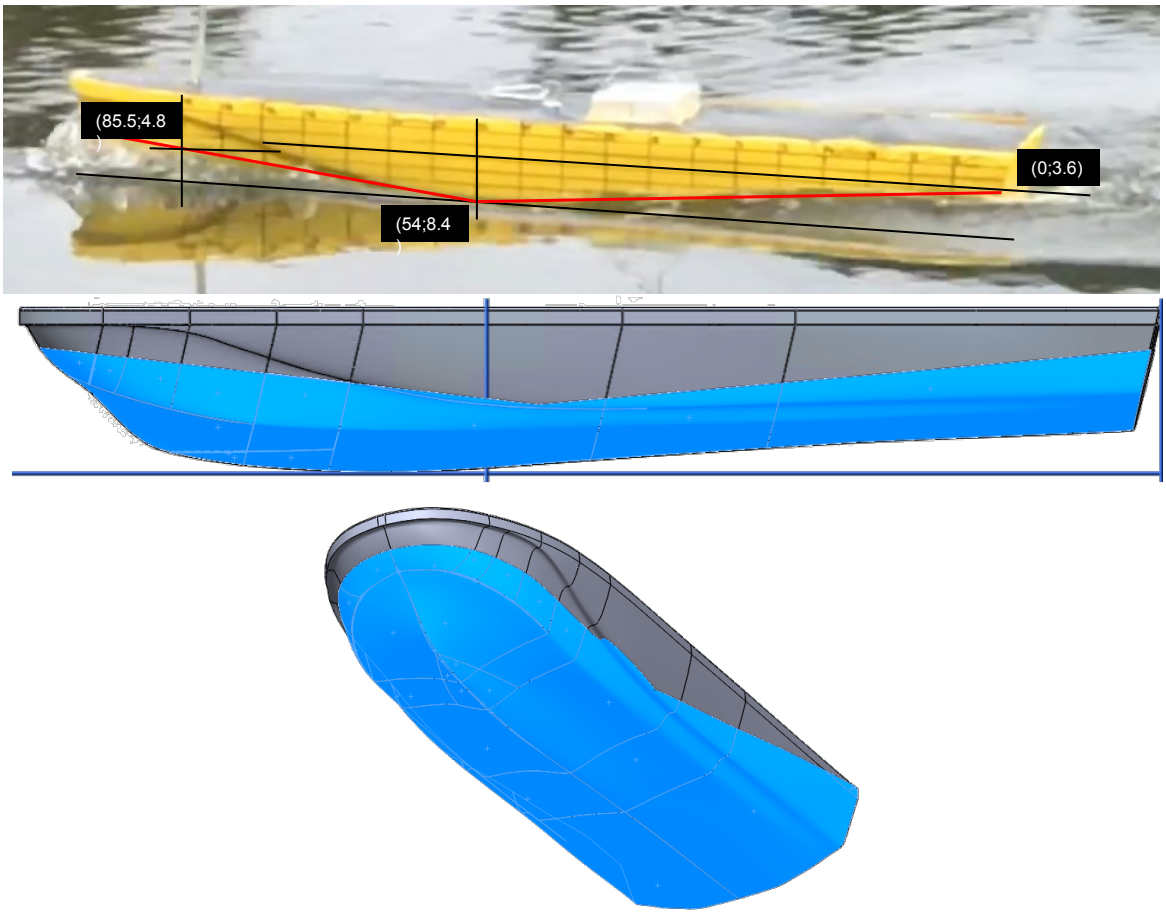

Figure E.1: Wetted area measurements (in centimeters) and CAD representation of the wetted areas for the monohull at a real scale speed of 4 m/s. Wetted area = 19.84 m^2. Wetted keel length = 7.6 m

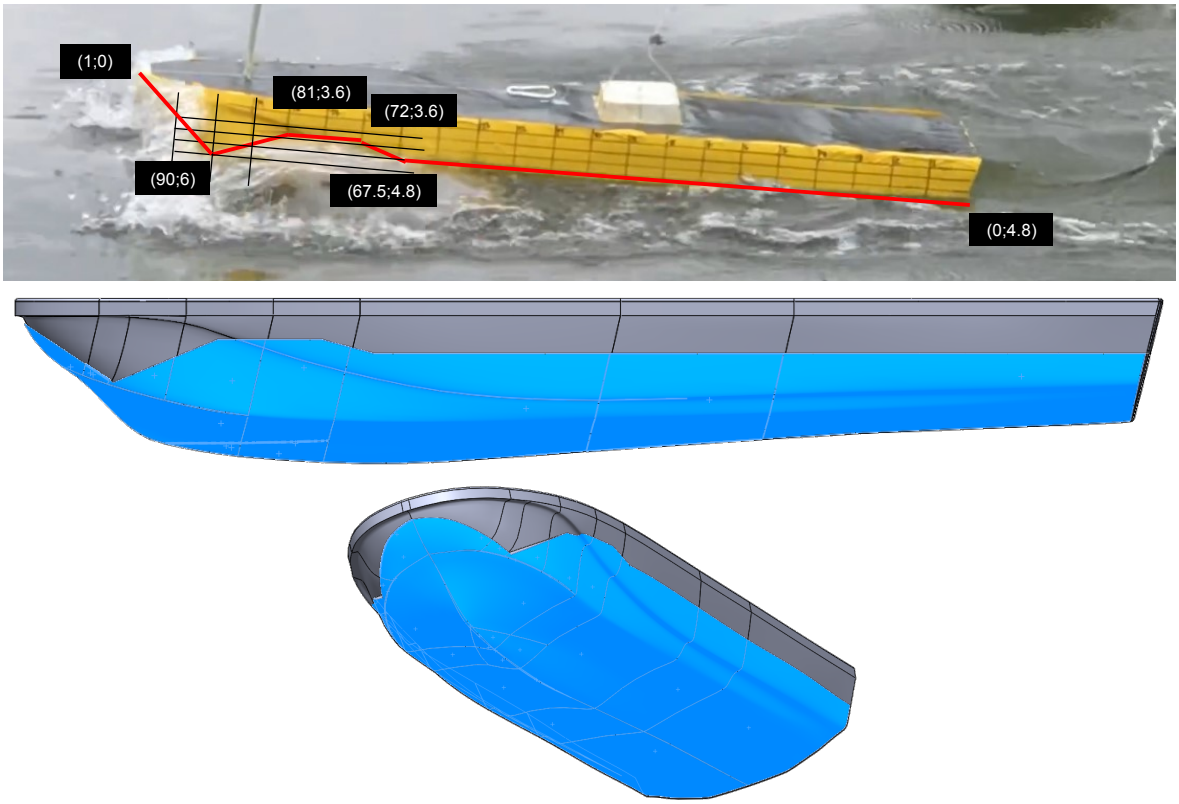

Figure E.2: Wetted area measurements (in centimeters) and CAD representation of the wetted areas for the monohull at a real scale speed of 6 m/s. Wetted area = 21.12 m^2. Wetted keel length = 8 m

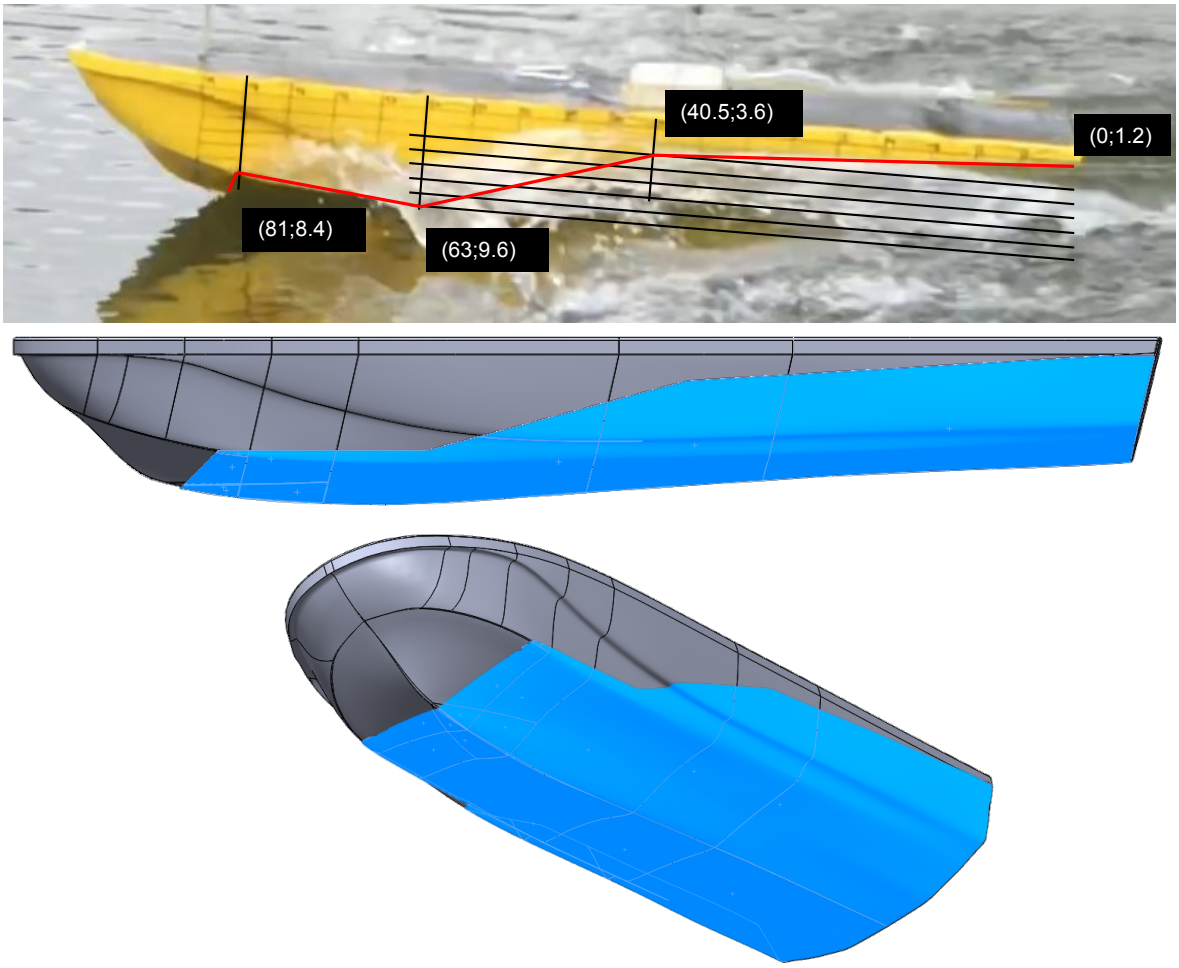

Figure E.3: Wetted area measurements (in centimeters) and CAD representation of the wetted areas for the monohull at a real scale speed of 10 m/s. Wetted area = 17.92 m^2. Wetted keel length = 6.48 m

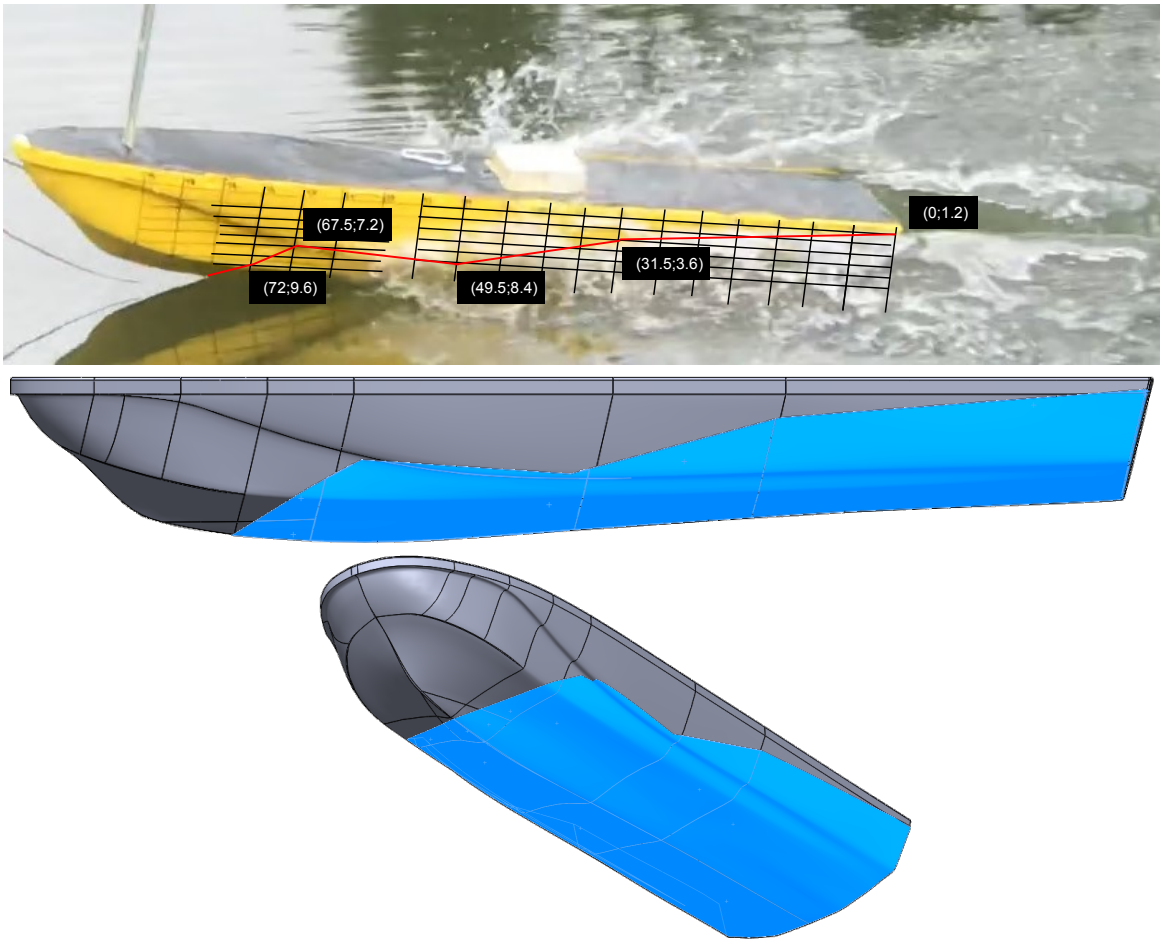

Figure E.4: Wetted area measurements (in centimeters) and CAD representation of the wetted areas for the monohull at a real scale speed of 13 m/s. Wetted area = 16.64 m^2. Wetted keel length = 5.76 m

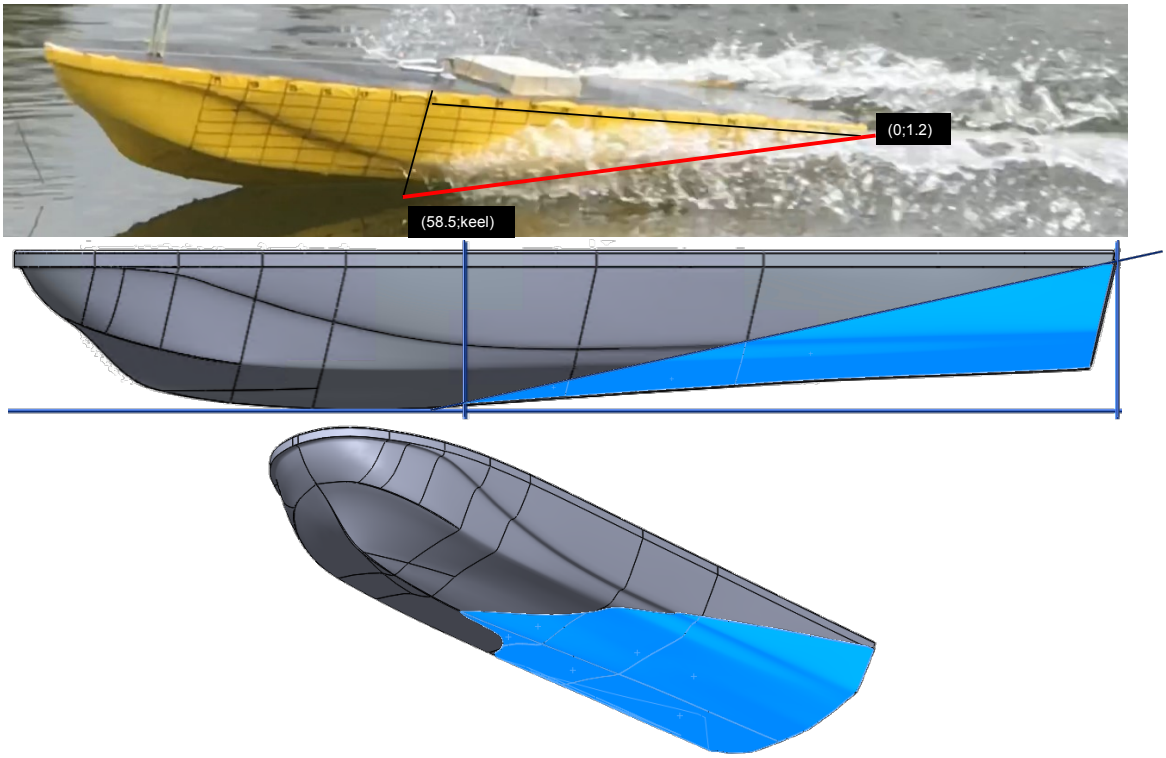

Figure E.5: Wetted area measurements (in centimeters) and CAD representation of the wetted areas for the monohull at a real scale speed of 15 m/s. Wetted area = 10.24 m^2. Wetted keel length = 4.68 m

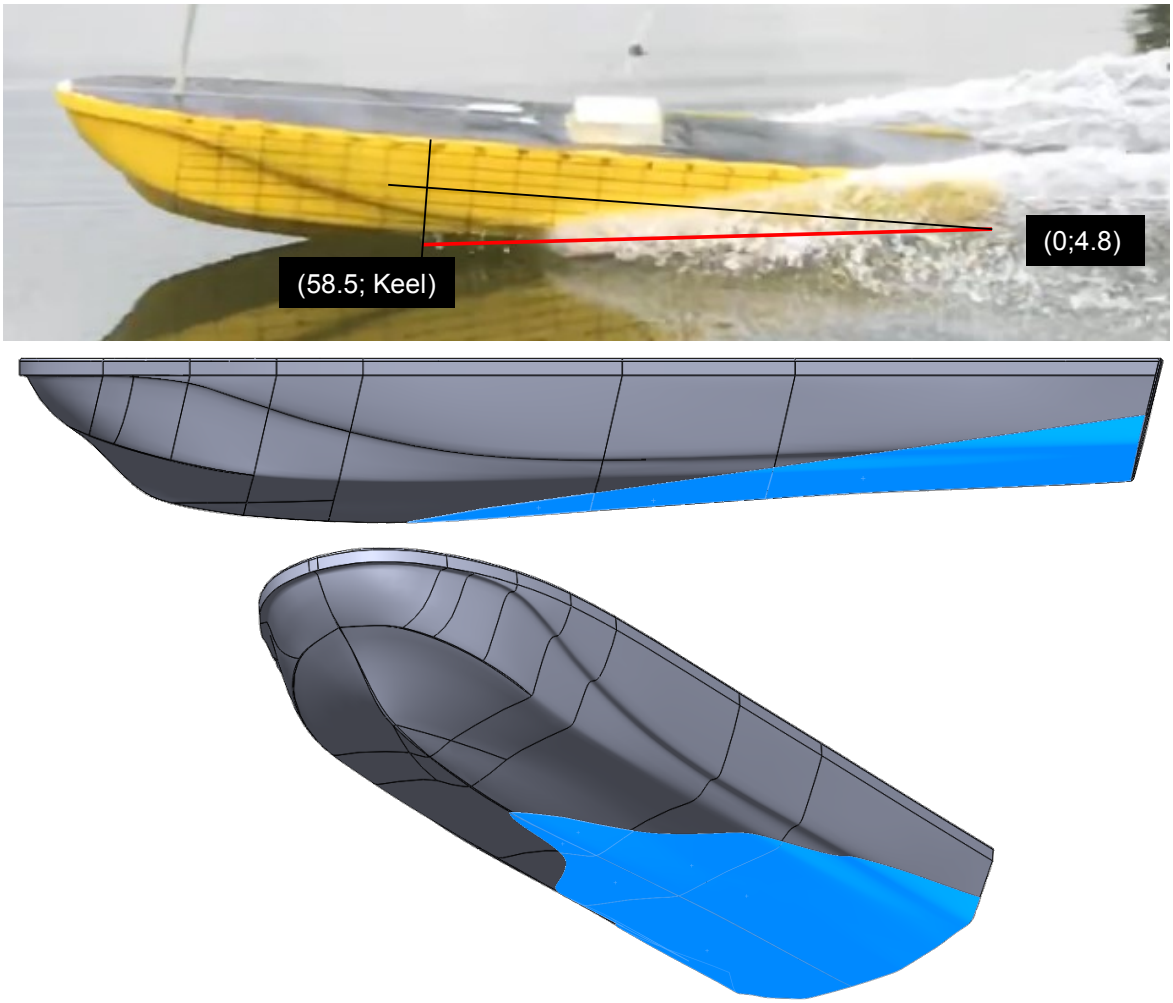

Figure E.6: Wetted area measurements (in centimeters) and CAD representation of the wetted areas for the monohull at a real scale speed of 17 m/s. Wetted area = 7.68 m^2. Wetted keel length = 4.68 m

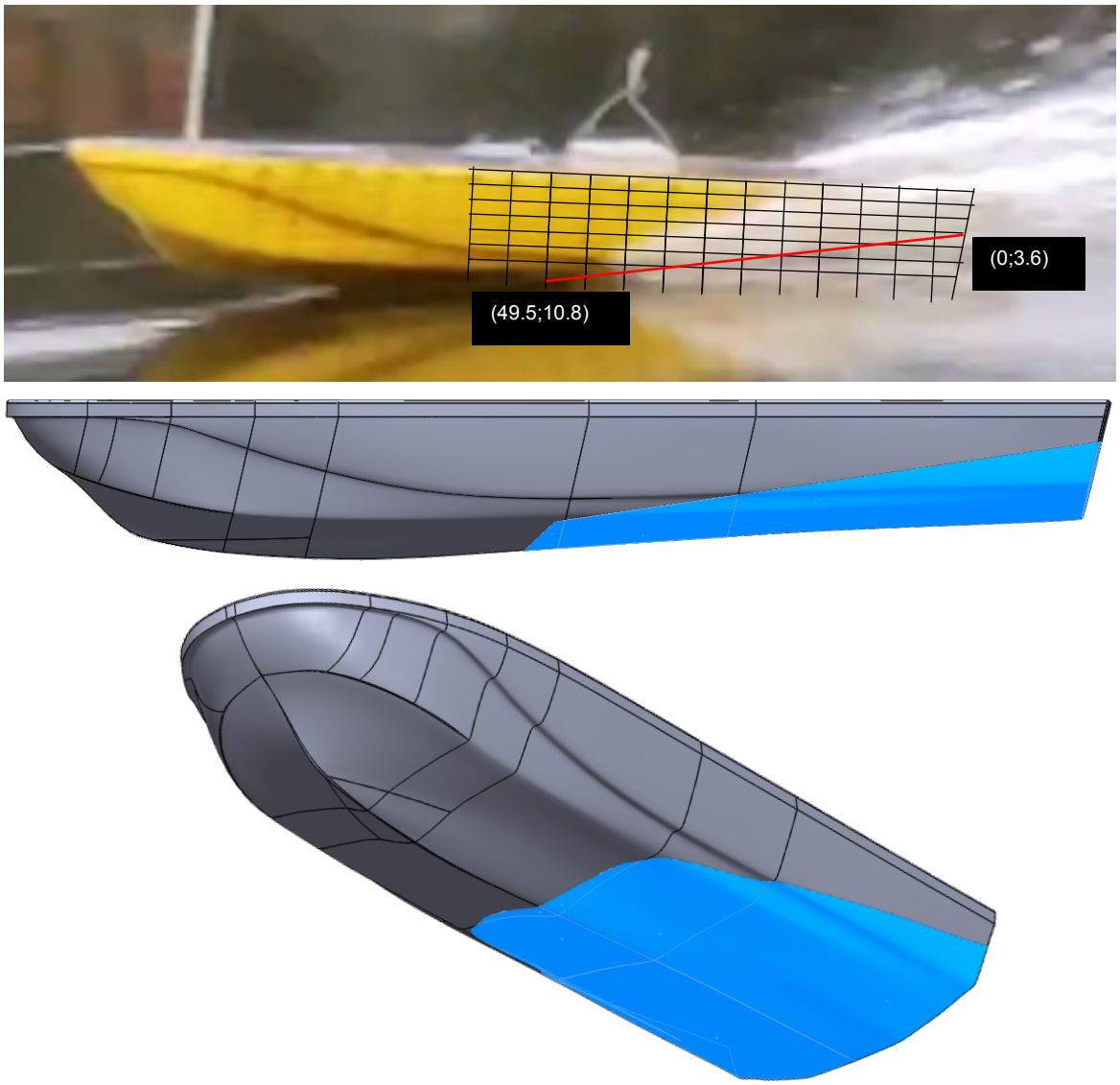

Figure E.7: Wetted area measurements (in centimeters) and CAD representation of the wetted areas for the monohull at a real scale speed of 17 m/s. Wetted area = 8.32 m^2. Wetted keel length = 3.96 m

E.2 Catamaran

Note: In some side photographs, the line indicating the wetted area seems to be overestimating the wetted area due to apparently there is not water making contact with the hull in that zone. However, from the videos from which the photographs were taken, in can be observed that those zones are also wetted due to, as it is explained at the end of section 5, the water tries to follow the contour of the catamaran hull. This also applies for the hysucat.

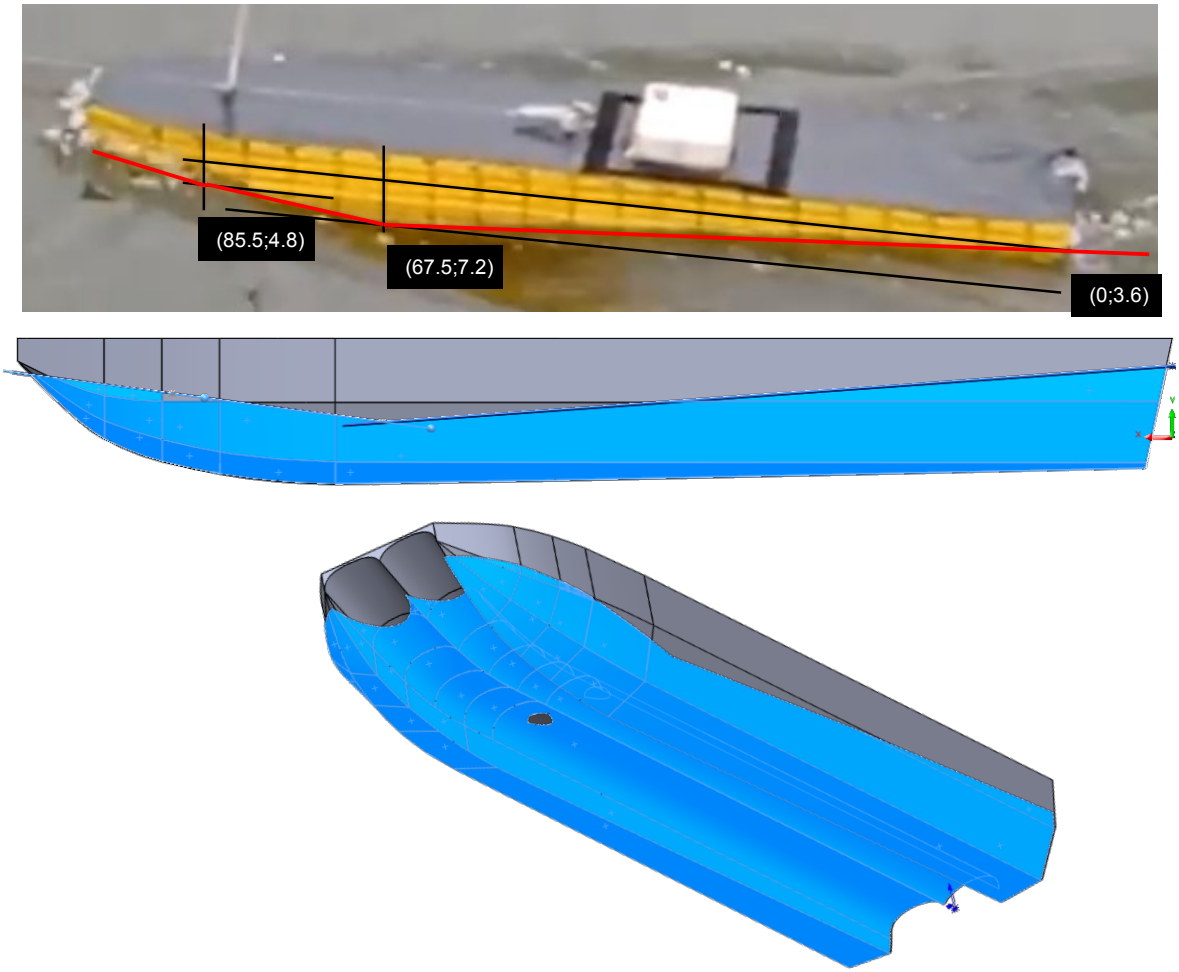

Figure E.8: Wetted area measurements (in centimeters) and CAD representation of the wetted areas for the catamaran (and the hysucat) at a real scale speed of 4 m/s. Wetted area = 24.96 m^2. Wetted keel length = 7.68 m

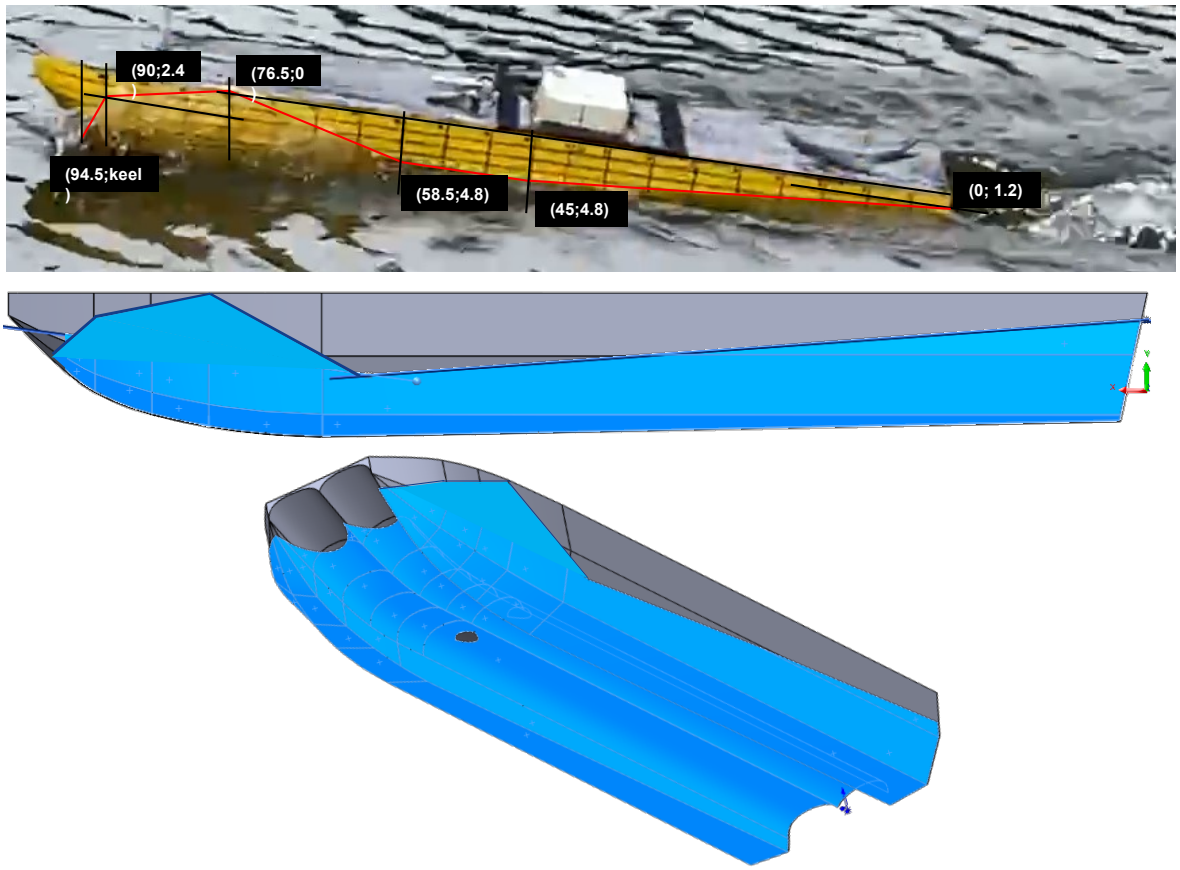

Figure E.9: Wetted area measurements (in centimeters) and CAD representation of the wetted areas for the catamaran (and the hysucat) at a real scale speed of 6 m/s. Wetted area = 26.24 m^2. Wetted keel length = 7.56 m

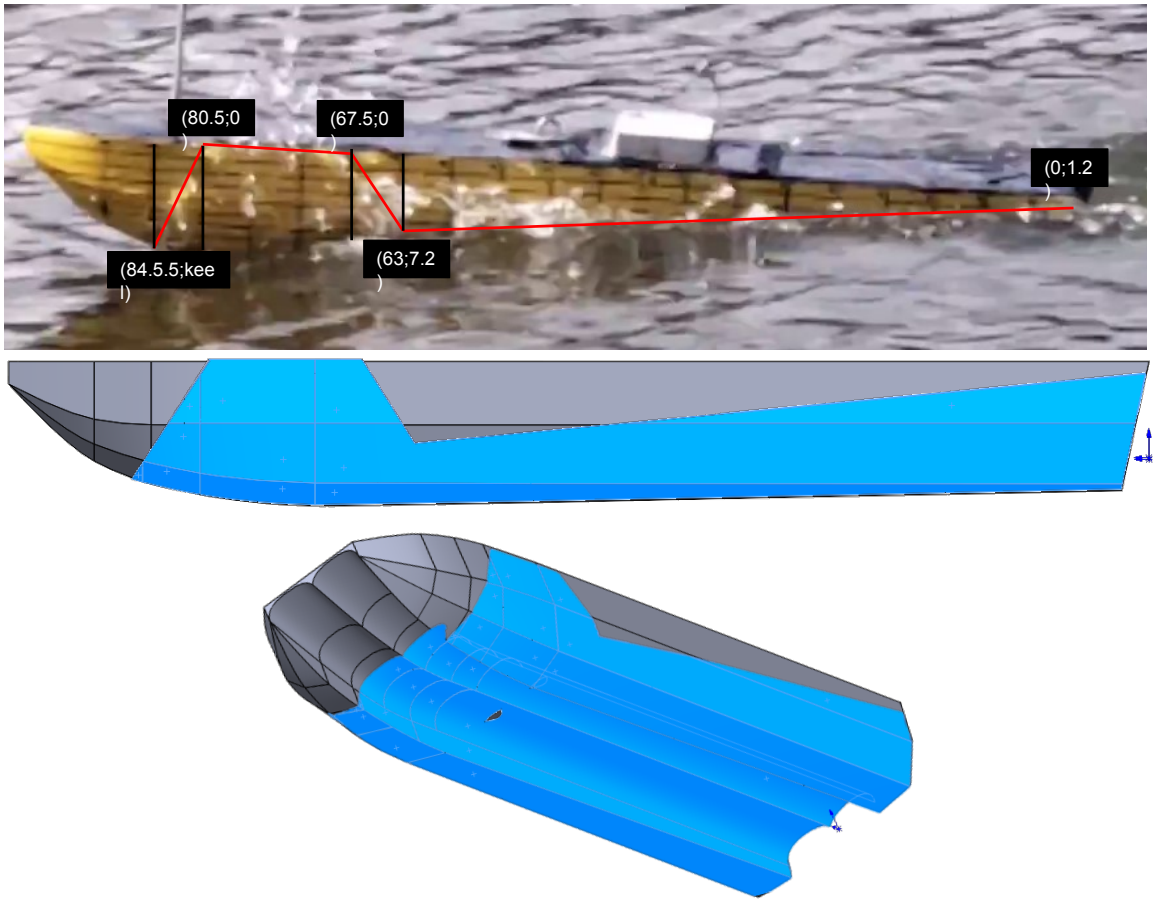

Figure E.10: Wetted area measurements (in centimeters) and CAD representation of the wetted areas for the catamaran at a real scale speed of 10 m/s. Wetted area = 24.96 m^2. Wetted keel length = 6.76 m

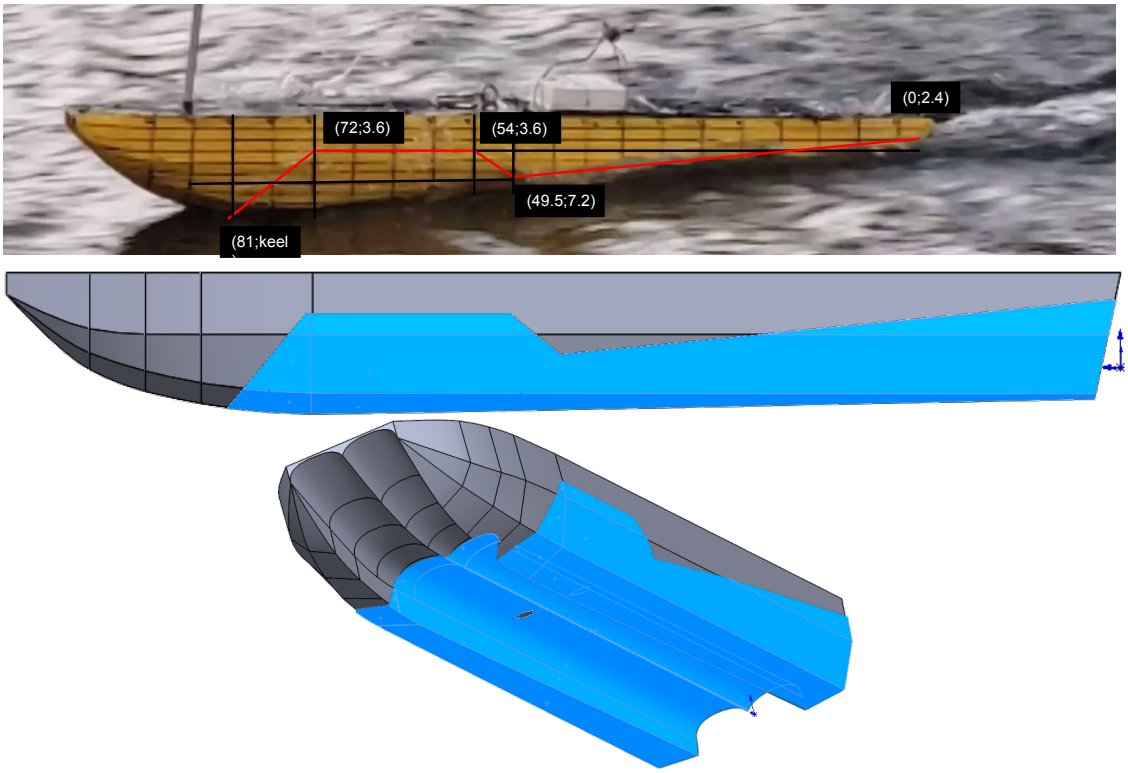

Figure E.11: Wetted area measurements (in centimeters) and CAD representation of the wetted areas for the catamaran at a real scale speed of 13 m/s. Wetted area = 20.48 m^2. Wetted keel length = 6.48 m

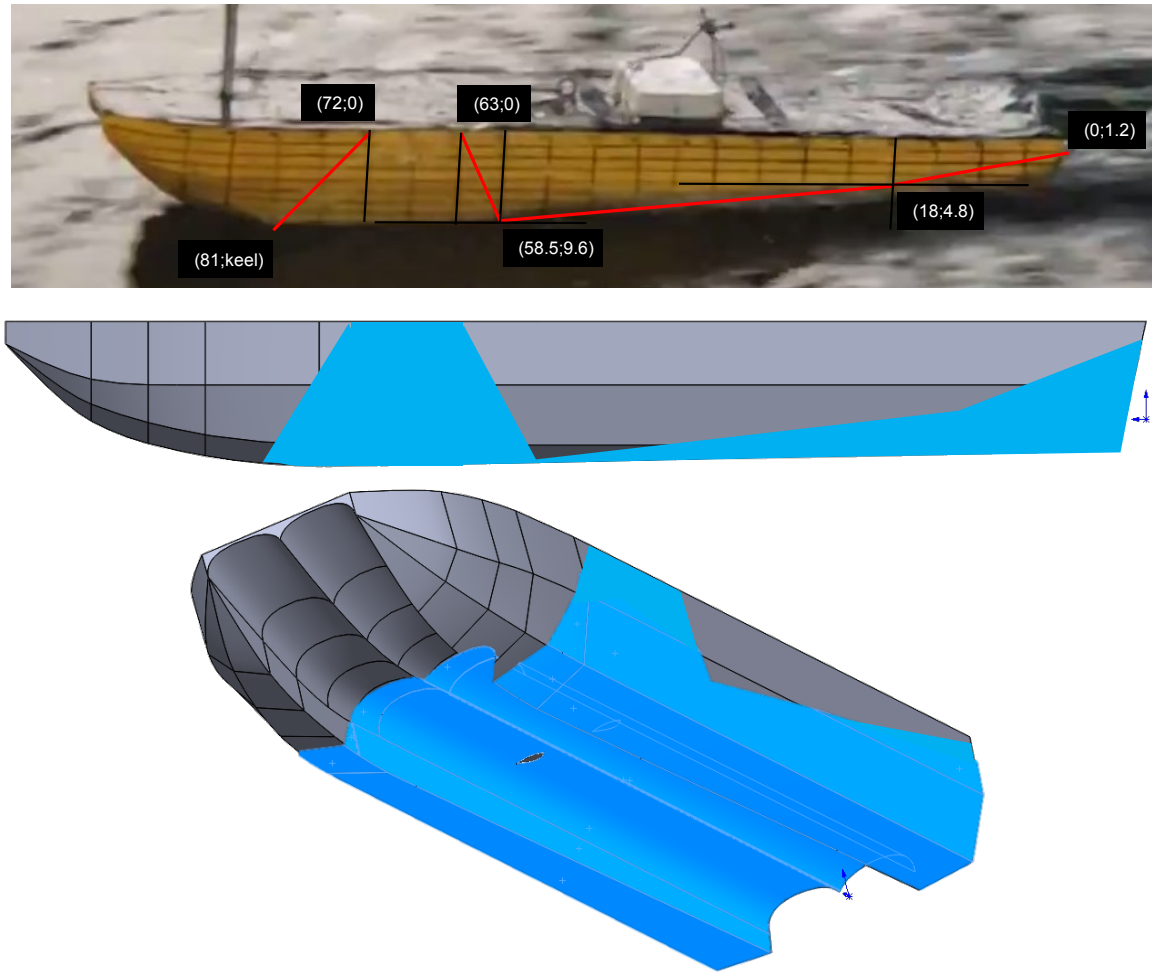

Figure E.12: Wetted area measurements (in centimeters) and CAD representation of the wetted areas for the catamaran at a real scale speed of 15 m/s. Wetted area = 17.92 m^2. Wetted keel length = 6.48 m

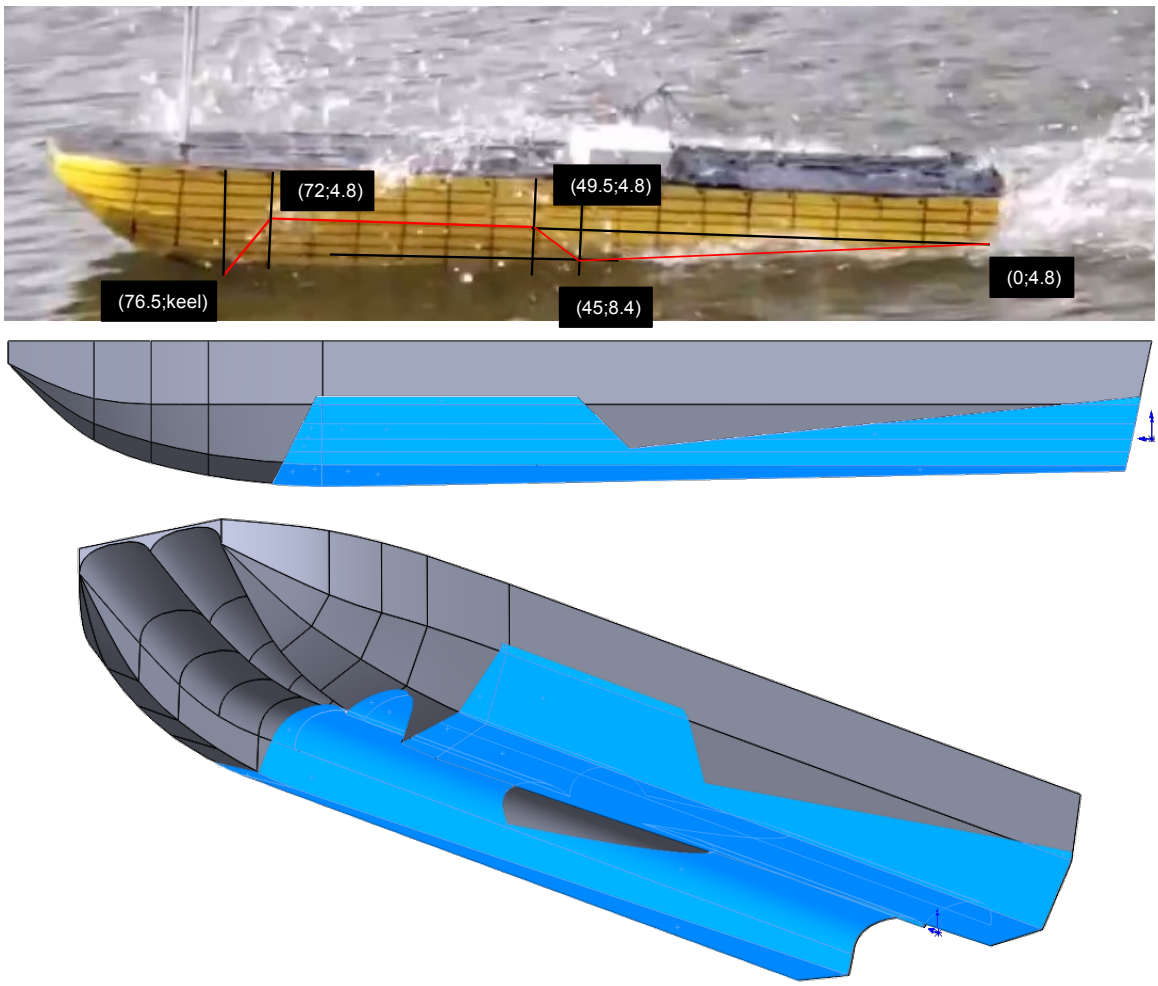

Figure E.13: Wetted area measurements (in centimeters) and CAD representation of the wetted areas for the catamaran at a real scale speed of 17 m/s. Wetted area = 17.28 m^2. Wetted keel length = 6.12 m

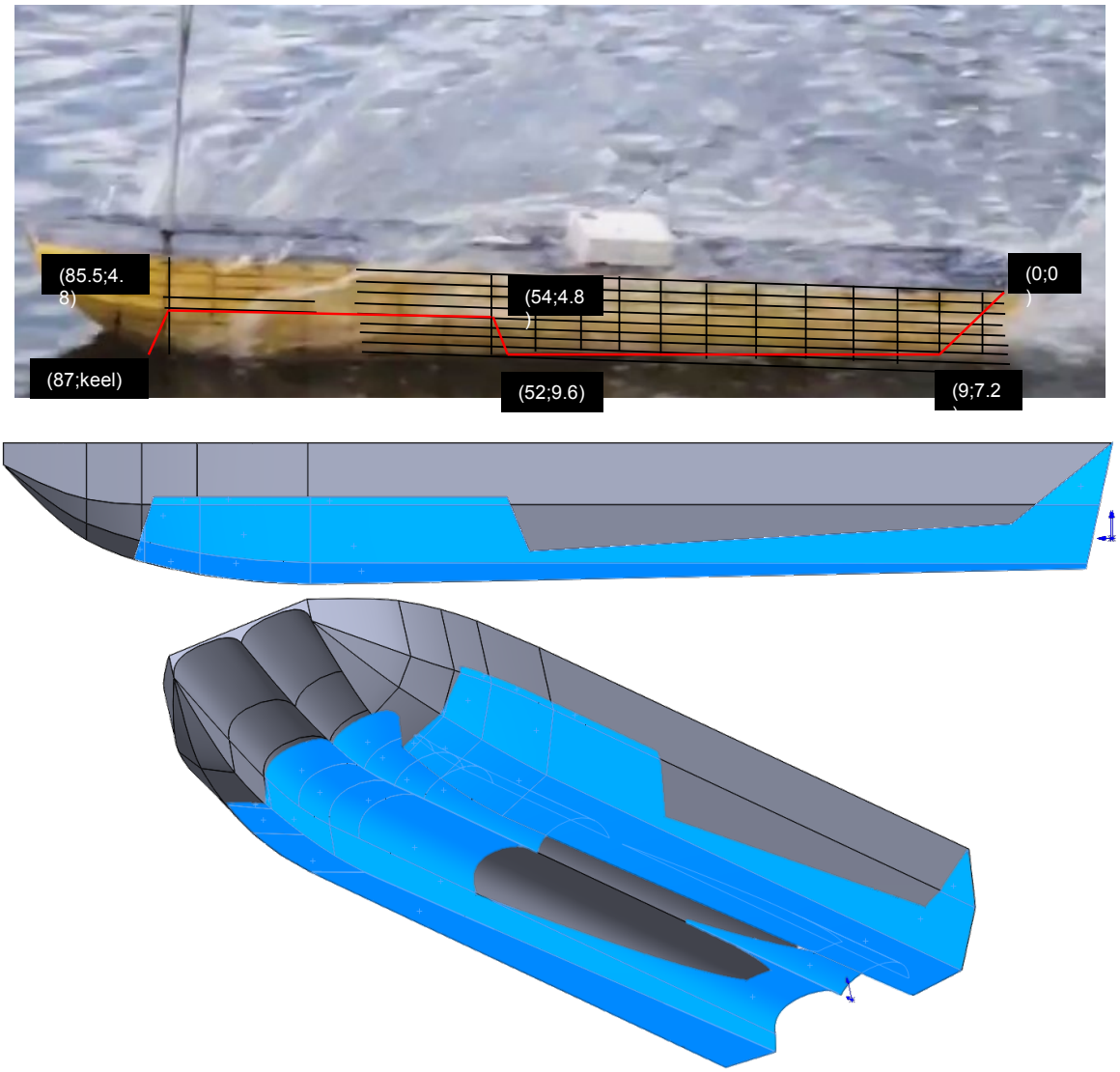

Figure E.14: Wetted area measurements (in centimeters) and CAD representation of the wetted areas for the catamaran at a real scale speed of 20 m/s. Wetted area = 17.28 m^2. Wetted keel length = 6.96 m

E.3 Hysucat

Wetted areas for the hysucat for 4 and 6 m/s are exactly the same than for the catamaran due to the hydrofoils start working at half the design speed, which is 7.4 m/s. For the hysucat, no CAD figures will be presented as they are very similar to those of the catamaran.

Figure E.15: Wetted area measurements (in centimeters) of the wetted area for the hysucat at a real scale speed of 10 m/s. Wetted area = 21.76 m^2. Wetted keel length = 6.48 m

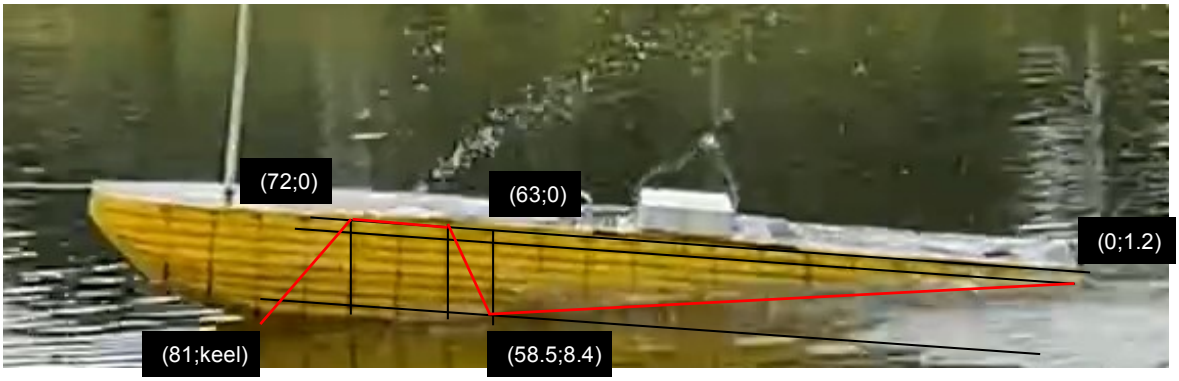

Figure E.16: Wetted area measurements (in centimeters) of the wetted area for the hysucat at a real scale speed of 13 m/s. Wetted area = 21.12 m^2. Wetted keel length = 6.48 m

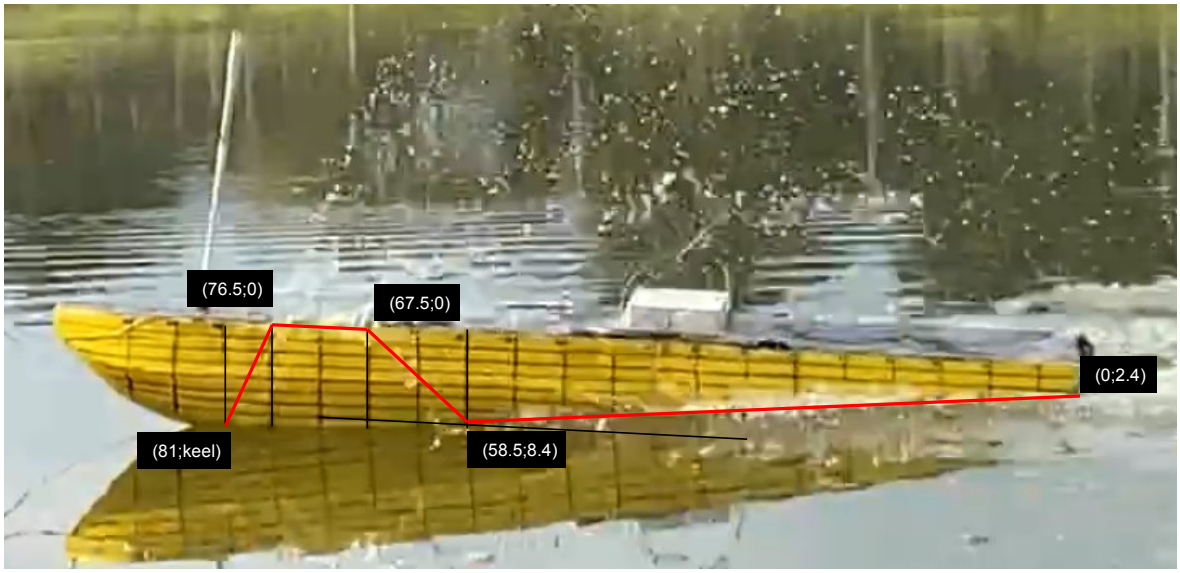

Figure E.17: Wetted area measurements (in centimeters) of the wetted area for the hysucat at a real scale speed of 15 m/s. Wetted area = 21.76 m^2. Wetted keel length = 6.48 m

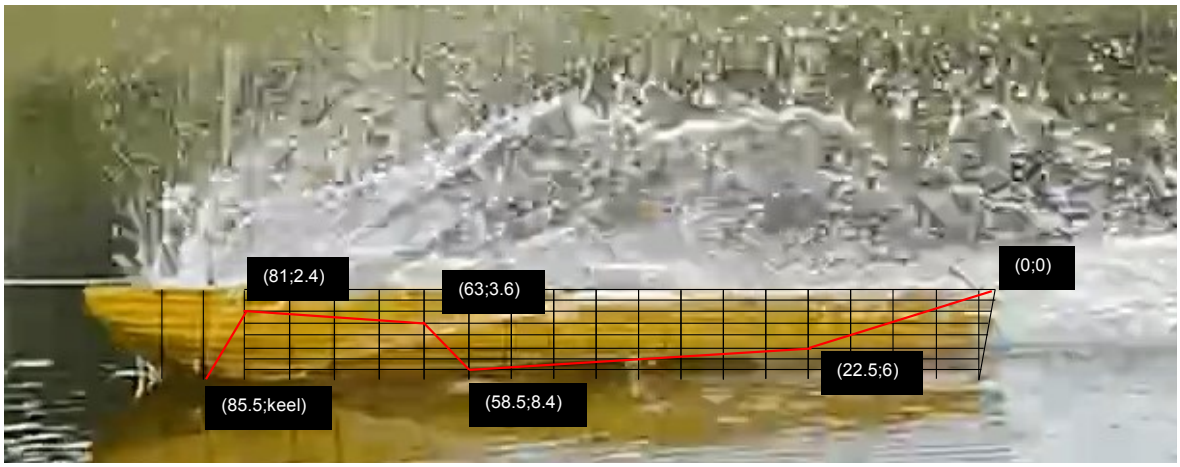

Figure E.18: Wetted area measurements (in centimeters) of the wetted area for the hysucat at a real scale speed of 17 m/s. Wetted area = 21.76 m^2. Wetted keel length = 6.48 m

Figure E.19: Wetted area measurements (in centimeters) of the wetted area for the hysucat at a real scale speed of 20 m/s. Wetted area = 18.56 m^2. Wetted keel length = 6.96 m